Università degli Studi di Palermo

SCUOLA POLITECNICA

Dipartimento di Ingegneria Civile, Ambientale, Aerospaziale, dei Materiali

Dottorato in Ingegneria Civile, Ambientale e dei Materiali

Ingegneria Strutturale e Geotecnica

ciclo XXX

Coordinatore.: Prof. Ing. Antonina Pirrotta

PH.D. THESIS

On the moving loads problem in discontinuous homogeneous beams and layered beams with interlayer slip

Candidato:

Ing. Salvatore Di Lorenzo

Relatori:

Ch.mo Prof. Antonina Pirrotta

Ch.mo Prof. Christoph Adam
(*University of Innsbruck*)

S.S.D. ICAR/08

On the moving loads problem in discontinuous homogeneous beams and layered beams with interlayer slip

Ph.D thesis submitted to the University of Palermo

by

Salvatore Di Lorenzo

Dipartimento di Ing. Civile, Ambientale, Aerospaziale, dei Materiali
Università degli Studi di Palermo
Scuola Politecnica
Viale delle Scienze, Ed. 8 - 90128 Palermo

SALVATORE DI LORENZO
Palermo, December 2017
e-mail:salvatore.dilorenzo@unipa.it

Thesis of the Ph.D. course in *Structural Engineering*
Dipartimento di Ingegneria Civile Ambientale, Aerospaziale, dei Materiali
Università degli Studi di Palermo
Scuola Politecnica
Viale delle Scienze, Ed.8 - 90128 Palermo, ITALY

Written in LaTeX
Examples and figures made with *Wolfram Mathematica*©

Contents

List of Figures

Preface

This manuscript contains the main part of my research performed in this last triennium at the Department of Civil, Environmental, Aerospace and Materials Engineering, University of Palermo, and at the Department of Basic Sciences in Engineering Sciences (Unit of Applied Mechanics), University of Innsbruck, Austria.

The research adheres to a common procedure of solving a scientistic problem. That is, introduction to the problem, selection of the mathematical and physical tools to model the problem, proposed solution, and numerical validation.

The thesis proposes a novel modal superposition approach to the moving loads problem on discontinuous homogeneous beam and layered beam with interlayer slip, carrying an arbitrary number of translational supports, rotational joints and alternatively tuned mass dampers (TMDs). The beams are referred to as discontinuous for the discontinuities of response variables at the application points of supports/joints/TMDs. Supports and TMDs are taken as representative of external devices while the rotational joints may model rotational dampers or connections with flexibility and damping arising from imperfections or damage.

Based on the theory of generalized functions to handle the discontinuities of response variables due to supports/joints/TMDs, exact beam modes are obtained regardless of the number of discontinuities. On using pertinent orthogonality condition for the de deflection modes, the dynamic response of the beam under moving loads is derived in time domain. All response variables are presented in a closed analytical form by using the relationship equations of the beam. Several numerical applications illustrate the efficiency of the proposed method.

Salvatore Di Lorenzo
Palermo, December 2017

Introduction

The main purpose of this thesis is to provide a novel modal superposition approach to the moving multi-loads problem in beam structures with external translational supports, internal rotational joints and alternatively tuned mass dampers (TMDs). The beams are referred to as discontinuous for the discontinuities of response variables at the application points of supports/joints and TMDs.

The reason for this kind of problem relates to the fact that, in recent years, lighter and more slender structures are being designed while vehicle speed progressively increases. In this contexts, investigations of dynamic effects have become crucial, stimulating a considerable interest in accurate and efficient solutions for the moving multi-loads problem on discontinuous beams.

In general, studies have adopted either a modal superposition or a finite element (FE) approach, but some inherent limitations still exist. Modal superposition methods generally use exact or approximate modes of the undamped beam and, for this reason, proportional damping is assumed or no damping is considered. Also the FE methods have some drawbacks: they generally require numerical integration, accuracy may depend on the grid mesh, and nodes must be inserted at any location of external translational/rotational supports, internal rotational joints, and dampers. This may be a significant disadvantage, especially in the early stages of design, when different solutions have to be built and compared at various locations of supports, joints or dampers.

To overcome these limitations, this thesis introduces a novel modal superposition approach to the moving multi-load problem in discontinuous beams. Exact modes are derived by the theory of generalised functions, along with pertinent orthogonality conditions. Based on the exact modes, the analytical expressions of the response under moving loads, by simple integration rules of generalised functions, are obtained. Analytical solutions for all response

variables and for any number of supports/joints/TMDs along the beam are built under moving loads with constant velocity.

In particular, in this thesis, the novel modal superposition approach is applied to two kind of beams: homogeneous beams and two-layered elastically bonded beams.

This thesis comprises five Chapters.

Chapter 1 concerns the vibration response of continuous Euler-Bernoulli beams under moving load. This Chapter is devoted to the introduction of the topic of the present thesis; i.e. moving loads on discontinuous Euler-Bernoulli beams.

Chapter 2 introduces a novel and efficient approach for studying the dynamic behavior under moving loads of discontinuous Euler-Bernoulli beams.

In Chapter 3 the aforementioned original and efficient approach is generalised to beams equipped with Kelvin-Voigt viscoelastic tuned mass dampers (TMDs).

Chapter 4 presents the moving multi-loads problem for two-layered elastically bonded beams.

Finally, Chapter 5 addresses the dynamic flexural behavior of the two-layered elastically bonded beams carrying an arbitrary number of elastic translational supports and rotational joints, under moving multi-loads.

Notation

In order to make reading of this manuscript easier, below the mainly used symbols and acronyms are summarised (in order of appearance).

X	coordinate in direction of the longitudinal axis
Z	coordinate in direction of the transverse axis
L	length of the beam
m_L	mass per unit length
EI	flexural rigidity
E	Young's modulus
I	moment of inertia of the cross section with respect to the Z-axis
$W(X,t)$	flexural deflection
$\Theta(X,t)$	bending rotation of the cross section
$Q(X,t)$	shear force
$M(X,t)$	bending moment
t	time instant
F	moving load
V_0	velocity of the moving load
δ	Dirac's Delta function

$\sigma(Z,X,t)$	stress
$\varepsilon(Z,X,t)$	strain
x	dimensionless longitudinal axis
f	dimensionless moving load
v_0	dimensionless velocity of the moving load
τ	dimensionless time instant
T	period of oscillator
$w(x,\tau)$	dimensionless flexural deflection
$\theta(x,\tau)$	dimensionless bending rotation of the cross section
$m(X,\tau)$	dimensionless bending moment
$q^*(X,\tau)$	dimensionless shear force
$\psi(x)$	dimensionless eigenfunction of deflection
$\vartheta(x)$	dimensionless eigenfunction of rotation
$\mu(x)$	dimensionless eigenfunction of bending moment
$\chi(x)$	dimensionless eigenfunction of shear force
σ	dimensionless eigenvalue
ω	eigenvalue
i	imaginary unit
$\mathbf{Y}(x)$	vector collecting the dimensionless eigenfunctions
$\mathbf{c}$	vector of integration constants
$\mathbf{\Omega}(x)$	matrix containing all the terms of the dimensionless eigenfunction of the bare beam

$\mathbf{B}$	matrix given by the response variables $\mathbf{Y}(x)$ computed at the end of the beam
det	determinant
δ_{jk}	Kronecker delta
M	number of modes
N	number of discontinuities
X_j	position of the discontinuities
$K_{W,j}$	spring stiffness of the viscoelastic support
$C_{W,j}$	damping coefficient of the viscoelastic support
$K_{\Delta\Theta,j}$	spring stiffness of the viscoelastic joint
$C_{\Delta\Theta,j}$	damping coefficient of the viscoelastic joint
$R(X,t)$	generalised function
$P_j(t)$	reaction force of the j-th support
$\Delta\Theta_j(t)$	relative rotation at the j-th joint
$r(x,\tau)$	dimensionless generalised function
$p_j(\tau)$	dimensionless reaction force of the j-th support
x_j	dimensionless position of the discontinuities
$\Delta\theta_j(\tau)$	dimensionless relative rotation at the j-th joint
$\delta^{(k)}$	k-th formal derivative of the Dirac's delta
$k_{w,j}$	dimensionless spring stiffness of the viscoelastic support
$c_{w,j}$	dimensionless damping coefficient of the viscoelastic support
$k_{\Delta\theta,j}$	dimensionless spring stiffness of the viscoelastic joint
$c_{\Delta\theta,j}$	dimensionless damping coefficient of the viscoelastic joint

$\rho(\sigma)$	dimensionless generalised function in the eigenfunction domain
$\varphi_j(\sigma)$	dimensionless reaction force of the jth support in the eigenfunction domain
$\Delta\vartheta_j(\sigma)$	dimensionless relative rotation at the jth joint in the eigenfunction domain
$\mathbf{\Lambda}_j$	vector of the dimensionless reaction forces and the dimensionless relative rotation in the eigenfunction domain
$\mathbf{J}(x, x_j)$	particular solutions associated with $\mathbf{\Lambda}_j$
F_{ii}	moving multi loads
NL	number of moving multi loads
t_{ii}^0	time instants of departure of the moving loads
t_{ii}^E	time instants of arrival of the moving loads
H	Heaviside function
S_{ii}	initial location of the moving loads
s_{ii}	dimensionless initial location of the moving loads
f_{ii}	dimensionless moving multi loads
τ_{ii}^0	dimensionless time instants of departure of the moving loads
τ_{ii}^E	dimensionless time instants of arrival of the moving loads
$K_{TMD,j}$	stiffness of the tuned mass damper
$C_{TMD,j}$	damping coefficient of the tuned mass damper
$M_{TMD,j}$	mass of the tuned mass damper
$k_{TMD,j}$	dimensionless stiffness of the tuned mass damper

$c_{TMD,j}$	dimensionless damping coefficient of the tuned mass damper
$m_{TMD,j}$	dimensionless mass of the tuned mass damper
β	frequency ratio of the tuned mass damper
ζ	damping ratio of the tuned mass damper
σ_{TMD}	natural frequency of the tuned mass damper
α	mass ratio
$\bar{m}$	dimensionless first modal mass of the beam
$N(X,t)$	axial force
$T(X,t)$	elastic interlaminar shear force
$Q_1(X,t)$	shear force in the upper layer
$Q_2(X,t)$	shear force in the lower layer
$M_1(X,t)$	bending moment in the upper layer
$M_2(X,t)$	bending moment in the lower layer
$N_1(X,t)$	axial force in the upper layer
$N_2(X,t)$	axial force in the lower layer
ρ_i	mass densities of the single layers
A_i	cross sectional areas of the single layers
r_i	distances between the centroids of the single layers and the interlayer
$U_1(X,t)$	longitudinal displacements at the centroid of the upper layer
$U_2(X,t)$	longitudinal displacements at the centroid of the lower layer
$\Delta U\,(X,t)$	interlaminar slip
EI_0	bending stiffness corresponding to non-composite action

EI_∞	bending stiffness corresponding to a rigid interlayer connection
EA_0	longitudinal stiffness for non-composite action
$\Phi(X)$	eigenfunction of deflection
$O(X)$	eigenfunction of rotation
$\Upsilon(X)$	eigenfunction of bending moment
$\Gamma(X)$	eigenfunction of shear force
$\Sigma(X)$	eigenfunction of the axial force in the upper layer
$\Psi(X)$	eigenfunction of the elastic interlaminar shear force
ζ_m	m-th proportional viscous damping coefficient
ω_{dm}	damped m-th natural frequency

Chapter 1

On the moving load problem in continuous Euler-Bernoulli beams

This chapter concerns the vibration response of Euler-Bernoulli beams under moving load. Based on pertinent orthogonality conditions for the deflection modes, the response under a moving load is built in time domain by modal superposition.

1.1 Preliminary remarks

Vibration analysis of beam-like structures under moving loads is a classical topic in structural dynamics, with relevant applications in many engineering fields such as, for instance, railway or highway bridges acted upon by travelling loads [1, 3–5]. In light of the fact that, in recent years, lighter and more slender structures are being designed while vehicle speed progressively increases, investigations of dynamic effects have become crucial, stimulating a considerable interest in accurate and efficient solutions for the moving load problem on beams [1, 3–6].

In the context of moving load analysis, this chapter serves as a foundation for the subsequent chapters, since it contains the well-known classical formulation of the moving load problem in Euler-Bernoulli beams. The modal superposition approach based on the exact modes is considered and analytical solutions for all response variables are built in time domain.

1.2 Equation of motion for beams under moving load

Consider the beam in Fig.1.1 where X is the longitudinal axis, Z the transverse axis, L the length, m_L the mass per unit length, EI the flexural rigidity, with E representing the Young's modulus and I the moment of inertia of the cross section with respect to the Z-axis; symbols $W(X,t)$, $\Theta(X,t)$ denote flexural deflection and bending rotation of the cross section; $Q(X,t)$ and $M(X,t)$ are shear force and bending moment, with t denoting the time instant. Positive sign conventions are shown in Fig.1.1.

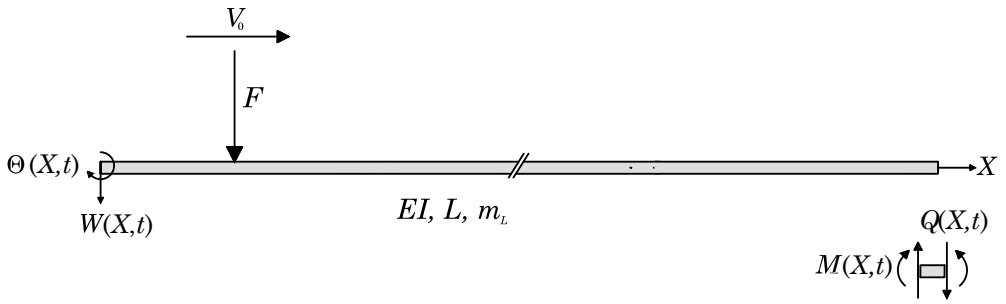

Figure 1.1: Euler-Bernoulli beam under moving load with constant velocity. Positive sign conventions are shown

The dynamic equilibrium equation for vibrations $W(X,t)$, in the Z-direction of the length dX of the beam, under a moving load F with constant velocity V_0 [7], is readily obtained by equating the inertial force to the sum of the forces exerted by the other parts of the beam and the external forces:

$$\frac{\partial^2 M(X,t)}{\partial X^2} = m_L \frac{\partial^2 W(X,t)}{\partial t^2} - F\delta(X - V_0 t) \tag{1.1}$$

where $\delta(X - X_j)$ is the Dirac's delta.

In virtue of the Euler- Bernoulli hypothesis, that is neglecting rotary inertia and shear deformation, the kinematic and the mechanical relations read respectively [8]:

$$\varepsilon(Z,X,t) = -Z\frac{\partial^2 W(X,t)}{\partial X^2} \tag{1.2}$$

$$\sigma\left(Z,X,t\right)=\frac{M\left(X,t\right)}{I}Z \tag{1.3}$$

Making use of Hooke's law, $\sigma\left(Z,X,t\right)=E\,\varepsilon\left(Z,X,t\right)$ which relates stress $\sigma\left(Z,X,t\right)$ to the axial strain $\varepsilon\left(Z,X,t\right)$, and substituting Eq. (1.2) and Eq. (1.3) into this relationship, the following relation for bending moment $M(X,t)$ is found [8]:

$$M\left(X,t\right)=-EI\frac{\partial^2 W\left(X,t\right)}{\partial X^2} \tag{1.4}$$

At this point, introducing Eq. (1.4) into Eq. (1.1) the equation of motion of the beam under a moving load F with constant velocity V_0 is [8]:

$$EI\frac{\partial^4 W\left(X,t\right)}{\partial X^4}+m_L\frac{\partial^2 W\left(X,t\right)}{\partial t^2}=F\delta\left(X-V_0 t\right) \tag{1.5}$$

In dimensionless form, Eq. (1.5), reverts to:

$$\frac{\partial^4 w\left(x,\tau\right)}{\partial x^4}+\frac{\partial^2 w\left(x,\tau\right)}{\partial \tau^2}=f\delta\left(x-v_0\tau\right) \tag{1.6}$$

In Eq. (1.6), $x=X/L$, $f=FL^2/EI$, $v_0=V_0T/L$, and $\tau=t/T$, with $T=\sqrt{m_L L^4/EI}$ and $\delta\left(X-X_j\right)=\delta\left(x-x_j\right)/L$. Also, the following symbols denote the dimensionless beam response variables: $w=W/L$, $\theta=\Theta$, $m=ML/EI$, $q^*=QL^2/EI$.

1.3 Beam modes

The free vibration problem of the beam in Fig.1.1 is reported here.

1.3.1 Eigenvalue problem

Based on the standard separate variables approach, let $w\left(x,\tau\right)=\psi\left(x\right)e^{\mathrm{i}\sigma\tau}$, $\theta\left(x,\tau\right)=\vartheta\left(x\right)e^{\mathrm{i}\sigma\tau}$, $m\left(x,\tau\right)=\mu\left(x\right)e^{\mathrm{i}\sigma\tau}$, $q^*\left(x,\tau\right)=\chi\left(x\right)e^{\mathrm{i}\sigma\tau}$, where $\psi\left(x\right)$, $\vartheta\left(x\right)$, $\mu\left(x\right)$, $\chi\left(x\right)$ are the dimensionless eigenfunctions of deflection, rotation, bending moment and shear force, respectively; σ is the dimensionless eigenvalue, with $\sigma^2=\omega^2 m_L L^4/EI$ where ω the dimensional eigenvalue and $\mathrm{i}=\sqrt{-1}$ is the imaginary unit. The free-vibration equation of the beam in Fig.1.1 reads:

$$\frac{\bar{d}^4\psi(x)}{dx^4} - \sigma^2\psi(x) = 0 \tag{1.7}$$

The eigenfunctions $\psi(x)$, $\vartheta(x)$, $\mu(x)$, $\chi(x)$ are related by the beam equations:

$$\frac{d\chi(x)}{dx} + \sigma^2\psi(x) = 0 \tag{1.8}$$

$$\frac{d\mu(x)}{dx} = \chi(x) \tag{1.9}$$

$$\frac{d\vartheta(x)}{dx} = -\mu(x) \tag{1.10}$$

$$\frac{d\psi(x)}{dx} = \vartheta(x) \tag{1.11}$$

Next, let $\mathbf{Y}(x) = \begin{bmatrix} \psi(x) & \vartheta(x) & \mu(x) & \chi(x) \end{bmatrix}^T$ be the vector collecting the eigenfunctions of the response variables. From Eq. (1.7), $\mathbf{Y}(x)$ can be cast in the following form:

$$\mathbf{Y}(x) = \mathbf{\Omega}(x)\,\mathbf{c} \tag{1.12}$$

where

$$\mathbf{\Omega}(x) = \begin{bmatrix} \Omega_{\psi 1} & \Omega_{\psi 2} & \Omega_{\psi 3} & \Omega_{\psi 4} \\ \Omega_{\vartheta 1} & \Omega_{\vartheta 2} & \Omega_{\vartheta 3} & \Omega_{\vartheta 4} \\ \Omega_{\mu 1} & \Omega_{\mu 2} & \Omega_{\mu 3} & \Omega_{\mu 4} \\ \Omega_{\chi 1} & \Omega_{\chi 2} & \Omega_{\chi 3} & \Omega_{\chi 4} \end{bmatrix} \tag{1.13}$$

and $\mathbf{c} = \begin{bmatrix} c_1 & c_2 & c_3 & c_4 \end{bmatrix}^T$ 4×1 vector of integration constants.

The above terms in Eq. (1.13) can be written in a simple analytical form:

$$\begin{array}{ll} \Omega_{\psi 1}(x) = \mathrm{e}^{-\sigma x}; & \Omega_{\psi 2}(x) = \mathrm{e}^{\sigma x} \\ \Omega_{\vartheta 1}(x) = -\sigma \mathrm{e}^{-\sigma x}; & \Omega_{\vartheta 2}(x) = \sigma \mathrm{e}^{\sigma x} \\ \Omega_{\mu 1}(x) = -\sigma^2 \mathrm{e}^{-\sigma x}; & \Omega_{\mu 2}(x) = -\sigma^2 \mathrm{e}^{\sigma x} \\ \Omega_{\chi 1}(x) = \sigma^3 \mathrm{e}^{-\sigma x}; & \Omega_{\chi 2}(x) = -\sigma^3 \mathrm{e}^{\sigma x} \\ \Omega_{\psi 3}(x) = \cos(\sigma x); & \Omega_{\psi 4}(x) = \sin(\sigma x) \\ \Omega_{\vartheta 3}(x) = -\sigma \sin(\sigma x); & \Omega_{\vartheta 4}(x) = \sigma \cos(\sigma x) \\ \Omega_{\mu 3}(x) = \sigma^2 \cos(\sigma x); & \Omega_{\mu 4}(x) = \sigma^2 \sin(\sigma x) \\ \Omega_{\chi 3}(x) = -\sigma^3 \sin(\sigma x); & \Omega_{\chi 4}(x) = \sigma^3 \cos(\sigma x) \end{array} \tag{1.14}$$

The 4×1 vector of integration constants $\mathbf{c}$ in Eq. (1.12) can be computed by enforcing the boundary condition (B.C.) of the beam. This leads to four equations with the general form:

$$\mathbf{B}\mathbf{c} = \mathbf{0} \tag{1.15}$$

Terms in matrix $\mathbf{B}$ are given by the response variables $\mathbf{Y}(x)$ computed at $x = 0$, $x = 1$ using Eq. (1.12). From Eq. (1.15), the characteristic equation can be built as determinant of the 4×4 matrix $\mathbf{B}$, i.e.

$$\det \mathbf{B} = 0 \tag{1.16}$$

Then, upon deriving the dimensionless eigenvalue σ from Eq. (1.16), and the vector of integration constants $\mathbf{c}$ from Eq. (1.15), the vector of eigenfunctions $\mathbf{Y}(x)$ is obtained, using Eq. (1.12).

1.4 Beam response to moving load

The modes, built as explained in section 1.3, serve as a basis to predict the beam response to the moving load. Then, taking into account the orthogonality condition that is:

$$\int_0^1 \psi_j(x)\, \psi_k(x)\, dx = \delta_{jk} \tag{1.17}$$

where δ_{jk} is the Kronecker delta defined as:

$$\delta_{jk} = \begin{cases} 1 & \text{if} \quad j = k \\ 0 & \text{if} \quad j \neq k \end{cases} \tag{1.18}$$

and considering the moving load $f(x,\tau) = \delta(x - v_0\tau)$ in Eq. (1.6), the beam deflection can be cast in the following form:

$$w(x,\tau) = \sum_{k=1}^{\infty} \psi_k(x) \int_0^{\tau} e^{\mathrm{i}\sigma_k(\tau-\tau')} g_k(\tau')\, d\tau' \tag{1.19}$$

In Eq. (1.19), $\psi_k(x)$ is the kth deflection eigenfunction, and $g_k(\cdot)$ is given as:

$$g_k(\tau') = (\mathrm{i}\sigma_k \Xi_k)^{-1} \eta_k(\tau') \tag{1.20}$$

where

$$\eta_k(\tau') = \int_0^1 \psi_k(x)\, \delta(x - v_0\tau')\, dx = \psi_k(v_0\tau') \tag{1.21}$$

$$\Xi_k = 2\int_0^1 \psi_k^2(x)\, dx \tag{1.22}$$

In practical applications, a few M modes in the modal superposition Eq. (1.19) will be sufficient to accurately represent the response.

1.5 Numerical Application

Consider the simply supported beam in Fig.1.2

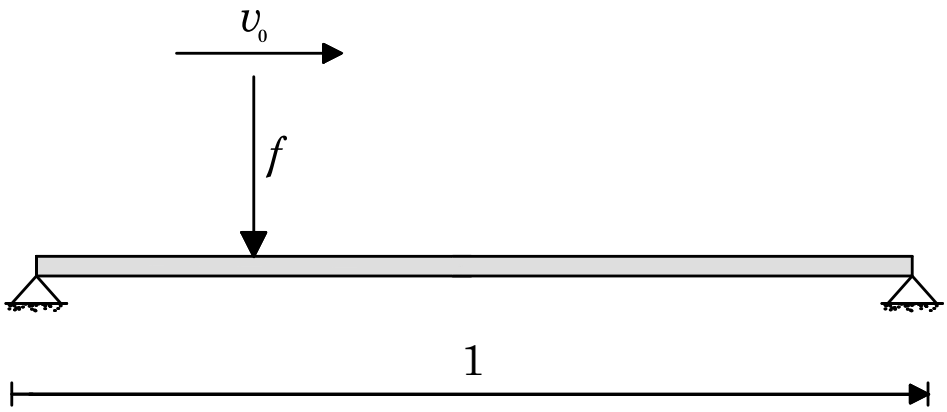

Figure 1.2: Simply-supported beam

Table 1.1: Dimensionless frequencies of beam in Fig.1.2

Mode	Frequency
1	9.8696
2	39.4784
3	88.8264
4	157.914
5	246.740

Table 1.2 reports the dimensionless eigenvalues of the first five modes while in Fig.1.3 the eigenfunctions of mode 1 are shown, for all response variables.

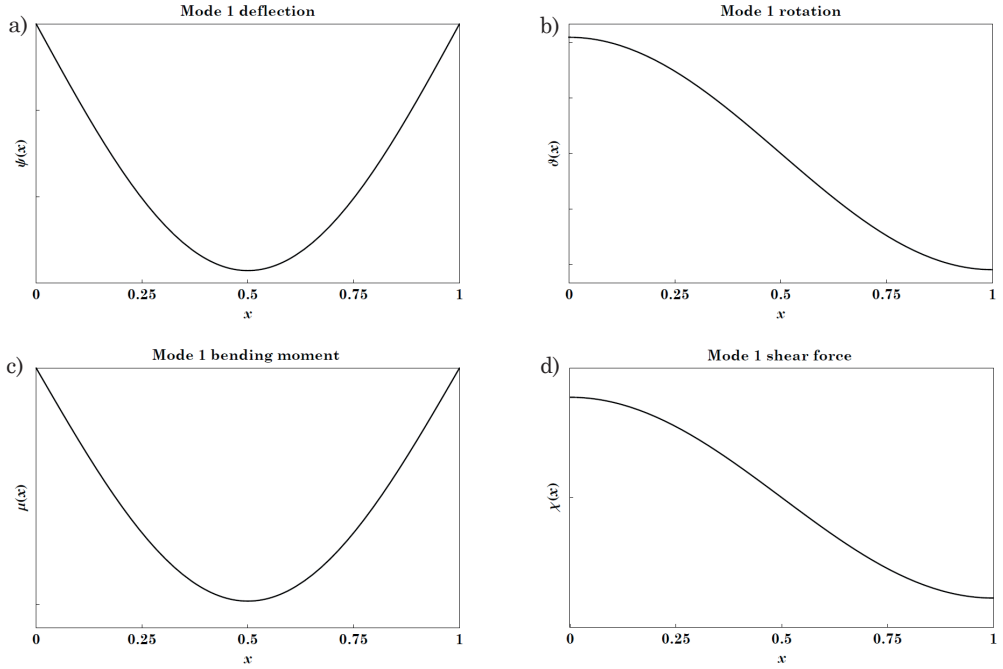

Figure 1.3: Mode 1 eigenfunctions of beam in Fig.1.2: (a) deflection; (b) rotation; (c) bending moment; (d) shear force

Next, the dynamic response to a moving force $f = 1$ is investigated. Fig.1.4 shows the mid-span deflection of the beam for various velocities of the moving force, as computed by Eq. (1.19) with M=3 modes. No significant changes are found when considering $M > 3$ modes.

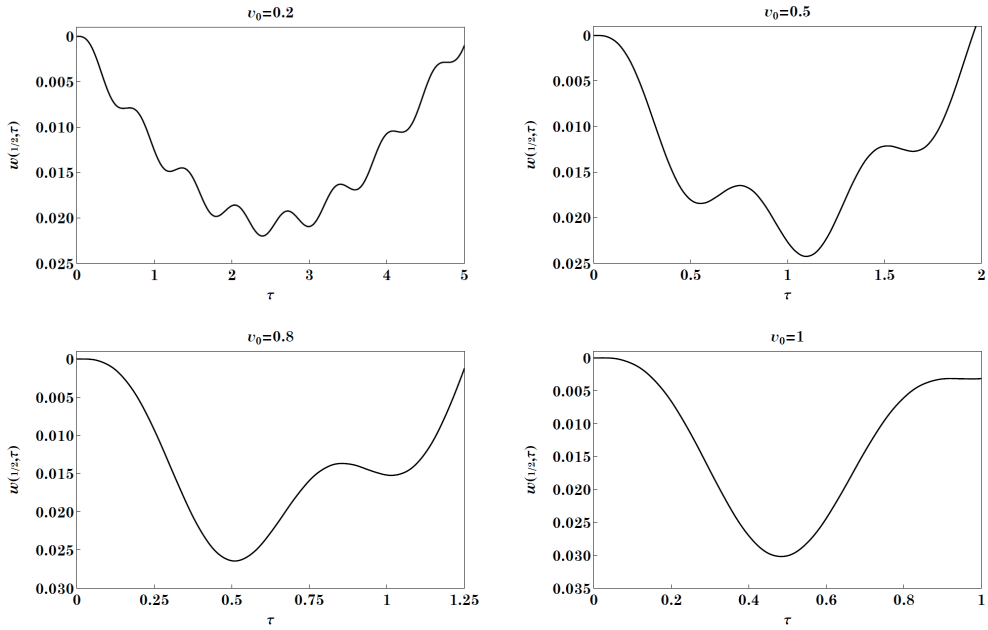

Figure 1.4: Mid-span deflection of beam in Fig.1.2 under a moving force with different velocities v_0

Finally, Fig.1.5 shows the beam deflection over the whole axis at certain time instants, for two load velocities, as computed by Eq. (1.19) with $M = 3$ modes.

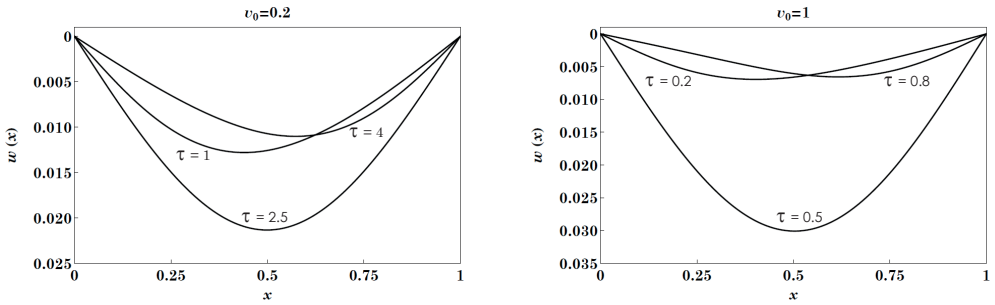

Figure 1.5: Deflection profile of beam in Fig.1.2 at different time instants, under a moving force with different velocities v_0

1.6 Concluding remarks

The vibration response of a beam under moving loads has been presented. To show the procedure used in the subsequent chapters, based on pertinent orthogonality conditions for the deflection modes, the response under a moving load is built in time domain by modal superposition.

Chapter 2

Novel approach to the moving load problem in discontinuous Euler-Bernoulli beams

This chapter concerns the vibration response under moving load of Euler-Bernoulli beams with translational supports and rotational joints, featuring Kelvin-Voigt viscoelastic behaviour. The beams are referred to as discontinuous for the discontinuities of response variables at the application points of supports/joints. Using the theory of generalised functions to handle the discontinuities of the response variables at the support/joint locations, exact beam modes are obtained from a characteristic equation built as the determinant of a 4×4 matrix, for any number of supports/joints. Based on pertinent orthogonality conditions for the deflection modes, the response under moving load is built in time domain by modal superposition. Remarkably, all response variables are built in a closed analytical form, regardless of the number of supports/joints.

2.1 Preliminary remarks

In the context of moving load problem analysis, much effort has been devoted to developing analytical or numerical methods that are capable of handling loads travelling on multi-span beams, beams with in-span external translational or rotational supports, beams with internal rotational joints modelling flexible connections or cracks, and beams with dampers. The dynamics of

such beams under moving loads has been investigated in several studies, and any review can hardly be exhaustive. In general, studies have adopted either a modal superposition [9–23] or a finite element (FE) approach [24–27], most of which focus on Euler-Bernoulli beam models [9–27].

Among modal superposition methods, some have addressed beams based on exact modes [9–14]. Specifically, for stepped [9] or uniform [10] beams with along-axis elastic translational/rotational supports [9, 10], and stepped beams with along-axis fixed translational supports [11], Johansson et al. [9], Zhu and Law [10], Chan and Ashebo [11], used exact modes built by the classical procedure, which requires representing the free vibration response of every beam segment with uniform cross-section properties, or between two consecutive translational/rotational supports, in a trigonometric-hyperbolic form with 4 integration constants, totalling $4 \times k$ constants for k segments, to be computed by matching conditions between responses over contiguous segments. By this approach, exact beam natural frequencies and modes are derived from a characteristic equation built as determinant of a $(4 \times k) \times (4 \times k)$ matrix. For non-prismatic [12] or stepped [13] beams with along-axis fixed translational supports [12, 13], Dugush and Eisenberger [12], Henchi et al.[13] used exact modes derived from a global dynamic stiffness matrix obtained by assembling the dynamic stiffness matrix of every span. For a uniform beam with end rotational dampers, Greco and Santini [14] used exact complex modes with pertinent orthogonality conditions. Notice that, in ref.[9–14] using exact modes, uncoupled equations of motion were always derived for the beam under moving load.

Among modal superposition methods for beams, a significant number of papers involving approximate modes also exists [15–23]. For instance, for non-prismatic beams with along-axis fixed translational supports, Martinez-Castro et al. [15] used modes from a FE discretisation of the beam, Zheng et al. [16] used modified vibration modes built as linear combination of the standard vibration modes of a uniform prismatic beam without along-axis supports, but featuring the same boundary conditions (B.C.) of the non-prismatic beam, and cubic splines fulfilling the in-span zero deflections at the rigid translational supports. Again for non-prismatic beams with along-axis fixed translational supports, De Salvo et al.[17] used a special variant of the component mode synthesis method, while Zhu and Law [18] utilized the Ritz method to build approximate modes as linear combination of exact modes of uniform beam. For stepped beams with along-axis elastic translational and rotational supports and internal translational and rotational joints cou-

pling adjacent spans, Xu and Li [19] applied a modified Fourier series representation of the deflection response including a suitable auxiliary polynomial function in each span to improve accuracy and convergence rate. For a beam connected to a retrofitted auxiliary beam with translational viscous dampers [20], a beam carrying a mass-damper with either linear or non-linear constitutive law [21], multi-span beams on fixed translational supports [22], Museros and Martinez-Rodrigo [20], Samani and Pellicano [21], Lee [22] used the exact modes of the bare beam, i.e. the uniform beam without in-span supports or attachments, to approximate the vibration modes (in ref. [20], they were used for both retrofitted and retrofitting beams). For a uniform beam with an elastic rotational joint modelling a crack, Lee and Ng [23] used a series of normalized characteristic functions over the two spans connected by the joint. Note that, in ref. [15–23] using approximate modes, uncoupled [15] and, more frequently, coupled [16–23] equations of motion were derived for the beam under moving load.

FE solutions in ref. [24–27] were generally built by numerical integration of the motion equations under moving load, and without recurring to modal truncation. A review may be found in the works by Wu et al. [24] and Rieker et al. [25]. A spectral FE approach was followed by Sarvestan et al.[26] for viscoelastic beams with elastic rotational joints modelling cracks, and by Azizi et al.[27] for multi-span non-uniform beams. An interesting and alternative approach to modal superposition methods [9–23] and FE solutions [24–27] has been proposed by Sun [28] for loads travelling on a uniform beam resting on a Winkler viscoelastic subgrade, by representing the deflection as a generalized integral which involves the beam Green's function.

Although modal superposition and FE methods provided effective solutions in all studies described above [9–27], some inherent limitations still exist. Modal superposition methods generally use exact or approximate modes of the undamped beam and, for this reason, proportional damping is assumed [9–11, 13] or no damping is considered [12]. For those applications where damping cannot be taken as proportional, as-in, for instance, cases where dampers are present, only a few modal superposition methods are available [14, 20, 21]. An exact solution for a uniform beam with end rotational dampers is provided in ref.[14], while approximate solutions for translational viscous dampers coupling retrofitted beams or one attached mass-damper are reported respectively in ref.[20] and ref.[21]. Also the FE methods have some drawbacks: they generally require numerical integration, accuracy may depend on the grid mesh, and nodes must be inserted at any location of exter-

nal translational/rotational supports, internal rotational joints, and dampers. This may be a significant disadvantage, especially in the early stages of design, when different solutions have to be built and compared at various locations of supports, joints or dampers.

Framed in the context above, this chapter introduces a novel modal superposition approach to the moving load problem in Euler-Bernoulli uniform beams with external translational supports and internal rotational joints, featuring linear elasticity and viscous damping according to a classical Kelvin-Voigt viscoelastic law. The formulation of the proposed approach has been published by myself and professors Di Paola, Failla and Pirrotta in an International journal "Acta Mechanica" [29] building upon a previous study [30] where, for such beams, exact modes were derived by the theory of generalised functions [31–42], along with pertinent orthogonality conditions. It will show that a modal superposition approach based on the exact modes provides analytical expressions of the response under moving loads, by simple integration rules of generalised functions. In particular, analytical solutions will be built under moving loads with constant velocity, and will be obtained for all response variables, for any number of supports/joints along the beam.

2.2 Equation of motion for discontinuous beam under moving load

Consider the beam in Fig.2.1 which carries an arbitrary number N of viscoelastic translational supports and rotational joints at abscissas X_j along the axis. In agreement with previous studies [43–48], a Kelvin-Voigt viscoelastic behaviour is assumed. The spring stiffness and damping coefficients are $K_{W,j}$ and $C_{W,j}$ for the jth translational support, $K_{\Delta\Theta,j}$ and $C_{\Delta\Theta,j}$ for the jth rotational joint.

In this study, translational supports are taken as representative of external devices such as grounded dampers applied for retrofitting purposes [20], or in-span supports with flexibility and damping. Likewise, rotational joints model rotational dampers such as, for instance, those applied at beam-to-column nodes for vibration control [46], or connections where flexibility and damping may arise from damage or imperfections [47, 48]. Obviously, purely elastic supports and joints can be considered in this study, as they are used in several applications to model in-span supports [9, 10, 17] and cracks [23, 35, 39, 40], respectively.

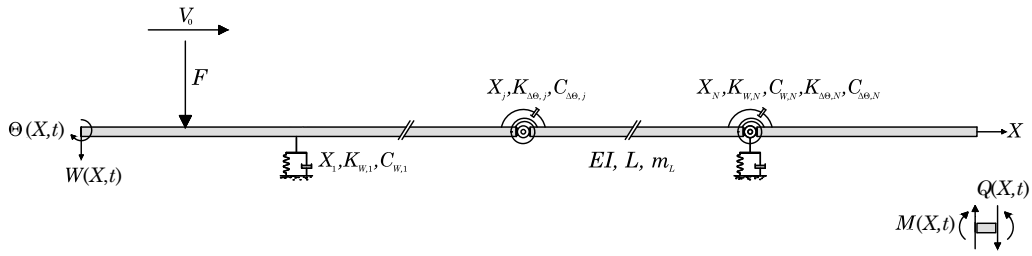

Figure 2.1: Euler-Bernoulli beam with translational supports and rotational joints under moving load with constant velocity. Positive sign conventions are shown.

Equations will be written for the most general case of supports and joints occurring simultaneously at the same location. However, changes will be straightforward to consider a single support or a single joint at a given location. Under this assumption, the theory of generalised functions leads to the following equation of motion of the beam under a moving load F with constant velocity V_0 [7]:

$$EI\frac{\bar{\partial}^4 W(X,t)}{\partial X^4} + m_L\frac{\partial^2 W(X,t)}{\partial t^2} + R(X,t) = F\delta(X - V_0 t) \tag{2.1}$$

Because of the discontinuities at support/joint locations, the fourth order derivative in Eq. (2.1) is a generalised derivative, as denoted by the over-bar. Further, $R(X,t)$ is a generalised function given as:

$$R(X,t) = -\sum_{j=1}^{N} P_j(t)\,\delta\left(X - X_j\right) - \sum_{j=1}^{N} EI\,\Delta\Theta_j(t)\,\delta^{(2)}\left(X - X_j\right) \tag{2.2}$$

In Eqs. (2.1 and 2.2), $\delta\left(X - X_j\right)$ is the Dirac's delta and $\delta^{(k)}\left(X - X_j\right)$ denotes its k-th formal derivative; $P_j(t)$ is the reaction force of the j-th support

$$P_j(t) = K_{W,j}W\left(X_j,t\right) + C_{W,j}\frac{\partial W\left(X_j,t\right)}{\partial t} \tag{2.3}$$

and $\Delta\Theta_j(t) = \Theta\left(X_j^+,t\right) - \Theta\left(X_j^-,t\right)$ is the relative rotation at the j-th joint (see Fig.2.1), related to the bending moment at that point of the beam according to the following equation:

$$M_j(t) = K_{\Delta\Theta,j}\Delta\Theta_j\left(X_j,t\right) + C_{\Delta\Theta,j}\frac{\partial\Delta\Theta_j\left(X_j,t\right)}{\partial t} \tag{2.4}$$

Note that if no support and joint occur at $X = X_j$, the reaction force P_j and the relative rotation $\Delta\Theta_j$ are equal to zero. Then being $R(X,t) = 0$, Eq. (2.1) returns to Eq. (1.5), valid for continuous Euler-Bernoulli beams.

In dimensionless form, Eqs. (2.1 and 2.2), revert to:

$$\frac{\bar{\partial}^4 w(x,\tau)}{\partial x^4} + \frac{\partial^2 w(x,\tau)}{\partial \tau^2} + r(x,\tau) = f\delta(x - v_0\tau) \tag{2.5}$$

$$r(x,\tau) = -\sum_{j=1}^{N} p_j(\tau)\,\delta\left(x - x_j\right) - \sum_{j=1}^{N}\Delta\theta_j(\tau)\,\delta^{(2)}\left(x - x_j\right) \tag{2.6}$$

In Eqs. (2.5) and (2.6), $\delta^{(k)}\left(X - X_j\right) = \delta^{(k)}\left(x - x_j\right)\Big/L^{k+1}$, while for the damper parameters, $k_{w,j} = K_{W,j}L^3/EI$, $c_{w,j} = C_{W,j}L/\sqrt{m_L EI}$, $k_{\Delta\theta,j} = K_{\Delta\Theta,j}L/EI$ and $c_{\Delta\theta,j} = C_{\Delta\Theta,j}/L\sqrt{m_L EI}$.

2.3 Beam complex modes

An original systematic procedure for the free vibration problem of the beam in Fig.2.1 is proposed here. In this context, this formulation allows the construction of a characteristic equation featuring all terms in a closed analytical form.

2.3.1 Eigenvalue problem

Based on the standard separate variables approach, used for the continuous beam in chapter 1, the free-vibration dimensionless equation of the discontinuous Euler-Bernoulli beam in Fig.2.1, reads:

$$\frac{\bar{d}^4\psi(x)}{dx^4} - \sigma^2\psi(x) + \rho(\sigma) = 0 \tag{2.7}$$

where $\rho(\sigma)$ denotes the presence of the supports and joints:

$$\rho(\sigma) = -\sum_{j=1}^{N} \varphi_j(\sigma)\,\delta(x - x_j) - \sum_{j=1}^{N} \Delta\vartheta_j(\sigma)\,\delta^{(2)}(x - x_j) \tag{2.8}$$

As said for the continuous beam, the eigenfunctions $\psi(x)$, $\vartheta(x)$, $\mu(x)$, $\chi(x)$ of the discontinuous beam are related by the beam equations:

$$\frac{\bar{d}\chi(x)}{dx} + \sigma^2\psi(x) + \sum_{j=1}^{N} \varphi_j(\sigma)\,\delta(x - x_j) = 0 \tag{2.9}$$

$$\frac{\bar{d}\mu(x)}{dx} = \chi(x) \tag{2.10}$$

$$\frac{\bar{d}\vartheta(x)}{dx} = -\mu(x) + \sum_{j=1}^{N} \Delta\vartheta_j(\sigma)\,\delta(x - x_j) \tag{2.11}$$

$$\frac{\bar{d}\psi(x)}{dx} = \vartheta(x) \tag{2.12}$$

In Eqs. (2.7) and (2.8), $\varphi_j(\sigma)$ and $\Delta\vartheta_j(\sigma)$ are the reaction force of the jth support and the relative rotation at jth joint, respectively. After Fourier-transforming Eqs. (2.3) and (2.4) written in dimensionless form, become:

$$\varphi_j(\sigma) = -\kappa_{w,j}(\sigma)\,\psi(x_j) \quad \kappa_{w,j}(\sigma) = k_{w,j} + \mathrm{i}\sigma c_{w,j} \tag{2.13}$$

$$\Delta\vartheta_j(\sigma) = -\frac{\mu(x_j)}{\kappa_{\Delta\theta,j}(\sigma)} \quad \kappa_{\Delta\theta,j}(\sigma) = k_{\Delta\theta,j} + \mathrm{i}\sigma c_{\Delta\theta,j} \tag{2.14}$$

Note that $\varphi_j(\sigma)$ and $\Delta\vartheta_j(\sigma)$ in Eqs. (2.7) and (2.8) are all unknown, for j=1,2,..,N. Next, considering $\mathbf{\Lambda}_j = \begin{bmatrix} \varphi_j & \Delta\vartheta_j \end{bmatrix}^T$ the vector of the unknown reaction forces $\varphi_j(\sigma)$ and the relative rotation $\Delta\vartheta_j(\sigma)$ at $x = x_j$, the vector $\mathbf{Y}(x)$ collecting the eigenfunctions of the response variables, can be cast from Eqs. (2.7) and (2.8), in the following general form, based on the linear superposition principle:

$$\mathbf{Y}(x) = \mathbf{\Omega}(x)\,\mathbf{c} + \sum_{j=1}^{N} \mathbf{J}(x, x_j)\,\mathbf{\Lambda}_j \tag{2.15}$$

That is, $\mathbf{Y}(x)$ is built as the sum of the solution to the homogeneous equation, $\mathbf{\Omega}(x)\,\mathbf{c}$, representing the eigenfunctions of the bare beam considered in chapter 1, Eqs. (1.13) and (1.14), and the particular solutions associated with the unknowns $\mathbf{\Lambda}_j$ at $x = x_j$, $\mathbf{J}(x, x_j)\,\mathbf{\Lambda}_j$, which account for the discontinuities at support/joint locations.

In the particular solution:

$$\mathbf{J}(x, x_j) = \begin{bmatrix} \mathbf{J}^{(p)} & \mathbf{J}^{(\Delta\theta)} \end{bmatrix} \quad \text{for} \quad \mathbf{J}^{(p)} = \begin{bmatrix} J_\psi^{(p)} \\ J_\vartheta^{(p)} \\ J_\mu^{(p)} \\ J_\chi^{(p)} \end{bmatrix}; \quad \mathbf{J}^{(\Delta\theta)} = \begin{bmatrix} J_\psi^{(\Delta\theta)} \\ J_\vartheta^{(\Delta\theta)} \\ J_\mu^{(\Delta\theta)} \\ J_\chi^{(\Delta\theta)} \end{bmatrix} \tag{2.16}$$

where superscripts (p), $(\Delta\theta)$ denote respectively the particular integrals associated with a unit transverse force $p = 1$, and a unit relative rotation $\Delta\theta = 1$, applied at $x = x_j$, all terms are available in a simple analytical form. In particular, the integrals $\mathbf{J}^{(p)}(x, x_j)$ for a point force $p = 1$ at $x = x_j$ are:

$$\begin{aligned}
J_\psi^{(p)}(x) &= 2^{-1}\sigma^{-3/2}\left[\sinh\left(\sqrt{\sigma}\,(x - x_j)\right) - \sin\left(\sqrt{\sigma}\,(x - x_j)\right)\right] H(x - x_j) \\
J_\vartheta^{(p)}(x) &= 2^{-1}\sigma^{-1}\left[\cosh\left(\sqrt{\sigma}\,(x - x_j)\right) - \cos\left(\sqrt{\sigma}\,(x - x_j)\right)\right] H(x - x_j) \\
J_\mu^{(p)}(x) &= -2^{-1}\sigma^{-1/2}\left[\sinh\left(\sqrt{\sigma}\,(x - x_j)\right) + \sin\left(\sqrt{\sigma}\,(x - x_j)\right)\right] H(x - x_j) \\
J_\chi^{(p)}(x) &= -2^{-1}\left[\cosh\left(\sqrt{\sigma}\,(x - x_j)\right) + \cos\left(\sqrt{\sigma}\,(x - x_j)\right)\right] H(x - x_j)
\end{aligned} \tag{2.17}$$

while the particular integrals $\mathbf{J}^{(\Delta\theta)}(x, x_j)$ for a relative rotation $\Delta\theta = 1$ at $x = x_j$ result to be:

$$\begin{aligned}
J_\psi^{(\Delta\theta)}(x) &= 2^{-1}\sigma^{-1/2}\left[\sinh\left(\sqrt{\sigma}\,(x - x_j)\right) + \sin\left(\sqrt{\sigma}\,(x - x_j)\right)\right] H(x - x_j) \\
J_\vartheta^{(\Delta\theta)}(x) &= 2^{-1}\left[\cosh\left(\sqrt{\sigma}\,(x - x_j)\right) + \cos\left(\sqrt{\sigma}\,(x - x_j)\right)\right] H(x - x_j) \\
J_\mu^{(\Delta\theta)}(x) &= -2^{-1}\sigma^{1/2}\left[\sinh\left(\sqrt{\sigma}\,(x - x_j)\right) - \sin\left(\sqrt{\sigma}\,(x - x_j)\right)\right] H(x - x_j) \\
J_\chi^{(\Delta\theta)}(x) &= -2^{-1}\sigma\left[\cosh\left(\sqrt{\sigma}\,(x - x_0)\right) - \cos\left(\sqrt{\sigma}\,(x - x_j)\right)\right] H(x - x_j)
\end{aligned} \tag{2.18}$$

Using Eq. (2.16) to express $\psi(x_j)$ and $\mu(x_j)$ on the r.h.s. of Eqs. (2.13) and

(2.14), it can be observed that the unit-step functions $H\left(x-x_j\right)$ involved in $\mathbf{J}\left(x,x_j\right)$ are not equal to zero only when computed at $x>x_j$. This makes it possible to cast vector $\mathbf{\Lambda}_1$ at the first damper location x_1, and vectors $\mathbf{\Lambda}_j$ at damper locations x_j, for $j=2...,N$, as follows:

$$\mathbf{\Lambda}_1=\mathbf{\Phi}_{\mathbf{\Omega}}\left(x_1\right)\mathbf{c} \tag{2.19}$$

$$\mathbf{\Lambda}_j=\mathbf{\Phi}_{\mathbf{\Omega}}\left(x_j\right)\mathbf{c}+\sum_{k=1}^{j-1}\mathbf{\Phi}_{\mathbf{J}}\left(x_j,x_k\right)\mathbf{\Lambda}_k \quad \text{for} \quad j=2,\ldots,N \tag{2.20}$$

where $\mathbf{\Phi}_{\mathbf{\Omega}}\left(x_j\right)$ is given by:

$$\mathbf{\Phi}_{\mathbf{\Omega}}\left(x_j\right)=\begin{bmatrix} -\kappa_{w,j}\left(\sigma\right)\left(\mathbf{\Omega}\left(x_j\right)\right)_1 \\ -\dfrac{\left(\mathbf{\Omega}\left(x_j\right)\right)_3}{\kappa_{\Delta\theta,j}\left(\sigma\right)} \end{bmatrix} \tag{2.21}$$

in which $\left(\mathbf{\Omega}\left(x_j\right)\right)_i$ are row vectors coinciding with the ith row of matrix $\mathbf{\Omega}\left(x\right)$. Further, $\mathbf{\Phi}_{\mathbf{J}}\left(x_j,x_k\right)$, for $k<j$, is the 4×2 matrix:

$$\mathbf{\Phi}_{\mathbf{J}}\left(x_j,x_k\right)=\begin{bmatrix} -\kappa_{w,j}\left(\sigma\right)\left(\mathbf{J}\left(x_j,x_k\right)\right)_1 \\ -\dfrac{\left(\mathbf{J}\left(x_j,x_k\right)\right)_3}{\kappa_{\Delta\theta,j}\left(\sigma\right)} \end{bmatrix} \tag{2.22}$$

where $\left(\mathbf{J}\left(x_j,x_k\right)\right)_i$ denotes the ith row of matrix $\mathbf{J}\left(x_j,x_k\right)$.

Eqs. (2.19 and 2.20) can be used to obtain $\mathbf{\Lambda}_j$ in terms of vector $\mathbf{c}$ only. Starting from Eq. (2.19) for $\mathbf{\Lambda}_1$, Eq. (2.20) allows to be expressed $\mathbf{\Lambda}_j$ in the following form:

$$\mathbf{\Lambda}_j=\mathbf{\Phi}_{\mathbf{\Omega}}\left(x_j\right)\mathbf{c}+$$

$$+\sum_{2\le q\le j}\ \sum_{(\underbrace{j,m,n,\ldots,r,s}_{N_q})\in N_q^{(j)}}\mathbf{\Phi}_{\mathbf{J}}\left(x_j,x_m\right)\mathbf{\Phi}_{\mathbf{J}}\left(x_m,x_n\right)\cdots\mathbf{\Phi}_{\mathbf{J}}\left(x_r,x_s\right)\mathbf{\Phi}_{\mathbf{\Omega}}\left(x_s\right)\mathbf{c} \tag{2.23}$$

where $N_q^{(j)} = \{(\underbrace{j,m,n,...r,s}_{q}) : j > m > n > ... > r > s; m,n,...r,s = 1,2,...,(j-1)\}$ is the set including all possible q-ples of indexes $(\underbrace{j,m,n,...r,s}_{q})$ such that $j > m > n > ... > r > s$ being $2 \leq q \leq j$. For instance, with $N = 4$ support/joint locations the following sets results to be:

Table 2.1: Sets of indexes $N_q^{(j)}$ for $N = 4$ support/joint locations

	$j=2$	$j=3$	$j=4$
$q=2$	$N_2^{(2)} = \{(2,1)\}$	$N_2^{(3)} = \{(3,1),(3,2)\}$	$N_2^{(4)} = \{(4,1),(4,2),(4,3)\}$
$q=3$	-	$N_3^{(3)} = \{(3,2,1)\}$	$N_3^{(4)} = \{(4,3,2),(4,3,1),(4,2,1)\}$
$q=4$	-	-	$N_4^{(4)} = \{(4,3,2,1)\}$

At this point substituting Eq. (2.23) into Eq. (2.15) it is possible to write the following general form of $\mathbf{Y}(x)$:

$$\mathbf{Y}(x) = \tilde{\mathbf{Y}}(x)\,\mathbf{c} \tag{2.24}$$

where $\tilde{\mathbf{Y}}(x)$ is given as:

$$\tilde{\mathbf{Y}}(x) = \mathbf{\Omega}(x) + \sum_{j=1}^{N} \mathbf{J}(x,x_j)\,\mathbf{\Phi_\Omega}(x_j) +$$

$$\sum_{j=2}^{N} \mathbf{J}(x,x_j) \sum_{2\leq q\leq j} \sum_{(\underbrace{j,m,n,...,r,s}_{q})\in N_q^{(j)}} \mathbf{\Phi_J}(x_j,x_m)\,\mathbf{\Phi_J}(x_m,x_n)\cdot\cdot\mathbf{\Phi_J}(x_r,x_s)\,\mathbf{\Phi_\Omega}(x_s) \tag{2.25}$$

As shown for the bare beam, the 4×1 vector of integration constants $\mathbf{c}$ in

Eq. (2.24) can be computed by enforcing the B.C. of the beam. This leads to four equations with the same general form written for the bare beam ($\mathbf{Bc} = \mathbf{0}$). Remarkably, matrix $\mathbf{B}$ will always be a 4×1 matrix, for any number of supports/joints along the beam. Terms in matrix $\mathbf{B}$ are given by the response variables $\mathbf{Y}(x)$ computed at $x = 0$, $x = 1$ and, therefore, can readily be obtained in a closed analytical form using Eqs. (2.24) and (2.25). The characteristic equation can be built as determinant of the 4×4 matrix $\mathbf{B}$, $(\det \mathbf{B} = 0)$, from which it is possible to find the dimensionless eigenvalue σ.

Upon deriving the non-trivial solution $\mathbf{c}$ from the characteristic equation, exact closed-form expressions can be built for the vector of eigenfunctions $\mathbf{Y}(x)$, using Eq. (2.24). Due to the fact that damping associated with supports/joints is in general not proportional, modes are expected to be complex. The same procedure is also valid for non-homogeneous B.C. due to end dampers. Modelling end dampers as internal dampers located at $x_1 = 0^+$ and $x_N = 1^-$, the B.C. can still be taken as homogeneous [49].
Changes to be made when a single translational support or rotational joint occur at a given abscissa x_j are straightforward. If no support occurs at $x = x_j$, $\kappa_{w,j}(\sigma) = 0$ shall be set at $x = x_j$. This will automatically set equal to zero the first row in matrices $\mathbf{\Phi_\Omega}(x_j)$, $\mathbf{\Phi_J}(x_j, x_k)$. Setting the reaction force $p_j = 0$ at $x = x_j$, the 1st column of matrix $\mathbf{\Phi_J}(x_m, x_j)$ shall be set equal to zero for all $x_m > x_j$. Obviously, if no joint occurs at $x = x_j$, $\kappa_{\Delta\theta,j}(\sigma) = \infty$ shall be set at $x = x_j$. As a result, the second row of matrices $\mathbf{\Phi_\Omega}(x_j)$, $\mathbf{\Phi_J}(x_j, x_k)$ will be equal to zero. Also, setting $\Delta\vartheta_j = 0$ at $x = x_j$, the 2nd column of matrix $\mathbf{\Phi_J}(x_m, x_j)$ shall be set equal to zero for all $x_m > x_j$.
At this stage, a few remarks are necessary to stress the advantages of the proposed approach. This procedure provides the exact eigenvalues, and the exact eigenfunctions of all response variables $\mathbf{Y}(x)$, in a closed form. Likewise, terms of the 4×4 matrix $\mathbf{B}$ can readily be computed in a closed form, for any number and positions of supports and joints, with no changes when their number and relative positions vary along the beam. These are significant advantages over the exact classical approach, which requires representing the free vibration response in every beam segment between two consecutive supports/joints in terms of four integration constants, totalling $4 \times (N + 1)$ constants for N support/joint locations. These integration constants have to be computed by a set of equations built by enforcing the B.C. and matching conditions between the responses over contiguous beam segments, to the left and right of any support/joint location. Through the use of this approach, the coefficient matrix associated with the set of equations has to be updated when-

ever the support/joint locations change along the axis, and its size increases with the number of supports/joints. Finally, it is noted that the proposed exact eigensolutions can serve as a benchmark for standard FE solutions with two-node beam elements. Advantages over the FE method are that, in a standard FE method, a mesh node must be inserted at the application point of any support or joint, and re-meshing may be required whenever they change position.

2.3.2 Orthogonality conditions

The derivation of the orthogonality conditions for the complex modes are now described. Firstly, Eq. (2.7) is written for $\psi_m(x)$ and multiplied by $\psi_n(x)$, using Eqs. (2.13) and (2.14) to express $\varphi_j(\sigma)$ and $\Delta\vartheta_j(\sigma)$ in terms of $\psi_m(x)$ and $\mu_m(x)$; likewise, Eq. (2.7) is written for $\psi_n(x)$ and multiplied by $\psi_m(x)$ using, in this case, Eqs. (2.13) and (2.14) for $\varphi_j(\sigma)$ and $\Delta\vartheta_j(\sigma)$ in terms of $\psi_n(x)$ and $\mu_n(x)$. Secondly, both equations are integrated by parts over the interval [0,1], taking into account the sampling property of Dirac's delta. The two equations are then used as follows: the first orthogonality condition is obtained by computing the difference between the two equations, while the second orthogonality condition is obtained by computing the difference between Eq. (2.7) in $\psi_m(x)$ multiplied by σ_n and Eq. (2.7) in $\psi_n(x)$ multiplied by σ_m. Therefore the two orthogonality conditions obtained read as:

$$\left(\sigma_m^2 - \sigma_n^2\right) \int_0^1 \psi_m \psi_n dx + \Delta_1(\sigma_m, \sigma_n) = 0 \tag{2.26}$$

$$(\sigma_m - \sigma_n) \int_0^1 \frac{d^2\psi_m}{dx^2} \frac{d^2\psi_n}{dx^2} dx + \sigma_m\sigma_n(\sigma_m - \sigma_n) \int_0^1 \psi_m \psi_n dx + \Delta_2(\sigma_m, \sigma_n) = 0 \tag{2.27}$$

where in Eq. (2.26)

$$\begin{aligned} \Delta_1(\sigma_m, \sigma_n) = \sum_{j=1}^{N} \{ &\left[\kappa_{w,j}(\sigma_n) - \kappa_{w,j}(\sigma_m)\right] \psi_m(x_j) \psi_n(x_j) + \\ &+ \left[\left(\kappa_{\Delta\theta,j}(\sigma_m)\right)^{-1} - \left(\kappa_{\Delta\theta,j}(\sigma_n)\right)^{-1}\right] \mu_m(x_j) \mu_n(x_j) \} \end{aligned} \tag{2.28}$$

while in Eq. (2.27)

$$\Delta_2(\sigma_m,\sigma_n)=\sum_{j=1}^{N}\Big\{\left[\sigma_m\kappa_{w,j}(\sigma_n)-\sigma_n\kappa_{w,j}(\sigma_m)\right]\psi_m(x_j)\,\psi_n(x_j)+$$
$$+\left[\sigma_n\left(\kappa_{\Delta\theta,j}(\sigma_m)\right)^{-1}-\sigma_m\left(\kappa_{\Delta\theta,j}(\sigma_n)\right)^{-1}\right] \tag{2.29}$$
$$\mu_m(x_j)\,\mu_n(x_j)+(\sigma_m-\sigma_n)\,\Gamma_j(\sigma_m,\sigma_n)\Big\}$$

where

$$\Gamma_j(\sigma_m,\sigma_n)=\left(\kappa_{\Delta\theta,j}(\sigma_m)\right)^{-1}\left(\kappa_{\Delta\theta,j}(\sigma_n)\right)^{-1}\mu_m(x_j) \tag{2.30}$$
$$\int_0^1\mu_n(x_j)\,\delta(x-x_j)\,\delta(x-x_j)\,dx$$

2.4 Beam response to moving loads

The complex modes, built as explained in section 2.3 serve as a basis to build the beam response to the moving load. The procedure and the formulation are the same as those described in section 1.4 concerning the continuous Euler-Bernoulli beam under moving load. The only difference is that in the case of discontinuous beams, the eigenfunctions include the contribution of supports and joints. Consequently

$$\Xi_k=2\int_0^1\psi_k^2(x)\,dx-\left\{\sum_{j=1}^{N}\frac{\mathrm{i}c_{w,j}}{\sigma_k}\psi_k^2(x_j)+\frac{\mathrm{i}c_{\Delta\theta,j}}{\sigma_k}\left[\frac{\mu_k(x_j)}{\kappa_{\Delta\theta,j}(\sigma_k)}\right]^2\right\} \tag{2.31}$$

Note that the B.C. of the beam are inherently fulfilled by the deflection eigenfunctions $\psi_k(x)$. Therefore, this method can be applied for any B.C.

In practical applications, a few M modes in the modal superposition will be sufficient to accurately represent the response and, upon summing up the contributions of complex-conjugate eigenfunction pairs, the beam deflection can be rewritten in the following real form [50, 51]:

$$w(x,\tau) \approx \mathrm{Re}\left[\sum_{k=1}^{M} \psi_k(x) \int_0^{\tau} e^{\mathrm{i}\sigma_k(\tau-\tau')} g_k(\tau')\, d\tau'\right] \tag{2.32}$$

Recognise that equations analogous to Eq. (2.32) may be written for the other response variables, i.e. rotation, bending moment and shear force, using pertinent eigenfunctions from Eq. (2.24). At this stage, a few remarks, in order to highlight some advantages of the proposed solution, are necessary. The first is that closed-form expressions can be derived for the convolution integral

$$\int_0^{\tau} e^{\mathrm{i}\sigma_k(\tau-\tau')} g_k(\tau')\, d\tau' \tag{2.33}$$

In light of Eq. (1.20) for $g_k(\tau')$, Eq. (2.24) for the kth eigenfunction $\psi_k(x)$, and Eqs. (2.17) and (2.18) for $\mathbf{J}(x, x_j)$, it may be seen that the integral Eq. (2.33) can be reverted as the sum of individual integrals with the general form:

$$\int_0^{\tau} \lambda(\tau')\, H(v_0\tau' - x_j)\, d\tau' \tag{2.34}$$

where $\lambda(\tau')$ is given by the product of the exponential function $e^{\mathrm{i}\sigma_k(\tau-\tau')}$ and trigonometric/hyperbolic functions:

$$\lambda(\tau') = e^{\mathrm{i}\sigma_k(\tau-\tau')} \quad 2^{-1}\sigma^{-3/2}\left[\sinh\left(\sqrt{\sigma}\left(v_0\tau' - x_j\right)\right) - \sin\left(\sqrt{\sigma}\left(v_0\tau' - x_j\right)\right)\right] \tag{2.35}$$

Using the theory of generalised functions [49], the integral (2.34) can be computed as:

$$\begin{aligned}\int_0^{\tau} \lambda(\tau')\, H(v_0\tau' - x_j)\, d\tau' &= \left\{H(\zeta - x_j)\left[\lambda^{[1]}\left(\zeta v_0^{-1}\right) - \lambda^{[1]}\left(x_j v_0^{-1}\right)\right]\right\}_0^{v_0\tau} = \\ &= H(v_0\tau - x_j)\left[\lambda^{[1]}(\tau) - \lambda^{[1]}\left(x_j v_0^{-1}\right)\right]\end{aligned} \tag{2.36}$$

where $\lambda^{[1]}(\cdot)$ denotes the first-order primitive function of $\lambda(\cdot)$. Note that, for functions $\lambda(\tau')$ given as the product of the exponential function $e^{\mathrm{i}\sigma_k(\tau-\tau')}$ and trigonometric or hyperbolic functions, the first-order primitive $\lambda^{[1]}(\cdot)$ can be obtained in a closed form by any symbolic package [52].

Secondly, it is worth remarking that Eq. (2.32) involves the exact modes of the beam and it is derived based on appropriate orthogonality conditions. The exact complex modes reflect the actual amount of damping introduced in the system by the viscoelastic supports and joints. No simplifying assumptions are made on such damping, unlike the alternative modal superposition approaches where proportional damping is assumed in order to use classical orthogonality conditions of undamped modes [9–11, 13].

2.5 Numerical Applications

Two numerical applications are presented in which free vibration solutions and dynamic response to moving loads, as obtained by the proposed method, are compared respectively to exact free vibration solutions built by the exact classical procedure and dynamic response built by the ADINA FE code [53], with time-dependent nodal forces modelled as explained in ref.[25].

2.5.1 Example A

Consider the four-span beam in Fig.2.2. Kelvin-Voigt viscoelastic translational supports and rotational joints occur at $x_1 = 1/4$, $x_2 = 1/2$ and $x_3 = 3/4$, while the two ends are assumed to be simply supported. The following dimensionless parameters are assumed: $k_{w,1} = k_{w,2} = k_{w,3} = 10^2$ and $c_{w,1} = c_{w,2} = c_{w,3} = 10^{-1}$; $k_{\Delta\theta,1} = k_{\Delta\theta,2} = k_{\Delta\theta,3} = 10$ and $c_{\Delta\theta,1} = c_{\Delta\theta,2} = c_{\Delta\theta,3} = 10^{-1}$.

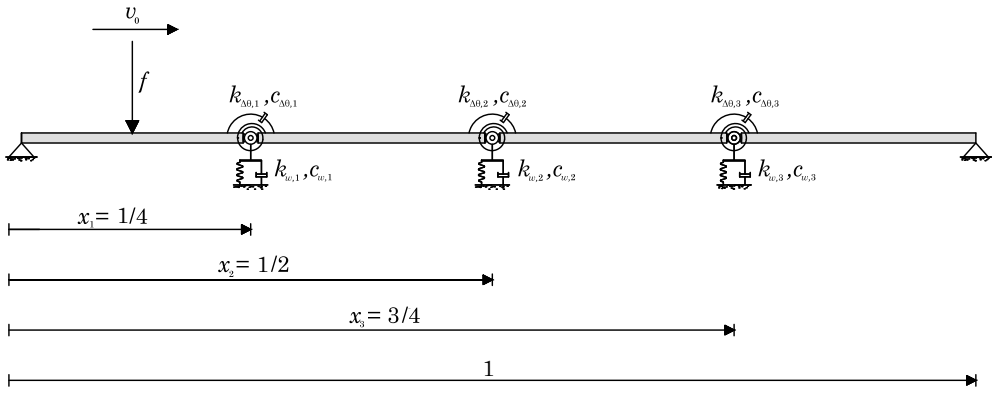

Figure 2.2: Simply-supported three-span beam with Kelvin-Voigt viscoelastic supports and joints.

Table 2.2 reports the dimensionless eigenvalues of the first three modes, as built by the proposed method, and the classical method, i.e. representing the free-vibration response in a trigonometric/hyperbolic form with four integration constants over each segment between two consecutive damper locations, and enforcing matching conditions at the subdivision points along with the B.C. Both methods provide the exact eigenvalues. However, using the proposed method the characteristic equation is given as determinant of a 4×4 matrix, with terms of matrix $\mathbf{B}$ given by analytical expressions Eq.(2.24). In contrast, the characteristic equation built by the classical exact procedure is given as determinant of a 16×16 matrix. Table 2.2 shows that the eigenvalues obtained by the two methods coincide up to the fourth decimal place (in this case, Newton's method is used to solve the characteristic equations). It can be observed that damping effects on the individual modes are not the same.

Table 2.2: Eigenvalues of beam in Fig.2.2 by exact proposed method (PM) and classical method (CM).

Mode	Eigenvalues (PM)	Eigenvalues (CM)	Damping ratio
1	$\pm$ 21.90371$+i$ 0.26292	$\pm$ 21.90370$+i$ 0.26292	0.0120
2	$\pm$ 39.89872$+i$ 1.54879	$\pm$ 39.89871$+i$ 1.54875	0.0388
3	$\pm$ 81.82443$+i$ 6.54101	$\pm$ 81.82442$+i$ 6.54108	0.0796

The eigenfunctions of mode 1 are shown in Fig.2.3, for all response variables (complex-conjugate eigenfunctions are not reported for conciseness). As observed, the rotational dampers induce a jump discontinuity at mode 1 rotation while the shear force is discontinuous at the translational supports.

Next, the dynamic response to a moving force $f = 1$ is investigated. Fig.2.4 shows the mid-span deflection of the beam for various velocities of the moving force, as computed by Eq. (2.32) with M=3 modes and the FE method in ADINA, with 4 and 16 elements. A very satisfactory agreement is encountered between the two solutions, when 16 elements are considered. No significant changes are found when considering $M > 3$ modes in the proposed solution and more than 16 elements in the FE solution and, for this reason, pertinent results are omitted.

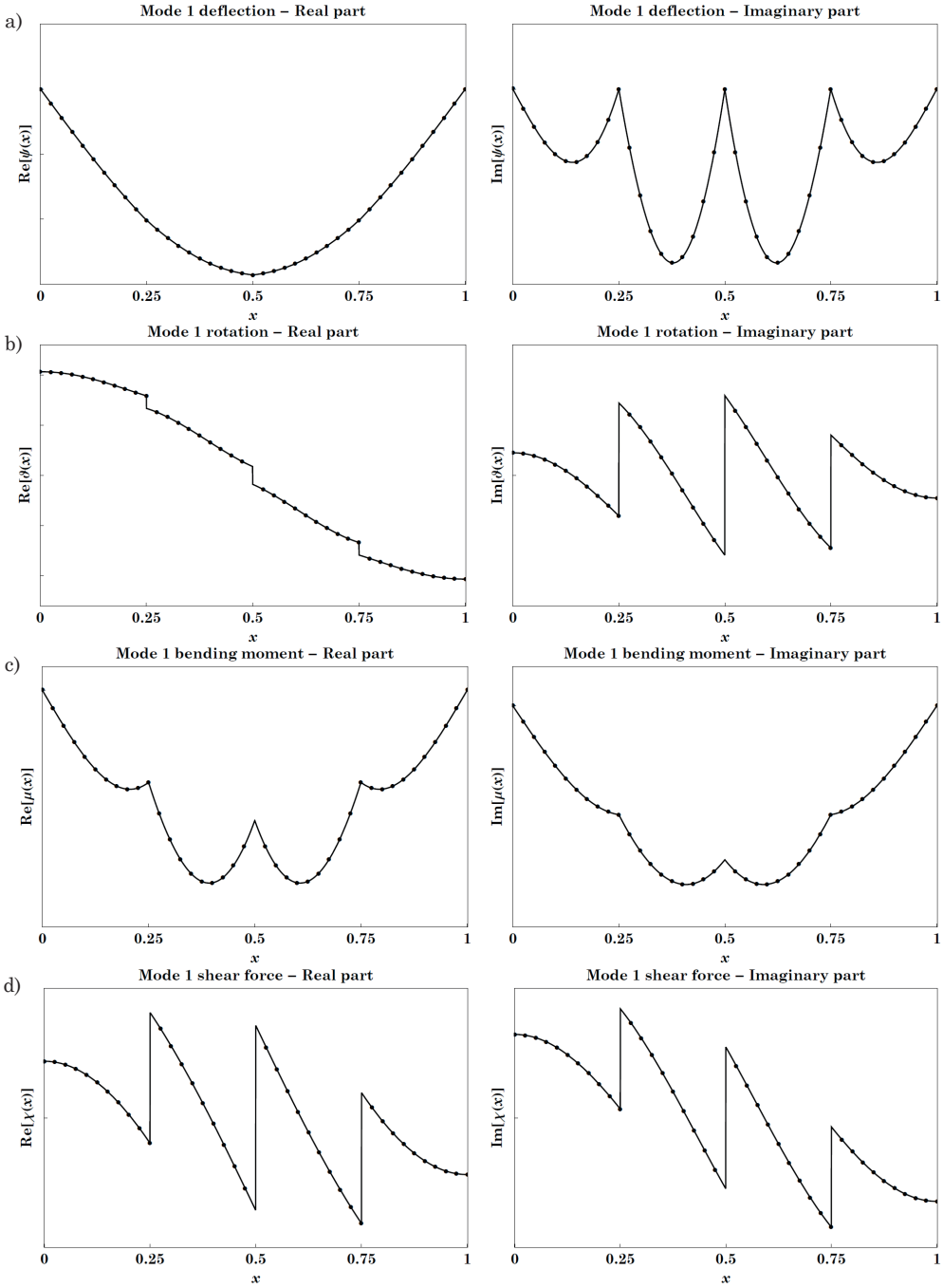

Figure 2.3: Mode 1 eigenfunctions of beam in Fig.2.2: (a) deflection; (b) rotation; (c) bending moment; (d) shear force. Left column: real part. Right column: imaginary part. Exact proposed solution (black line); exact classical solution (black circle).

Figure 2.5 shows the mid-span deflection, as computed by Eq. (2.32) with $M = 1$, $M = 2$ and $M = 3$ modes, and FE method with 16 elements. It is evident that contributions of various modes change depending on the velocity and that, in general, one mode is not sufficient to describe the mid-span deflection with due accuracy.

Figure 2.6 shows the beam deflection over the whole axis at certain time instants, for two load velocities, as computed by Eq. (2.32) with $M = 3$ modes and FE method with 16 elements. With previous results at the mid-span shown in Figs.2.4-2.6, the agreement between the two solutions is very satisfactory over the whole beam axis.

A final remark is that all proposed solutions rely on closed-form analytical expressions of Eq. (2.32), while the FE solution in ADINA requires numerical integration, with a considerable computational effort.

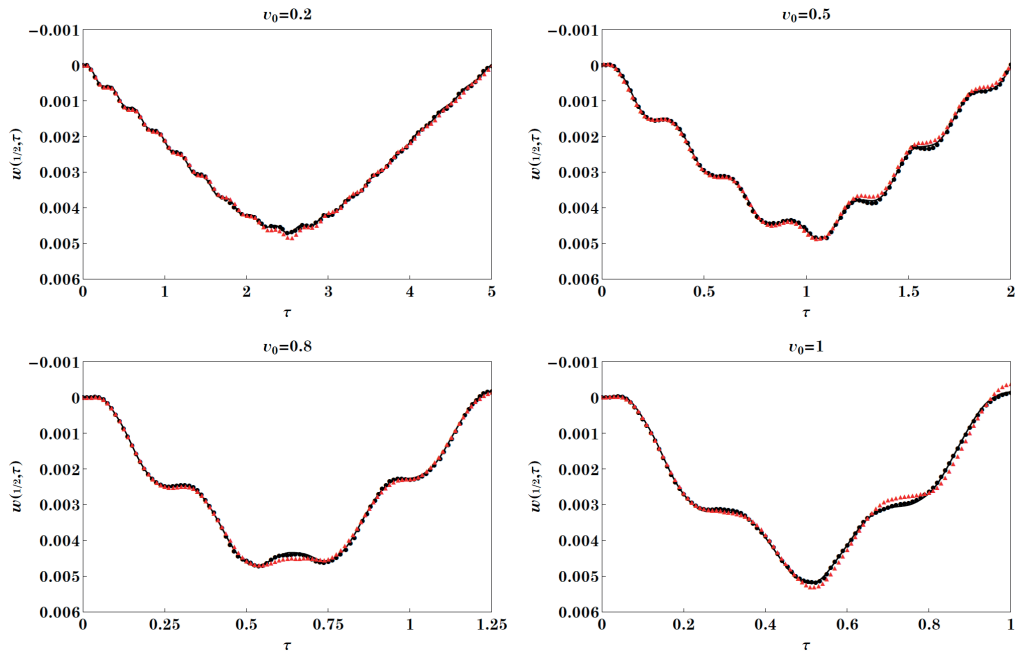

Figure 2.4: Mid-span deflection of beam in Fig.2.2 under a moving force with different velocities v_0: proposed solution with $M = 3$ modes (black line); FE solution with 4 (red triangle) and 16 (black circle) elements.

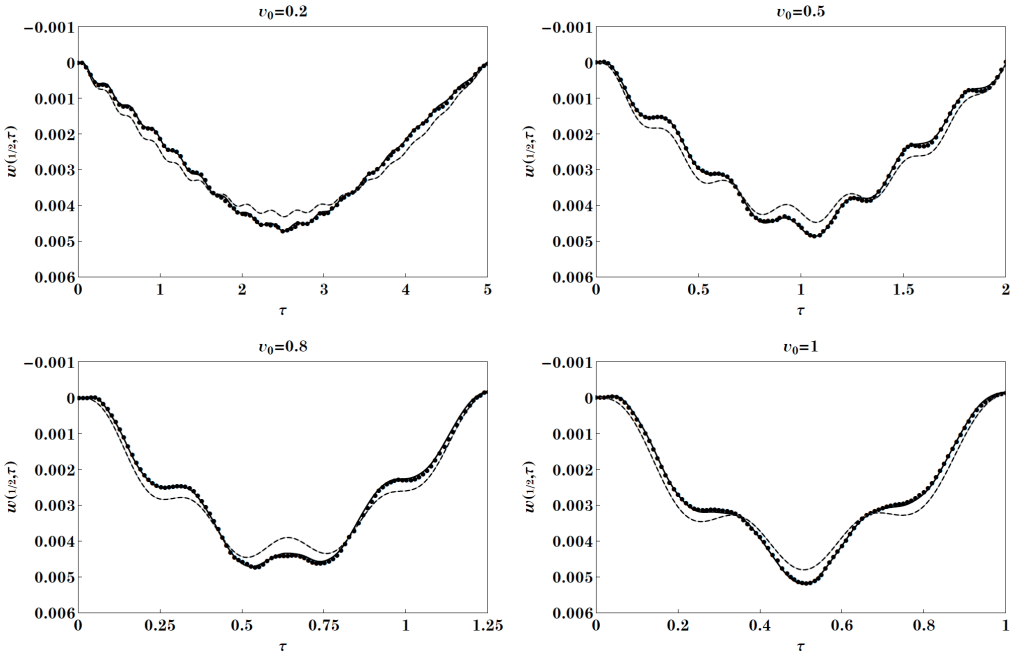

Figure 2.5: Mid-span deflection of beam in Fig.2.2 under a moving force with different velocities v_0: proposed solution with $M = 1$ (gray line), $M = 2$ (dashed line) and $M = 3$ (black line) modes; FE solution with 16 elements (black circle).

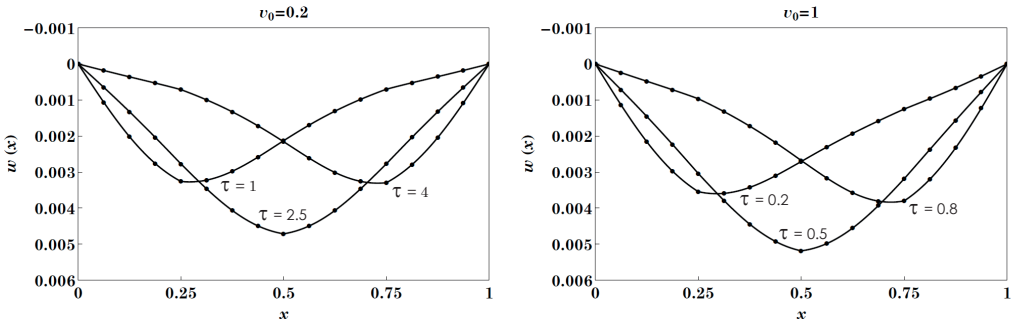

Figure 2.6: Deflection profile of beam in Fig.2.2 at different time instants, under a moving force with different velocities v_0: proposed solution with $M = 3$ modes (black line); FE solution with 16 elements (black circle).

2.5.2 Example B

Consider the three-span beam in Fig.2.7. Two viscoelastic translational supports are located at $x = 1/4$ and $x = 3/4$, while two viscoelastic rotational dampers are applied at the beam ends. Examples of end rotational dampers may be found in ref.[14, 51, 54].

The proposed method is implemented assuming clamped-clamped B.C. and considering the end rotational dampers as internal dampers at x $=0^+$ and x $=1^-$, totalling four damper locations: x $=0^+$, $x_2 = 1/4$, $x_3 = 3/4$ and x$_4$=1^-. The corresponding sets $N_q^{(j)}$, for $j = 1, 2, 3, 4$, to be considered in Eq. (2.25), are given in Table 2.3. Dimensionless parameters are selected as follows: $k_{w,2} = k_{w,3} = 10^2$, $c_{w,2} = c_{w,3} = 10^{-1}$ for the translational supports; $k_{\Delta\theta,1} = k_{\Delta\theta,4} = 10$ and $c_{\Delta\theta,1} = c_{\Delta\theta,4} = 10^{-1}$ for the rotational dampers. Numerical values for x $=0^+$ and x$_4$=1^- are as follows: $x_1 = \varepsilon$ and $x_4 = 1 - \varepsilon$, with $\varepsilon = 10^{-10}$.

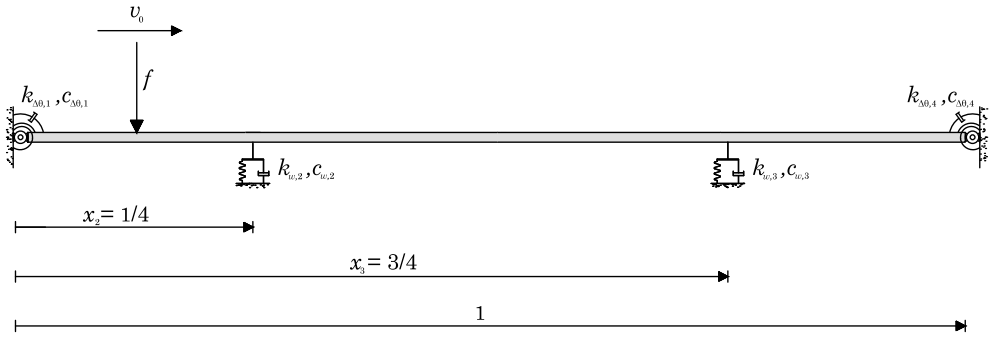

Figure 2.7: Three-span beam with Kelvin-Voigt viscoelastic supports and end dampers.

The exact eigenvalues, as obtained from the proposed procedure and the classical method, are listed in Table 2.3. Again, an excellent agreement is found. As in the previous case, however, recognize that the characteristic equation is built as determinant of a 4×4 matrix using the proposed approach, and a 12×12 matrix using the classical one.

Table 2.3: Eigenvalues of beam in Fig.2.7 by exact proposed method (PM) and classical method (CM).

Mode	Eigenvalues (PM)	Eigenvalues (CM)	Damping ratio
1	$\pm$ 21.68703$+i$ 0.52471	$\pm$ 21.68701$+i$ 0.52470	0.0242
2	$\pm$ 54.45782$+i$ 2.92061	$\pm$ 54.45783$+i$ 2.92060	0.0536
3	$\pm$ 105.16203$+i$ 7.60262	$\pm$ 105.16201$+i$ 7.60263	0.0723

The eigenfunctions of mode 1 are shown in Fig.2.8, for all response variables (complex-conjugate eigenfunctions are not reported for conciseness). There is a non-zero rotation at the end rotational dampers, and the shear force is discontinuous at the translational supports. The same consideration holds for the eigenfunctions of the all other modes. Figure 2.9 through Fig.2.11 show the dynamic response to a moving force $f = 1$, as computed by the proposed method using Eq. (2.32), and ADINA FE code [53]. In particular, Fig.2.9 shows that the two solutions for the mid-span deflection agree very well when $M = 3$ modes are used in Eq. (2.32) and 16 elements are considered in the FE solution (for various velocities of the moving force). Again, it should be emphasised that no significant changes are found when $M > 3$ modes are used in Eq. (2.32) and more than 16 elements in the FE solution. Figure 2.10 shows that M=3 modes are needed in Eq. (2.32) to accurately describe the mid-span deflection. Finally, Fig.2.11 demonstrates that the agreement between proposed solution with $M = 3$ modes and FE solution with 16 elements is very satisfactory over the whole axis, at given time instants for two load velocities. As in the previous case, closed-form analytical expressions (2.32) prove computationally more efficient than numerical integration required by ADINA.

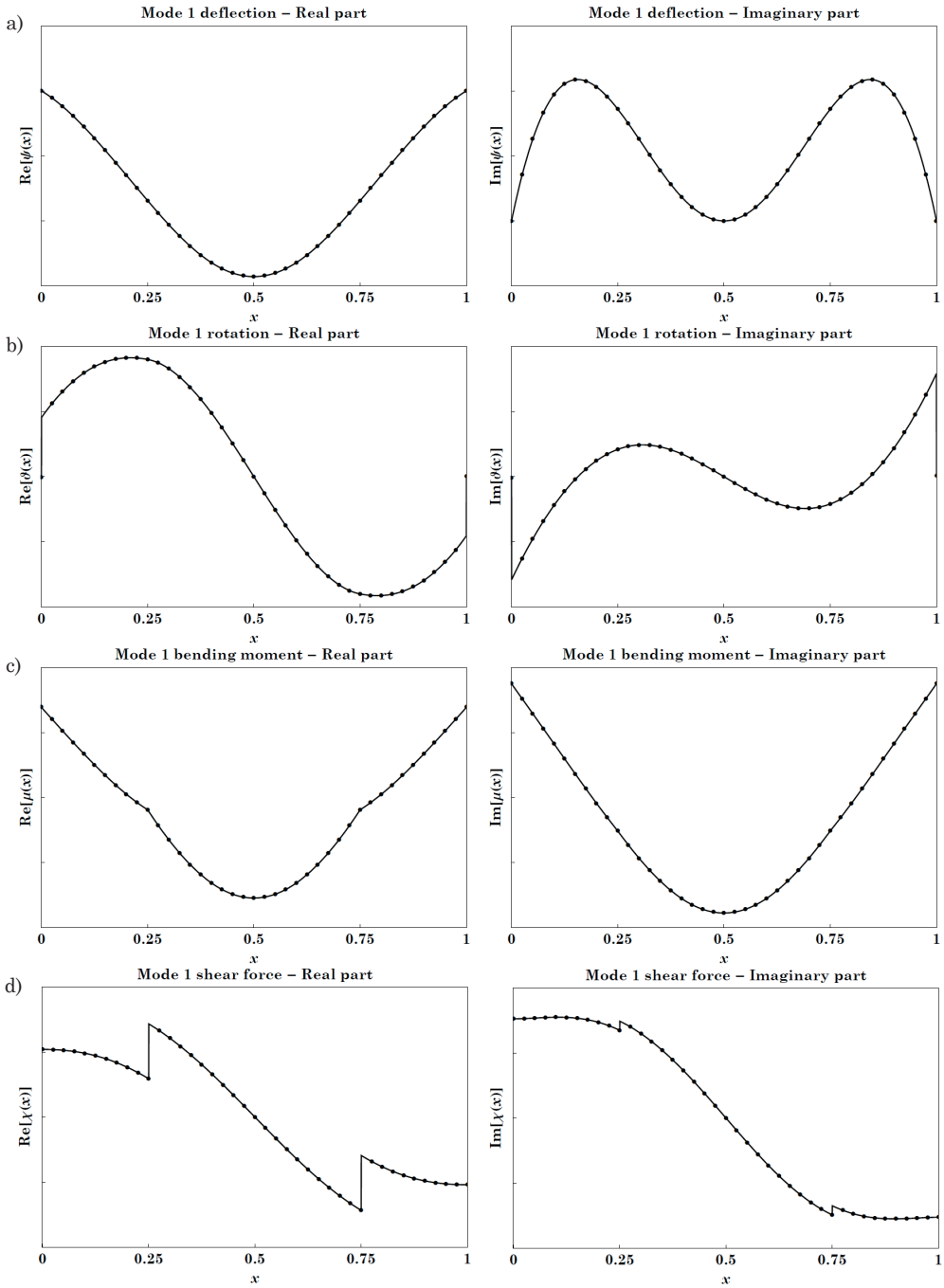

Figure 2.8: Mode 1 eigenfunctions of beam in Fig.2.7: (a) deflection; (b) rotation; (c) bending moment; (d) shear force. Left column: real part. Right column: imaginary part. Exact proposed solution (black line); exact classical solution (black circle).

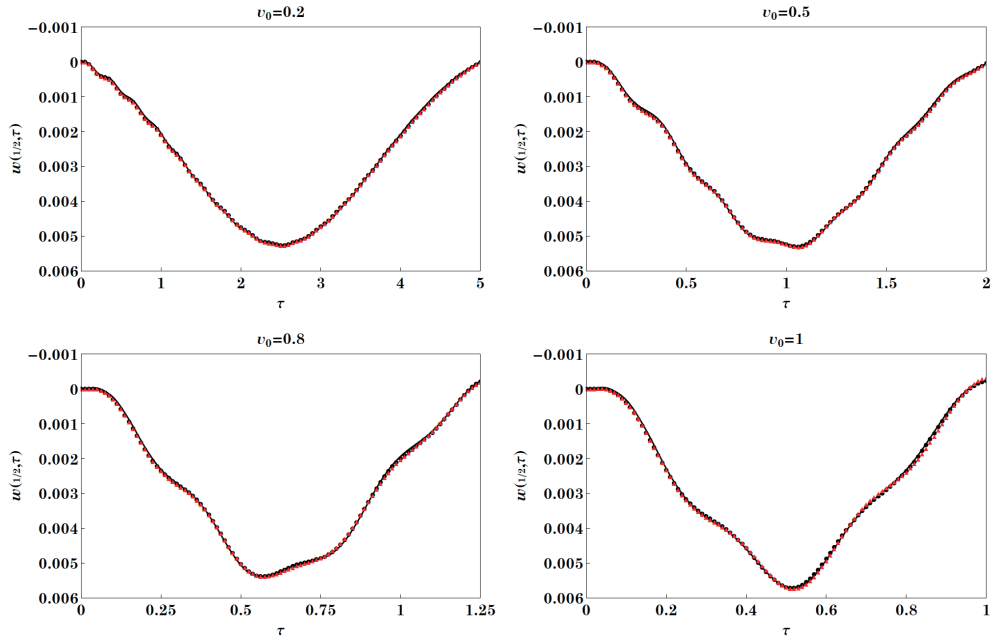

Figure 2.9: Mid-span deflection of beam in Fig.2.7 under a moving force with different velocities v_0: proposed solution with $M = 3$ modes (black line); FE solution with 4 (red triangle) and 16 (black circle) elements.

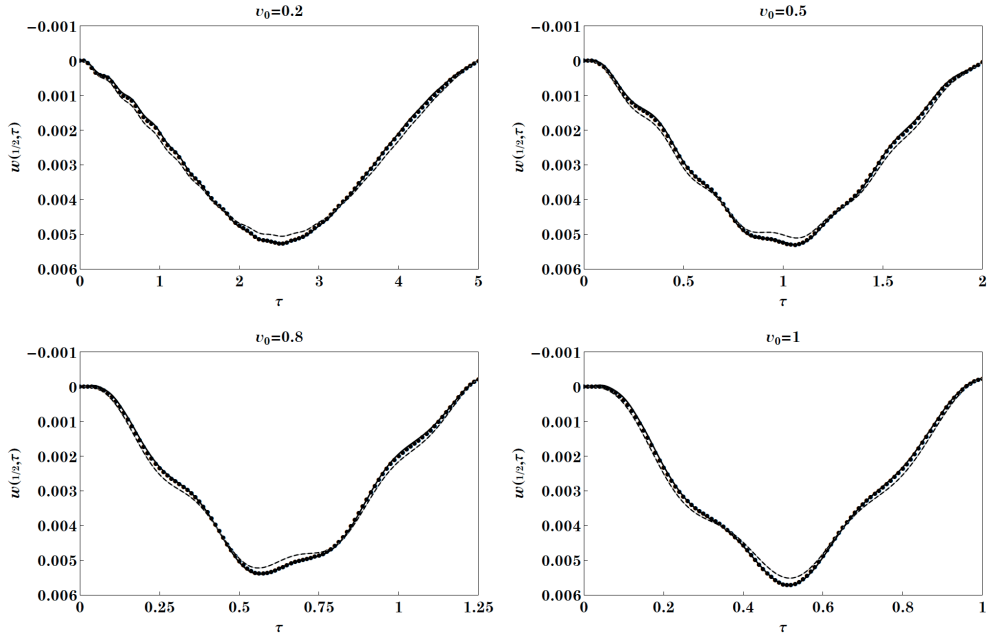

Figure 2.10: Mid-span deflection of beam in Fig.2.7 under a moving force with different velocities v_0: proposed solution with $M = 1$ (gray line), M=2 (dashed line) and $M = 3$ (black line) modes; FE solution with 16 elements (black circle).

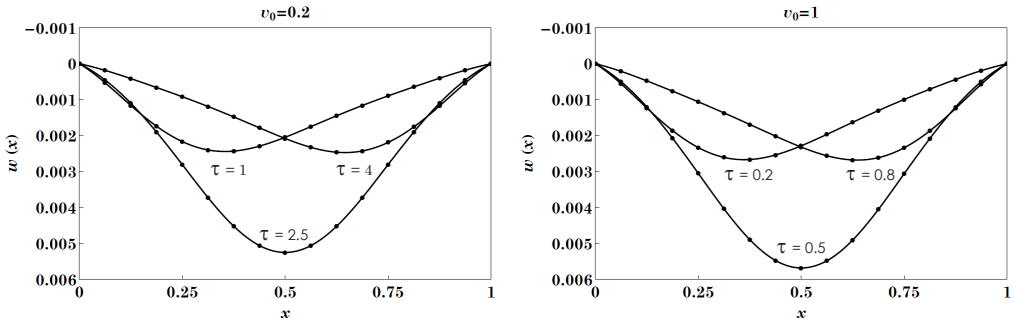

Figure 2.11: Deflection profile of beam in Fig.2.7 at different time instants, under a moving force with different velocities v_0: proposed solution with $M = 3$ modes (black line); FE solution with 16 elements (black circle).

2.6 Concluding remarks

A method has been presented to analyse the vibration response under moving loads of beams with Kelvin-Voigt viscoelastic translational supports and rotational joints. The method relies on exact complex modes and pertinent orthogonality conditions to express all response variables by appropriate time-domain convolution integrals, which can be reverted to closed-form analytical expressions using simple integration rules of generalised functions. No numerical integration is required. This allows considerable computational advantages over standard numerical solutions built by FE method. The method accounts for non-proportional damping due to supports and joints, since exact complex modes with pertinent orthogonality conditions are used, with a significant benefit with respect to alternative modal superposition methods where proportional damping is assumed or no damping is considered.

Chapter 3

Extension of the proposed approach to the moving load problem in discontinuous Euler-Bernoulli beams with tuned mass dampers

In this chapter the original and efficient approach to the moving load problem on Euler-Bernoulli beams, with Kelvin-Voigt viscoelastic translational supports and rotational joints, proposed in chapter 2, is generalised to be applied if such beams are equipped with Kelvin-Voigt viscoelastic tuned mass dampers (TMDs). The proposed solution holds for any number of TMDs and along-axis supports/joints. To show its applicability, accuracy and efficiency, a numerical application concerning a beam with multiple supports/joints is considered, subjected to a moving concentrated force and a series of concentrated forces, respectively. In two different configurations, the beam is equipped with one TMD and three TMDs, respectively.

3.1 Preliminary remarks

A beam crossed by a single load or a sequence of loads travelling with critical speed may be excited to a state of resonance. An effective way to reduce

the moving load induced vibration amplitudes is the application of TMDs [55–64]. In a pioneering work, Chen and Chen [65] discussed the appropriate design of TMDs for vibration control of Timoshenko beams subjected to constant and harmonic moving loads, as well as critical speed and structural resonance. Solutions were built by the modal superposition method for uniform beams with TMDs, but no external supports or internal joints were considered. Further studies on the application of TMDs for beam vibration control under moving loads were carried out in ref.[66], where the effectiveness of one versus multiple TMDs was investigated, and in ref.[67], where the uncertainty in dynamic excitation for robust design optimisation of TMDs was discussed. This chapter introduces a novel modal superposition approach to the moving-load problem in Euler-Bernoulli beams with TMDs, translational supports and rotational joints, all featuring a Kelvin-Voigt viscoelastic behaviour. This work has been published by myself and professors Adam, Failla and Pirrotta in the International journal "Meccanica" [68]. The approach uses the generalised functions theory [29–31, 34–37, 39, 40] to derive exact complex modes with pertinent orthogonality conditions, and closed-form expressions for all response variables. Specifically, analytical solutions will be built under loads with constant velocity, for any number of TMDs, supports, and joints. After describing the beams under study in Section 3.2, Section 3.3 will present exact modes and orthogonality conditions. Analytical solutions for the moving-loads problem will be presented in Section 3.4. Numerical applications will be discussed in Section 3.5.

3.2 Equation of motion for discontinuous beam equipped with Kelvin-Voigt viscoelastic tuned mass dampers under moving loads

The Euler-Bernoulli beam in Fig.3.1 carries an arbitrary number N of viscoelastic TMDs, translational supports and rotational joints at abscissas X_j. Kelvin-Voigt viscoelastic behaviour is assumed, in agreement with previous studies [44–48]. Spring stiffness and damping coefficients for the jth TMD are respectively $K_{TMD,j}$, $C_{TMD,j}$, with $M_{TMD,j}$ mass of the jth TMD. Equations will be presented to satisfy the most general case of TMDs, supports and joints occurring simultaneously at the same location. Under this assumption, the theory of generalised functions leads to the following equation of motion of the beam subjected to series of NL concentrated loads F_{ii} ($ii = 1, ..., NL$), with

constant velocity V_0 [1, 7]:

$$EI\frac{\bar{\partial}^4 W(X,t)}{\partial X^4} + m_L\frac{\partial^2 W(X,t)}{\partial t^2} + R(X,t) = \\ = \sum_{ii=1}^{NL} F_{ii}\delta(x - V_0 t + S_{ii})\left[H\left(t - t_{ii}^0\right) - H\left(t - t_{ii}^E\right)\right] \tag{3.1}$$

where Heaviside function H indicates the arrival and the departure of F_{ii} at time instants $t_{ii}^0 = S_{ii}/V_0$ and $t_{ii}^E = (S_{ii} + L)/V_0$ respectively, depending on the constant speed V_0 and the initial location S_{ii} of F_{ii}.

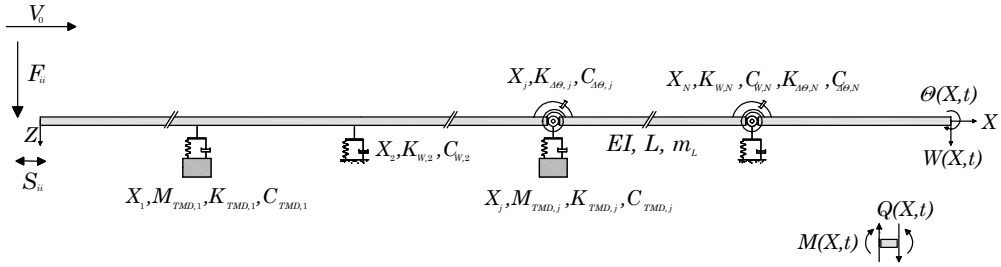

Figure 3.1: Euler-Bernoulli beam with TMDs, translational supports and rotational joints under moving load with constant velocity V_0.

Because of the discontinuities at support/joints locations, the fourth order derivative in Eq. (3.1) is a generalised derivative, as denoted by the over-bar. Further, $R(X,t)$ is a generalised function given as (2.2). However in this case $P_j(t)$ includes the reaction force of the jth TMD as well as that of the j-th support. In a non-dimensional form, Eq. (3.1) reverts to:

$$\frac{\bar{\partial}^4 w(x,\tau)}{\partial x^4} + \frac{\partial^2 w(x,\tau)}{\partial \tau^2} + r(x,\tau) = \\ = \sum_{ii=1}^{NL} f_{ii}\delta(x - v_0\,\tau + s_{ii})\left[H\left(\tau - \tau_{ii}^0\right) - H\left(\tau - \tau_{ii}^E\right)\right] \tag{3.2}$$

where $s_{ii} = S_{ii}/L$, $f_{ii} = F_{ii}L^2/EI$, $\tau_{ii}^0 = t_{ii}^0/T$ and $\tau_{ii}^E = t_{ii}^E/T$. For the jth TMD: $k_{TMD,j} = K_{TMD,j}L^3/EI$, $c_{TMD,j} = C_{TMD,j}L/\sqrt{m_L EI}$ and $m_{TMD,j} = M_{TMD,j}/m_L L$.

The solution of Eq. (3.2) will be obtained based on the complex mode superposition principle.

3.3 Beam complex modes

In this section the free vibration problem of the beam shown in Fig.3.1 is discussed.

3.3.1 Eigenvalue problem

The free vibration equation of the beam in Fig.3.1 is solved using Eq. (2.7) and Eq. (2.8), where $\varphi_j(\sigma)$ includes the reactions of the jth TMD and jth support:

$$\varphi_j(\sigma) = -\kappa_{T,j}(\sigma)\,\psi(x_j) \tag{3.3}$$

$$\kappa_{T,j}(\sigma) = \kappa_{TMD,j}(\sigma) + \kappa_{w,j}(\sigma) \tag{3.4}$$

with:

$$\kappa_{TMD,j}(\sigma) = \frac{\left(k_{TMD,j} + \mathrm{i}\sigma\, c_{TMD,j}\right) M_{TMD,j}\sigma^2}{M_{TMD,j}\sigma^2 - \left(k_{TMD,j} + \mathrm{i}\sigma\, c_{TMD,j}\right)} \quad \kappa_{w,j}(\sigma) = k_{w,j} + \mathrm{i}\sigma\, c_{w,j} \tag{3.5}$$

Eq. (3.5) shows that a TMD can be treated as a grounded damper, i.e. its reaction force depends on the deflection of the attachment point only through a frequency-dependent term involving stiffness, damping and mass [36,43]. Also, note that an attached lumped mass can be modelled by assuming that $k_{TMD,j} = \infty$ in Eq. (3.5). At this point, following the same procedure described in Chapter 2 for a discontinuous beam without TMDs, it is possible to find the exact closed-form expressions for the eigenfunctions responses of a discontinuous beam equipped with an arbitrary numbers of TMDs, using the same equations and solutions reported before by only adding the contribution of the TMDs in the stiffness $\kappa_{T,j}(\sigma)$. Since, in general, damping associated with TMDs/supports/joints is not proportional, complex modes are expected [50].

If no TMD and no support is attached at $x = x_j$, $\kappa_{T,j}(\sigma) = 0$ at $x = x_j$. This will set the first row in matrices $\mathbf{\Phi_\Omega}(x_j)$ and $\mathbf{\Phi_J}(x_j, x_k)$ equal to zero. Accordingly, the first column of matrix $\mathbf{\Phi_J}(x_m, x_j)$ shall be set equal to zero for all values $x_m > x_j$, due to the reaction $p_j = 0$ at $x = x_j$. Naturally the same

considerations made for the rotational joints reported in the chapter 1 are also valid for this case.

Terms of the 4×4 matrix $\mathbf{B}$ can readily be computed in a closed form, for any number and positions of TMDs, supports and joints, with no changes when their number and relative positions vary along the beam. These are significant advantages over the exact classical approach, which requires to be represented in terms of four integration constants. The vibration response in each beam segment between two consecutive application points of TMDs-supports-joints (totalling $2 \times (N+1)$ constants for N application points) is computed by enforcing the B.C. and matching conditions between the responses over continuous beam segments. By using this approach, the coefficient matrix associated with the equations to be solved is updated whenever positions of TMDs, supports and joints change, and its size inevitably increases with the number of TMDs, supports, joints.

Advantages over a FE method are also that a mesh node shall be inserted at the application point of any TMD, support or joint, and re-meshing may be required whenever they change position.

3.4 Beam response to moving loads

Generalising the approach devised in chapter 2, and using the same orthogonality conditions as in Eqs. (2.26) and (2.27), the response to the moving loads in Eq. (3.2) can be represented in terms of complex modes in the form:

$$w(x,\tau) = \sum_{ii=1}^{NL} f_{ii} \sum_{k=1}^{\infty} \psi_k(x) \begin{bmatrix} \int_{\tau_{ii}^0}^{\tau} e^{i\sigma_k(\tau-\tau')} g_{k,ii}(\tau')\, d\tau' - \\ \\ \int_{\tau_{ii}^E}^{\tau} e^{i\sigma_k(\tau-\tau')} g_{k,ii}(\tau')\, d\tau' \end{bmatrix} \tag{3.6}$$

where $\psi_k(x)$ is the kth deflection eigenfunction, and $g_{k,ii}(\cdot)$ is given as

$$g_{k,ii}(\tau) = (i\sigma_k \Xi_k)^{-1} \eta_{k,ii}(\tau) \tag{3.7}$$

In Eq. (3.7), $\eta_{k,ii}(\tau)$ depends on the moving loads,

$$\eta_{k,ii}(\tau) = \int_0^1 \psi_k(x)\, \delta(x - v_0\, \tau + s_{ii})\, dx \tag{3.8}$$

while term Ξ_k involves the parameters of TMDs, as well as those of the supports and joints according to

$$\Pi_k = \sum_{j=1}^{N} \left\{ \begin{array}{l} \dfrac{\mathrm{i}c_{w,j}}{\sigma_k}\psi_k^2\left(x_j\right) + \dfrac{\mathrm{i}c_{\Delta\theta,j}}{\sigma_k}\left[\dfrac{\mu_k\left(x_j\right)}{\kappa_{\Delta\theta,j}\left(\sigma_k\right)}\right]^2 - \\ \dfrac{m_{TMD,j}\left[2\left(k_{TMD,j}+\mathrm{i}\sigma_k c_{TMD,j}\right)^2 - \mathrm{i}\sigma_k^3 m_{TMD,j}c_{TMD,j}\right]}{\left[\left(k_{TMD,j}+\mathrm{i}\sigma_k c_{TMD,j}\right) - m_{TMD,j}\sigma_k^2\left(x_j\right)\right]^2}\psi_k^2\left(x_j\right) \end{array} \right\} \tag{3.9}$$

In practical applications, a few NM modes in Eq. (3.6) will be sufficient to accurately represent the response and, upon summing up the contributions of complex-conjugate eigenfunction pairs, Eq. (3.6) can be reverted to the following real form [50, 51]:

$$w\left(x,\tau\right) \approx \mathrm{Re}\left[\sum_{ii=1}^{NL} f_{ii} \sum_{k=1}^{NM} \psi_k\left(x\right) \left[\begin{array}{l} \int_{\tau_{ii}^0}^{\tau} e^{\mathrm{i}\sigma_k\left(\tau-\tau'\right)} g_{k,ii}\left(\tau'\right) d\tau' - \\ \int_{\tau_{ii}^E}^{\tau} e^{\mathrm{i}\sigma_k\left(\tau-\tau'\right)} g_{k,ii}\left(\tau'\right) d\tau' \end{array} \right]\right] \tag{3.10}$$

Equations analogous to Eq. (3.10) may be written for all response variables, i.e. rotation, bending moment and shear force, using pertinent eigenfunctions from Eq. (2.25). At this stage, some remarks on the advantages of the proposed approach must be made. The first is that closed-form expressions can be derived for the convolution integral

$$\int_0^{\tau} e^{\mathrm{i}\sigma_k\left(\tau-\tau'\right)} g_{k,ii}\left(\tau'\right) d\tau' \tag{3.11}$$

or as shown in the previous chapter, for the sum of integrals with general form

$$\int_0^{\tau} \lambda\left(\tau'\right) H\left(v_0\tau' - s_{ii} - x_j\right) d\tau' \tag{3.12}$$

Once again, using the generalised functions theory [29, 49], Eq. (3.12) can be computed as

$$\int_0^\tau \lambda(\tau') H\left(v_0\tau' - s_{ii} - x_j\right) d\tau' =$$

$$\left\{H\left(\xi - s_{ii} - x_j\right)\left[\lambda^{[1]}\left(\xi v_0^{-1}\right) - \lambda^{[1]}\left(x_j v_0^{-1} + s_{ii} v_0^{-1}\right)\right]\right\}_0^{v_0\tau} = \tag{3.13}$$

$$= H\left(v_0\tau - s_{ii} - x_j\right)\left[\lambda^{[1]}(\tau) - \lambda^{[1]}\left(x_j v_0^{-1} + s_{ii} v_0^{-1}\right)\right]$$

Secondly, it is worth noting that the exact complex modes of the beam in Eq. (3.6) and Eq. (3.10) reflect the actual amount of damping introduced by viscoelastic TMDs, supports and joints. This means that no simplifying assumptions are made on system damping, as is the case in modal superposition approaches where proportional damping is assumed in order to use classical orthogonality conditions of undamped modes [9–11, 13].

3.5 Numerical Applications

3.5.1 Example A: Beam subjected to a single moving load

Consider a simply-supported beam of unit length with Kelvin-Voigt viscoelastic translational supports and rotational joints located at $x_1 = 1/4$ and $x_3 = 3/4$ in two different configurations. In the first configuration the beam is equipped with one viscoelastic TMD at mid-span, whereas in the second configuration three viscoelastic TMDs are attached, located at $x_2 = 0.5$, $x_4 = 0.45$ and $x_5 = 0.55$, as shown in Fig.3.2. Non-dimensional parameters are selected as follows: Translational supports $k_{w,1} = k_{w,3} = 10^2$, $c_{w,1} = c_{w,3} = 10^{-1}$; Rotational dampers $k_{\Delta\theta,1} = k_{\Delta\theta,3} = 10$, $c_{\Delta\theta,1} = c_{\Delta\theta,3} = 10^{-1}$. The beam is subjected to a non-dimensional unit single force $f_1 = 1$ moving with constant speed $v_0 = 3.5$ and starting from $s_1 = 0$. In an initial numerical study, performing repeated time history analysis of the beam without TMDs with incrementally increased speed, speed v_0 was found to yield at the largest displacement response in the speed range [0,8]. At this speed the force leaves the beam at time instant $\tau = 0.286$. The maximum deflection $w_{\max} = 0.01289$ of the beam without TMDs undergoes at $x = 0.6$ and time $\tau = 0.219$ when the unit force f_1, travelling with speed v_0, is located at $x = 0.763$. Although the peak deflection occurs at $x = 0.6$, the TMDs (or the single TMD in the first configuration) are symmetrically placed along the beam because the structure may be crossed in both directions.

In the single TMD configuration, the mass ratio $\alpha = m_{TMD}/\bar{m}_1$ is chosen to be 5%, i.e. $\alpha = 0.05$. In this relationship m_{TMD} is the non-dimensional TMD mass while $\bar{m}_1 = \left(\int_0^1 \psi_1^2(x)\,dx\right) / \left(\psi_1^2(x = x_{TMD} = 0.5)\right)$ is the non-dimensional first modal mass of the beam without TMD. In a simplified approach, tuning of the frequency ratio β (i.e. TMD natural frequency σ_{TMD} over the real part of the fundamental eigenvalue $\mathrm{Re}[\sigma_1]$ of the beam without TMD), and the TMD damping ratio ζ is accomplished according to Den Hartog [69],

$$\beta \equiv \frac{\sigma_{TMD}}{\mathrm{Re}[\sigma_1]} = \frac{1}{1+\alpha}\ ,\quad \zeta = \sqrt{\frac{3\alpha}{8\,(1+\alpha)}} \tag{3.14}$$

yielding the frequency ratio $\beta = 0.952$ and TMD damping ratio $\zeta = 0.133$. Then, the non-dimensional TMD stiffness coefficient and TMD damping coefficient are found from:

$$k_{TMD} = m_{TMD}(\beta \mathrm{Re}[\sigma_1])^2\ ,\quad c_{TMD} = 2\zeta\sqrt{k_{TMD} m_{TMD}} \tag{3.15}$$

where $\sigma_1 = 16.9419 + \mathrm{i}0.1158$ is considered. A more elaborate tuning procedure yielding optimal TMD parameters can be found in [65].

The three TMDs of the second structural configuration are attached in proximity to the mid-span of the beam in accordance with the fundamental mode shape [65–67]. The mass ratio of each TMD is chosen equal to $\alpha = 1.67\%$, i.e., the total mass of the three TMDs corresponds to the mass of the single TMD in the first configuration. Again, Den Hartog's relations are used to tune the TMD parameters. Thus, the non-dimensional stiffness coefficients and damping coefficients of the TMDs are given by Eqs. (3.15), considering the mass ratio $\alpha = 1.67\%$. It should be noted that optimal tuning of TMD parameters is no objective of this work. For this issue it is referred to, for instance, [65]. In Tables 3.1 to 3.3 the exact non-dimensional eigenvalues of the first eight modes of the beam without TMDs, the beam in the first configuration (equipped with one TMD) and the beam in the second configuration (equipped with three TMDs) are specified, derived by the proposed method using Eq. (1.16), and the classical method. In the latter method the free-vibration response is represented in trigonometric/hyperbolic form with four integration constants over each segment between two consecutive damper/support locations, and the matching conditions are enforced at the subdivision points along with the boundary conditions. Whereas for the proposed method the characteristic equation is derived from a determinant of a

4×4 matrix, as oppose to in the classical procedure where the underlying determinant is of a 12×12 matrix. All modes of this non-classically damped problem are complex, and thus, the equivalent modal damping coefficients of the individual modes are not the same. According to these tables, the first mode of the beam without TMDs is split into two modes when applying one or three TMDs, respectively [65]. However, the TMDs have almost no impact on the higher modes, as it has already found in previous studies such as [65].

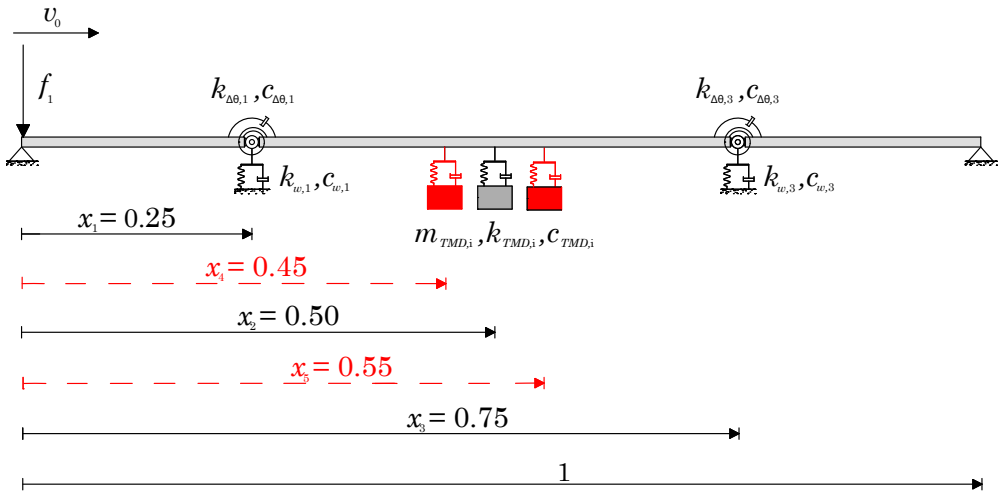

Figure 3.2: Simply-supported beam with Kelvin-Voigt viscoelastic supports and joints and one viscoelastic TMD (first configuration) or three viscoelastic TMDs (second configuration) attached.

Figure 3.3 shows the mode 1 eigenfunctions of the beam without TMDs (red lines), the beam in the first configuration (blue lines), and the beam in the second configuration (black lines). In particular the real part (left column) and the imaginary part (right column) of the mode 1 deflection (first line), the mode 1 rotation (second line), the mode 1 bending moment (third line), and the mode 1 shear force (fourth line) are depicted. As observed, the rotational dampers induce a jump discontinuity at mode 1 rotation while the translational dampers induce a jump discontinuity at the mode 1 shear force. The TMDs greatly affect the shape of the imaginary part of the considered mode 1 eigenfunctions, reflecting the introduced non-classical damping to the system. In contrast, the global shape of the real part remains similar. The TMDs create a kink in the mode 1 bending moment, and a jump discontinuity in the

Table 3.1: Eigenvalues of the beam without TMDs obtained by the proposed method (PM) and the classical method (CM).

Mode	Eigenvalues (PM)	Eigenvalues (CM)	Damping ratio
1	$\pm$ 16.9419$+i$ 0.1158	$\pm$ 16.9417$+i$ 0.1159	0.0068
2	$\pm$ 39.8987$+i$ 1.5487	$\pm$ 39.8985$+i$ 1.5484	0.0387
3	$\pm$ 85.5111$+i$ 3.0840	$\pm$ 85.5113$+i$ 3.0838	0.0360
4	$\pm$ 157.914	$\pm$ 157.916	—
5	$\pm$ 242.810$+i$ 7.6555	$\pm$ 242.808$+i$ 7.6557	0.0315
6	$\pm$ 348.718$+i$ 17.468	$\pm$ 348.715$+i$ 17.470	0.0500
7	$\pm$ 480.920$+i$ 9.2064	$\pm$ 480.922$+i$ 9.2062	0.0191
8	$\pm$ 631.655	$\pm$ 631.653	—

Table 3.2: Eigenvalues of the structural configuration with one TMD obtained by the proposed method (PM) and the classical method (CM).

Mode	Eigenvalues (PM)	Eigenvalues (CM)	Damping ratio
1	$\pm$ 15.0493$+i$ 1.0641	$\pm$ 15.0495$+i$ 1.0643	0.0705
2	$\pm$ 18.0474$+i$ 1.2957	$\pm$ 18.0472$+i$ 1.2955	0.0716
3	$\pm$ 39.8987$+i$ 1.5487	$\pm$ 39.8985$+i$ 1.5486	0.0387
4	$\pm$ 85.5856$+i$ 3.1932	$\pm$ 85.5858$+i$ 3.1985	0.0372
5	$\pm$ 157.914	$\pm$ 157.916	—
6	$\pm$ 242.820$+i$ 7.7563	$\pm$ 242.822$+i$ 7.7565	0.0319
7	$\pm$ 348.718$+i$ 17.468	$\pm$ 348.716$+i$ 17.469	0.0500
8	$\pm$ 480.944$+i$ 9.3117	$\pm$ 480.947$+i$ 9.3115	0.0193

mode 1 shear force, at the point of attachment.

Now, the dynamic response of the beam with and without TMDs when subjected to a moving single force with speed v_0 is considered.

Figure 3.4 shows the beam deflection over the span of the beam at time instant $\tau = 0.219$, computed by the proposed method, based on a four-mode approximation, and by FE analysis using ADINA [53] with time-dependent nodal forces built as explained in ref.[25]. At this time instant the displacement of the beam without TMDs is at maximum value in the forced vibration phase. As observed in Fig.3.4, the TMDs do not significantly affect the beam response in the forced vibration phase. Attaching one or three TMDs to the beam, leads to a peak displacement reduction of only 1%.

Table 3.3: Eigenvalues of the structural configuration with three TMDs obtained by the proposed method (PM) and the classical method (CM).

Mode	Eigenvalues (PM)	Eigenvalues (CM)	Damping ratio
1	$\pm$ 15.0692+i 1.0700	$\pm$ 15.0665+i 1.0703	0.0708
2	$\pm$ 18.0270+i 1.2895	$\pm$ 18.0272+i 1.2892	0.0713
3	$\pm$ 39.9084+i 1.5574	$\pm$ 39.9082+i 1.5557	0.0389
4	$\pm$ 85.5752+i 3.1780	$\pm$ 85.5757+i 3.1778	0.0371
5	$\pm$ 157.922+i 0.0241	$\pm$ 157.924+i 0.0243	0.0001
6	$\pm$ 242.817+i 7.7300	$\pm$ 242.819+i 7.7304	0.0317
7	$\pm$ 348.724+i 17.513	$\pm$ 348.727+i 17.515	0.0501
8	$\pm$ 480.932+i 9.2560	$\pm$ 480.934+i 9.2563	0.0192

It can be also observed that the agreement between the proposed solution and the FE solution is very satisfactory.

No significant changes are found when taking into account more than four modes, as shown in Fig.3.5, where the deflection at $x = 0.6$ of the beam with three TMDs is shown with respect to time τ using one, two, three modes, four and five modes, respectively. Additionally, the FE solution is depicted. It is evident that, in general, one mode is not sufficient to describe the deflection of the beam.

Figure 3.6 shows the beam deflection at $x = 0.6$ with respect to time τ for the considered structural configurations. As is well known, the peak response induced by a single moving load is not greatly affected by TMDs, in the forced vibration phase.

However, the results of Fig.3.6 highlight the importance of the TMDs to reduce the free-vibration response after the single force has left the beam to increase the fatigue life of the structure. No significant changes are found with one or three TMDs attached, as shown in Fig.3.6. With one or three TMDs equipped, the beam is almost at rest after eight free-vibration cycles, whereas the displacement amplitude of the beam without TMDs is only 25.3% less than its initial value at $\tau = 0.423$.

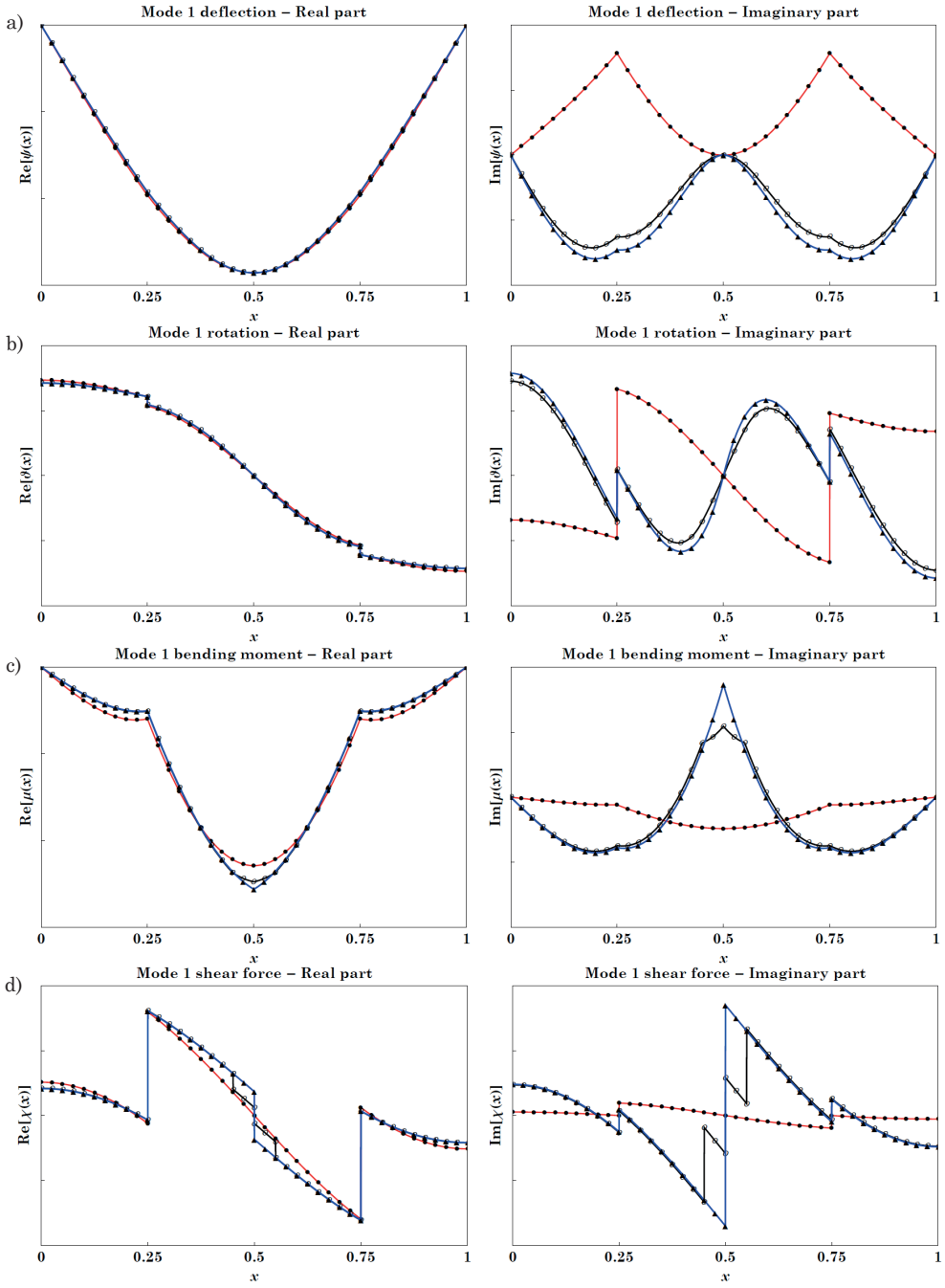

Figure 3.3: Mode 1 eigenfunctions of the beam (i) without TMDs (red line), (ii) with one TMD (blue line) and (iii) with three TMDs (black line) shown in Fig.3.2: (a) deflection; (b) rotation; (c) bending moment; (d) shear force. Left column: real part. Right column: imaginary part. Solution based on the proposed method (solid line) and on the classical procedure (black markers).

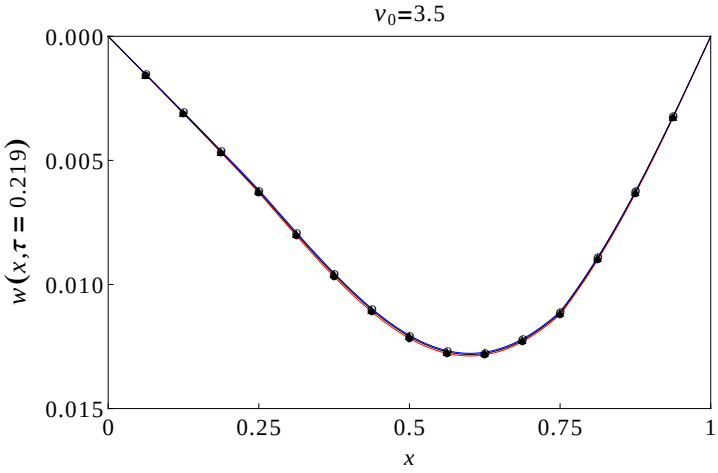

Figure 3.4: Deflection profile at time $\tau = 0.219$, subjected to moving concentrated force with speed v_0: Proposed solution for the beam (i) without TMDs (red line), (ii) with one TMD (blue dashed line), (iii) with three TMDs (black line); corresponding FE solution (black markers).

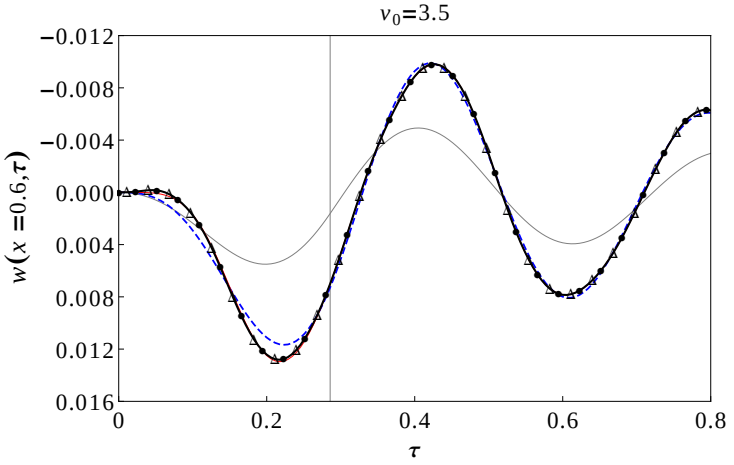

Figure 3.5: Deflection at $x = 0.6$ of the beam with three TMDs subjected to moving concentrated force with speed v_0. Proposed solution with one mode (gray line), two modes (dashed blue line), three modes (red line), four modes (black thick line) and five modes (triangle markers) approximation; corresponding FE solution (black markers).

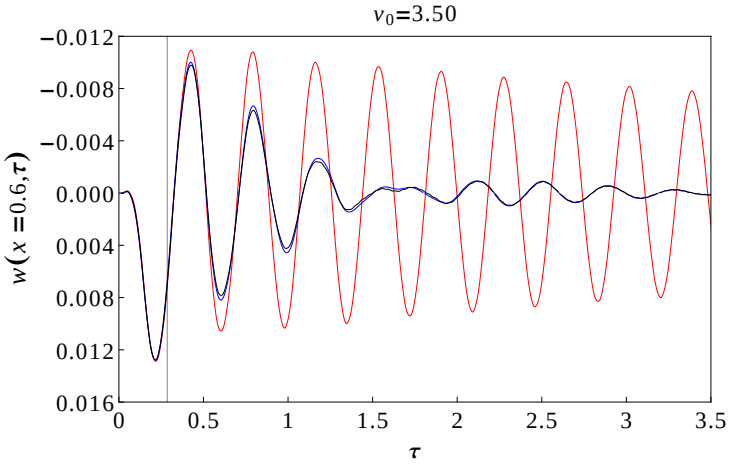

Figure 3.6: Beam deflection at $x = 0.6$ subjected to moving concentrated force with speed v_0: proposed solution for the beam (i) without TMDs (red line), (ii) with one TMD (blue line), (iii) with three TMDs (black line).

3.5.2 Example B: Beam subjected to a series of moving loads

In the second application the previously considered structural configurations shown in Fig.3.2 are subjected to a series of concentrated forces. In this particular example the series of concentrated forces represent the axle loads of a train composed of one rail car and seven passenger cars [4], as shown in Fig.3.7. Each car has at both ends a bogie with two axles each, with non-dimensional distances specified in Fig.3.7: $h = c = 0.115$, $b = e = 0.093$, $g = 0.493$, $d = 1$. The non-dimensional axle loads of the rail cars and passenger cars are respectively 1.0 and 0.5. At critical speeds of the passing load series, the dynamic response of the bridge is severely amplified and driven into resonance. The critical speeds depend on the natural structural frequencies and load distance d [49]. In the current application it is assumed that the loads cross the beam with the critical speed of first order [49, 50], i.e.

$$v_0 = \frac{\mathrm{Re}[\sigma_1]d}{2\pi} \tag{3.16}$$

with the non-dimensional complex fundamental eigenvalue of the beam without TMDs, σ_1, yielding $v_0 = 2.69$.

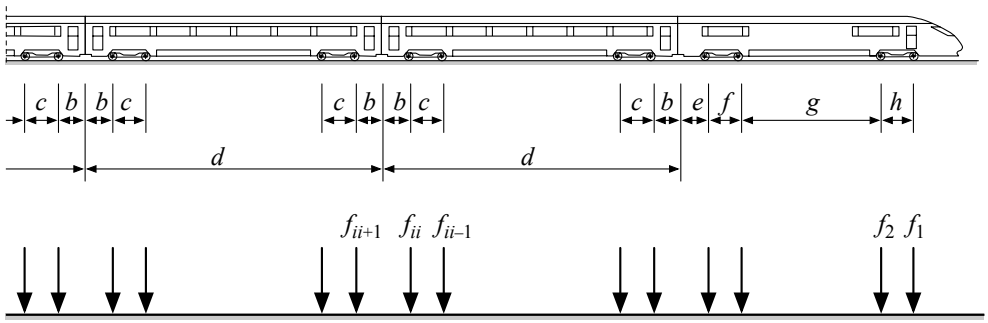

Figure 3.7: Idealization of the train loads (modified from [1]).

Figure 3.8 shows the beam deflection at $x = 0.5$ with respect to time τ for the structural configurations: (i) beam without TMDs (red line), (ii) beam with one TMD (blue line), and (iii) beam with three TMDs (black line). The results of Fig.3.8 highlight the importance of using TMDs to reduce the response of the beam subjected to a series of repetitive loads at critical speed. The difference of the response of the two structural configurations with one TMD and three TMDs is negligible for the considered problem (about 1%), as shown in Fig.3.8. The vibrations decrease significantly in the forced vibration phase, unlike in the previous case of a single passing force, in which TMDs are only useful to reduce the free-vibration response. In this example the decrease of the peak response is about 60% when attaching three TMDs to the beam.

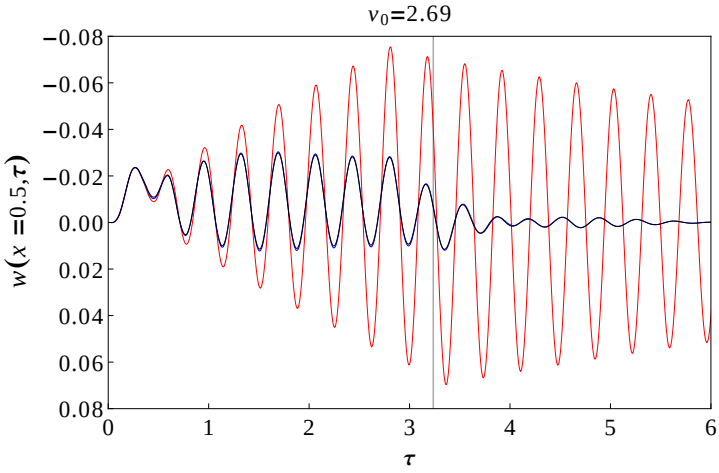

Figure 3.8: Beam deflection at $x = 0.5$ subjected to a series of moving concentrated forces with critical speed v_0 : proposed solution for the beam (i) without TMDs (red line), (ii) with one TMD (blue line), (iii) with three TMDs (black line).

3.6 Concluding remarks

Euler-Bernoulli beams with Kelvin-Voigt viscoelastic tuned mass dampers (TMDs), translational supports and rotational joints subjected to moving loads have been studied. A generalised function approach has been proposed, which uses exact complex modes and pertinent orthogonality conditions to express all response variables by time-domain convolution integrals in closed analytical form. No numerical integration is required, as is the case in finite element approaches. Unlike in a FE method where a mesh node must be inserted at the application point of any TMD, support or joint, and re-meshing may be required whenever they change position, in the proposed method this is not required. The proposed solution accounts for non-proportional damping due to TMDs, viscoelastic supports and joints, with significant benefits over existing modal superposition methods, where only proportional damping or, alternatively, no damping can be considered. The applicability, accuracy, and efficiency of the proposed procedure has been tested on a beam with multiple supports/joints and TMDs, acted under moving concentrated forces.

Chapter 4

On the moving multi-loads problem in beam structures with interlayer slip

The moving multi-loads problem for two-layered elastically bonded beams with interlayer slip is considered here. Bernoulli-Euler hypothesis is assumed to hold for each layer separately, and a linear constitutive equation between the horizontal slip and the interlaminar shear force is considered. On using pertinent orthogonality condition for the deflection modes, the dynamic response of the beam is derived in time domain.

4.1 Preliminary remarks

In engineering applications, beams composed of two or more layers are widely used to increase the strength-to-weight and stiffness-to-weight ratio of structural components. If bonded by strong adhesives, the layers can be assumed to be rigidly interconnected, and a full composite action between the layers is developed. During the last decades a large amount of studies has been devoted to static and dynamic analysis of rigidly bonded composite structures for various engineering problems [70–83], providing engineers with various well established methods.

However, in certain structural components such as composite steel-concrete beams and layered wood beams with flexible shear connectors, a rigid bond between the layers cannot be achieved. The deformation of the connectors

results in an interlayer slip, which affects both strength and deformation of the structure. Existing literature has focused on static and dynamic analysis of layered elastically bonded beams. For instance, linear static analysis is performed in [84–93], and vibration problems are addressed in [2, 94–104].

In this Chapter, the vibration problem of two-layer elastically bonded beams under moving loads is analysed. Firstly, the governing motion equations are presented. Then, a modal superposition approach is applied to build the dynamic response. Finally two illustrative examples are reported.

4.2 Equation of motion for layered beams under moving loads

In this section the dynamic response under moving loads of the two-layered beam shown in Fig.4.1 is analyzed. The layers are disposed about the transverse (Z-) beam axis, with otherwise arbitrary shape and constant cross section.

The beam is subjected to a series of NL concentrated loads F_{ii} $(i = 1, ..., NL)$ along the longitudinal (X-), with constant velocity V_0 and initial location S_{ii}, inducing the dynamic lateral beam deflection $W(X,t)$, which, under the assumption of small deformations, is assumed to be the same for each fiber at given X (no uplift between the layers). Variable t denotes time.

The equation of flexural motion in terms of deflection $W(X,t)$ is derived neglecting the effect of rotatory and longitudinal inertia and in absence of external axial forces [95]. With these assumptions, conservation of momentum in transverse direction, conservation of the angular momentum about the (Y-) axis, and conservation of momentum in axial direction for the beam element yield the following equilibrium equations:

$$\begin{aligned}
\frac{\partial Q\left(X,t\right)}{\partial X} &= -\sum_{ii=1}^{NL} F_{ii}\delta\left(X - V_0 t + S_{ii}\right)\left[H\left(t - t_{ii}^{0}\right) - H\left(t - t_{ii}^{E}\right)\right] + m_L \frac{\partial^2 W\left(X,t\right)}{\partial t^2} \\
\frac{\partial M\left(X,t\right)}{\partial X} &= Q\left(X,t\right) \\
\frac{\partial N\left(X,t\right)}{\partial X} &= -T_1(X,t) + T_2(X,t) = 0
\end{aligned} \tag{4.1}$$

in which $Q(X,t)$, $M(X,t)$, $N(X,t)$, $T_1(X,t) = T_2(X,t) = T(X,t)$ denote the total shear force, the total bending moment, the total axial force, and the elastic interlaminar shear force transmitted between the upper and lower layer, respectively. The mass per unit length m_L is calculated as $m_L = \sum_{i=1}^{2} \rho_i A_i$ with mass densities ρ_i and cross sectional areas A_i $(i = 1, 2)$ of the upper (subscript 1) and the lower layer (subscript 2).

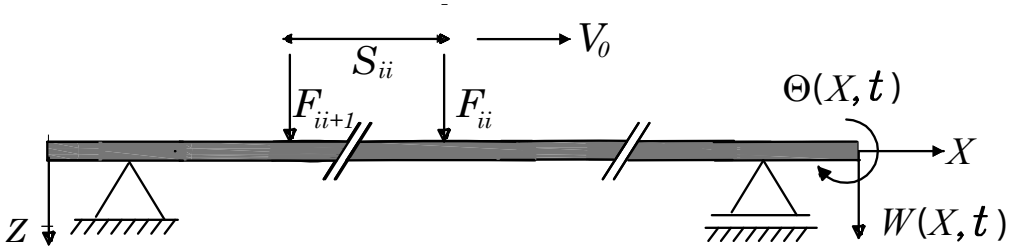

Figure 4.1: Two-layered elastically bonded beam under moving loads

The total shear force $Q(X,t)$, the total bending moment $M(X,t)$ and the total axial force $N(X,t)$ are expressed in terms of the layer stress resultants as shown in Fig.4.2 and discussed in [2]:

$$\begin{aligned} Q(X,t) &= Q_1(X,t) + Q_2(X,t) \\ M(X,t) &= M_1(X,t) + M_2(X,t) - N_1(X,t)\, r \\ N(X,t) &= N_1(X,t) + N_2(X,t) = 0 \end{aligned} \tag{4.2}$$

where r represents the distance between the layer centroids, see Fig.4.2.

Considering that Euler-Bernoulli hypothesis is not applicable to the total cross-section of the beam due to interlayer slip, but remains valid for each individual layer, and referring once more to Fig.4.2, the individual layer stress resultants are:

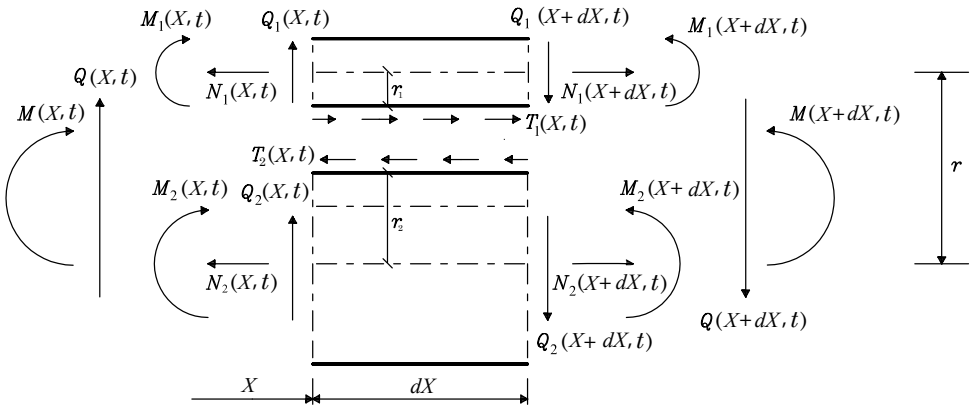

Figure 4.2: Infinitesimal two-layered beam element (according to [2])

$$
\begin{aligned}
Q_i(X,t) &= \frac{\partial M_i\,(X,t)}{\partial X} + T_i(X,t)\; r_i \\
M_i(X,t) &= -E_i I_i\;\; \frac{\partial^2 W\,(X,t)}{\partial X^2} \qquad i = 1,2 \\
N_i(X,t) &= E_i A_i\;\; \frac{\partial U_i\,(X,t)}{\partial X}
\end{aligned}
\tag{4.3}
$$

where E_1 and E_2 denote Young's moduli, and I_1 and I_2 are the principal moments of inertia of the cross-sectional areas of the upper and lower layer, respectively. The distances between the centroids of the single layers and the interlayer are referred to as r_1 and r_2 (see Fig.4.2). Furthermore, $U_1(X,t)$ and $U_2(X,t)$ are the longitudinal displacements at the centroid of the upper and lower layer, respectively.

The elastic interlaminar shear force $T(X,t) = T_1(X,t) = T_2(X,t)$ between the upper and lower layer is a force per unit length and is related to the interlaminar slip (see Fig.4.3)

$$
\Delta U\,(X,t) = U_2\,(X,t) - U_1\,(X,t) + r\frac{\partial W\,(X,t)}{\partial X} \tag{4.4}
$$

via Hooke's law, i.e.

$$
T(X,t) = k_s\;\Delta U(X,t) \tag{4.5}
$$

with k_s being the elastic slip modulus.

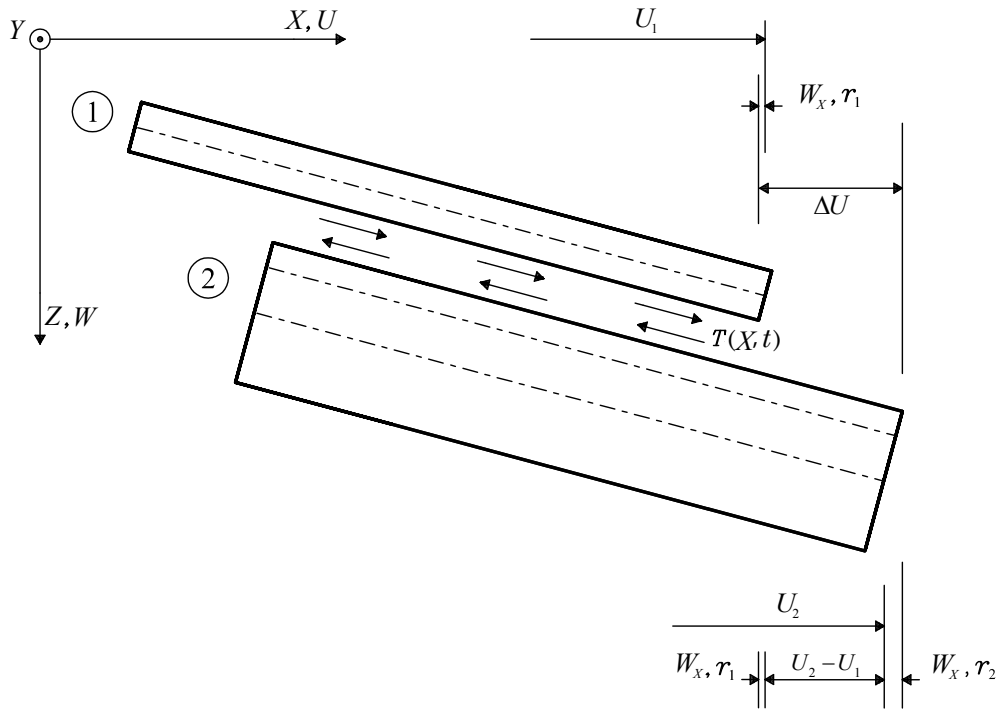

Figure 4.3: Deformed two-layered beam (according to [2])

Differentiation of Eq.(4.5) with respect to X, together with Eqs.(4.4),(4.3c), (4.2c), and taking into account that $\partial N_1(X,t)/\partial X = -T(X,t)$, yields after some algebra to the following equation:

$$r\frac{\partial^2 W(X,t)}{\partial X^2} + \frac{1}{k_s}\frac{\partial^2 N_1(X,t)}{\partial X^2} - N_1(X,t)\left(\frac{1}{E_1 A_1} + \frac{1}{E_2 A_2}\right) = 0 \tag{4.6}$$

Combining Eq.(4.3b) and Eq.(4.2b) allows the axial force in the upper layer $N_1(X,t)$ to be expressed as a function of the total bending moment $M(X,t)$ and the kinematic variables $W(X,t)$:

$$N_1(X,t) = -\frac{1}{r}\left[M(X,t) + EI_0\frac{\partial^2 W(X,t)}{\partial X^2}\right] \tag{4.7}$$

with EI_0 denoting the bending stiffness corresponding to non-composite action (subscript 0),

$$EI_0 = \sum_{i=1}^{2} E_i I_i \tag{4.8}$$

Subsequently, Eq.(4.7) and its second derivative with respect to X are substituted into Eq.(4.6), yielding:

$$\frac{\partial^4 W(X,t)}{\partial X^4} - \alpha^2 \frac{\partial^2 W(X,t)}{\partial X^2} = \frac{\alpha^2}{EI_\infty} M(X,t) - \frac{1}{EI_0} \frac{\partial^2 M(X,t)}{\partial X^2} \tag{4.9}$$

In this equation, $EA_p = E_1 A_1 E_2 A_2$, EI_∞ is the bending stiffness corresponding to a rigid interlayer connection (subscript ∞) and EA_0 is the longitudinal stiffness for non-composite action, respectively defined as:

$$EI_\infty = EI_0 + \frac{r^2\, EA_p}{EA_0} \quad , \quad EA_0 = \sum_{i=1}^{2} E_i A_i \tag{4.10}$$

while coefficient α^2 reads [96]:

$$\alpha^2 = k_s \left(\frac{EA_0}{EA_p} + \frac{r^2}{EI_0} \right) \tag{4.11}$$

Twice differentiation of Eq.(4.9) with respect to X and using Eqs.(4.1a,b) finally yields the equation of motion in terms of $W(X,t)$:

$$\begin{aligned} &\frac{\partial^6 W(X,t)}{\partial X^6} - \alpha^2 \frac{\partial^4 W(X,t)}{\partial X^4} + \frac{m_L}{EI_0} \frac{\partial^4 W(X,t)}{\partial X^2 \partial t^2} - \frac{m_L\, \alpha^2}{EI_\infty} \frac{\partial^2 W(X,t)}{\partial t^2} = \\ &-\frac{\alpha^2}{EI_\infty} \sum_{ii=1}^{NL} F_{ii} \delta\left(X - V_0\, t + S_{ii}\right) \left[H\left(t - t_{ii}^0\right) - H\left(t - t_{ii}^E\right) \right] \\ &+\frac{1}{EI_0} \sum_{ii=1}^{NL} F_{ii} \delta^{(2)}\left(X - V_0\, t + S_{ii}\right) \left[H\left(t - t_{ii}^0\right) - H\left(t - t_{ii}^E\right) \right] \end{aligned} \tag{4.12}$$

In the present formulation, both limits $\alpha \to \infty$ (rigidly bonded beam) and $\alpha \to 0$ (no bonded beam) can be taken into account without numerical difficulties [96].

The solution of Eq.(4.12) is found together with the initial conditions $W(X, t = 0) = 0$, $\partial W(X, t = 0)/\partial t = 0$, and the beam boundary conditions. In the following, three classical boundary conditions are reported [96], with $X_b = 0, L$ denoting the beam ends.

(*i*) Simply supported end:

$$W\left(X_b, t\right) = 0 \qquad M_1\left(X_b, t\right) = M_2\left(X_b, t\right) = 0 \qquad N_1\left(X_b, t\right) = 0 \tag{4.13}$$

(*ii*) Free end:

$$M_1\left(X_b, t\right) = M_2\left(X_b, t\right) = 0 \qquad N_1\left(X_b, t\right) = 0 \qquad Q\left(X_b, t\right) = 0 \tag{4.14}$$

(*iii*) Clamped end:

$$W\left(X_b, t\right) = 0 \qquad \frac{\partial W\left(X_b, t\right)}{\partial X} = 0 \qquad \Delta U\left(X_b, t\right) = 0 \tag{4.15}$$

After solving Eq.(4.12) for $W(X, t)$, it is possible to built the stress resultants $M(X, t)$, $Q(X, t)$, $N_1(X, t)$ and the interlaminar shear force per unit length $T(X, t)$.

In particular, the bending moment from Eqs.(4.9) and (4.1a,b) reads

$$\begin{aligned} M\left(X, t\right) = & -EI_\infty \frac{\partial^2 W\left(X, t\right)}{\partial X^2} + \frac{EI_\infty}{\alpha^2}\left(\frac{\partial^4 W\left(X, t\right)}{\partial X^4} + \frac{m_L}{EI_0}\frac{\partial^2 W\left(X, t\right)}{\partial t^2}\right) \\ & + \frac{EI_\infty}{EI_0\alpha^2}\left(-\sum_{ii=1}^{NL} F_{ii}\delta\left(X - V_0\, t + S_{ii}\right)\left[H\left(t - t_{ii}^0\right) - H\left(t - t_{ii}^E\right)\right]\right) \end{aligned} \tag{4.16}$$

the transverse shear force from Eq.(4.1b)) reads

$$Q\left(X, t\right) = -EI_\infty \frac{\partial^3 W\left(X, t\right)}{\partial X^3} + \frac{EI_\infty}{\alpha^2}\left(\frac{\partial^5 W\left(X, t\right)}{\partial X^5} + \frac{m_L}{EI_0}\frac{\partial^3 W\left(X, t\right)}{\partial X \partial t^2}\right) \tag{4.17}$$

the axial force in the upper layer, from Eq.(4.7)) reads

$$N_1(X,t) = -\frac{1}{r}\left[(EI_0 - EI_\infty)\frac{\partial^2 W(X,t)}{\partial X^2} + \frac{EI_\infty}{\alpha^2}\left(\frac{\partial^4 W(X,t)}{\partial X^4} + \frac{m_L}{EI_0}\frac{\partial^2 W(X,t)}{\partial t^2}\right)\right]$$
$$-\frac{EI_\infty}{r\,EI_0\alpha^2}\left(-\sum_{ii=1}^{NL} F_{ii}\delta\left(X - V_0\,t + S_{ii}\right)\left[H\left(t - t_{ii}^0\right) - H\left(t - t_{ii}^E\right)\right]\right) \tag{4.18}$$

the axial force in the lower layer reads

$$N_2(X,t) = -N_1(X,t) \tag{4.19}$$

and the interlaminar shear force from Eqs.(4.7), and (4.1c) reads

$$T(X,t) = -\frac{\partial N_1(X,t)}{\partial X} =$$
$$\frac{1}{r}\left[(EI_0 - EI_\infty)\frac{\partial^3 W(X,t)}{\partial X^3} + \frac{EI_\infty}{\alpha^2}\left(\frac{\partial^5 W(X,t)}{\partial X^5} + \frac{m_L}{EI_0}\frac{\partial^3 W(X,t)}{\partial X \partial t^2}\right)\right] \tag{4.20}$$
$$+\frac{EI_\infty}{r\,EI_0\alpha^2}\left(-\sum_{ii=1}^{NL} F_{ii}\delta\left(X - V_0\,t + S_{ii}\right)\left[H\left(t - t_{ii}^0\right) - H\left(t - t_{ii}^E\right)\right]\right)$$

4.3 Beam modes

The free vibration problem of the beam shown in Fig.4.1 is solved here.

4.3.1 Eigenvalue problem

Based on the standard separate variables approach ($W(X,t) = \Phi(X)e^{I\omega t}$), the following sixth order ordinary differential equation for the deflection eigenfunction $\Phi(X)$ of the two-layered elastically bonded beam, is obtained:

$$\frac{d^6\Phi(X)}{dX^6} - \alpha^2\frac{d^4\Phi(X)}{dX^4} - \frac{m_L\,\omega^2}{EI_0}\frac{d^2\Phi(X)}{dX^2} + \frac{m_L\,\alpha^2\omega^2}{EI_\infty}\Phi(X) = 0 \tag{4.21}$$

The eigenfunctions for the bending moment $\Upsilon(X)$, the shear force $\Gamma(X)$, the

axial force in the upper layer $\Sigma(X)$, and the elastic interlaminar shear force $\Psi(X)$, are similarly obtained from Eqs.(4.16), (4.17), (4.18) and (4.20):

$$\Upsilon(X) = -EI_\infty \frac{d^2\Phi(X)}{dX^2} + \frac{EI_\infty}{\alpha^2}\left(\frac{d^4\Phi(X)}{dX^4} - \frac{m_L\,\omega^2}{EI_0}\Phi(X)\right) \tag{4.22}$$

$$\Gamma(X) = -EI_\infty \frac{d^3\Phi(X)}{dX^3} + \frac{EI_\infty}{\alpha^2}\left(\frac{d^5\Phi(X)}{dX^5} - \frac{m_L\,\omega^2}{EI_0}\frac{d\Phi(X)}{dX}\right) \tag{4.23}$$

$$\Sigma(X) = -\frac{1}{r}\left[(EI_0 - EI_\infty)\frac{d^2\Phi(X)}{dX^2} + \frac{EI_\infty}{\alpha^2}\left(\frac{d^4\Phi(X)}{dX^4} - \frac{m_L\,\omega^2}{EI_0}\Phi(X)\right)\right] \tag{4.24}$$

$$\Psi(X) = \frac{1}{r}\left[(EI_0 - EI_\infty)\frac{d^3\Phi(X)}{dX^2} + \frac{EI_\infty}{\alpha^2}\left(\frac{d^5\Phi(X)}{dX^4} - \frac{m_L\omega^2}{EI_0}\frac{d\Phi(X)}{dX}\right)\right] \tag{4.25}$$

The eigenfunction of rotation $\mathrm{O}(X)$ is found considering that:

$$\mathrm{O}(X) = \frac{d\Phi(X)}{dX} \tag{4.26}$$

Next, the eigenfunctions of the response variables are collected in vector $\mathbf{\Upsilon}(X) = \left[\ \Phi(X) \quad \mathrm{O}(X) \quad \Upsilon(X) \quad \Gamma(X) \quad \Sigma(X) \quad \Psi(X)\ \right]^T$, expressed thought the following expression, from Eq.(4.21):

$$\mathbf{\Upsilon}(X) = \mathbf{\Omega}(X)\,\mathbf{c} \tag{4.27}$$

where $\mathbf{c} = \left[\ c_1 \quad c_2 \quad c_3 \quad c_4 \quad c_5 \quad c_6\ \right]^T$ is a 6×1 vector of integration constants, while:

$$\mathbf{\Omega}(X) = \begin{bmatrix} \Omega_{\Phi_1} & \Omega_{\Phi_2} & \Omega_{\Phi_3} & \Omega_{\Phi_4} & \Omega_{\Phi_5} & \Omega_{\Phi_6} \\ \Omega_{O_1} & \Omega_{O_2} & \Omega_{O_3} & \Omega_{O_4} & \Omega_{O_5} & \Omega_{O_6} \\ \Omega_{Y_1} & \Omega_{Y_2} & \Omega_{Y_3} & \Omega_{Y_4} & \Omega_{Y_5} & \Omega_{Y_6} \\ \Omega_{\Gamma_1} & \Omega_{\Gamma_2} & \Omega_{\Gamma_3} & \Omega_{\Gamma_4} & \Omega_{\Gamma_5} & \Omega_{\Gamma_6} \\ \Omega_{\Sigma_1} & \Omega_{\Sigma_2} & \Omega_{\Sigma_3} & \Omega_{\Sigma_4} & \Omega_{\Sigma_5} & \Omega_{\Sigma_6} \\ \Omega_{\Psi_1} & \Omega_{\Psi_2} & \Omega_{\Psi_3} & \Omega_{\Psi_4} & \Omega_{\Psi_5} & \Omega_{\Psi_6} \end{bmatrix} \tag{4.28}$$

All terms in Eq.(4.28) are available in a simple analytical form; in particular, the terms of the first row of matrix $\mathbf{\Omega}(X)$ concerning the deflection eigenfunction are:

$$\begin{aligned} &\Omega_{\Phi_1}(X) = e^{-X\sqrt{R_1}} \qquad \Omega_{\Phi_2}(X) = e^{X\sqrt{R_1}} \qquad \Omega_{\Phi_3}(X) = e^{-X\sqrt{R_2}} \\ &\Omega_{\Phi_4}(X) = e^{X\sqrt{R_2}} \qquad \Omega_{\Phi_5}(X) = e^{-X\sqrt{R_3}} \qquad \Omega_{\Phi_6}(X) = e^{X\sqrt{R_3}} \end{aligned} \tag{4.29}$$

where R_1, R_2 and R_3 are the roots of the characteristic polynomial associated with the homogeneous differential Eq.(4.21):

$$R_1 = \frac{1}{6}\left(2\alpha^2 + \frac{2^{4/3}\left(EI_0\,\alpha^4 + 3m_L\,\omega^2\right)}{a} + \frac{2^{2/3}a}{EI_0}\right) \tag{4.30}$$

$$R_2 = \frac{1}{12}\left(4\alpha^2 - \frac{4(-2)^{1/3}\left(EI_0\,\alpha^4 + 3m_L\,\omega^2\right)}{a} + \frac{i\,2^{2/3}\left(i+\sqrt{3}\right)a}{EI_0}\right) \tag{4.31}$$

$$R_3 = \frac{1}{12}\left(4\alpha^2 + \frac{2^{7/3}(-1)^{2/3}\left(EI_0\,\alpha^4 + 3m_L\,\omega^2\right)}{a} - \frac{i\,2^{2/3}\left(-i+\sqrt{3}\right)a}{EI_0}\right) \tag{4.32}$$

Symbol a is a constant defined as:

$$a = \left[2{EI_0}^3\,\alpha^6 + 9{EI_0}^2\,\alpha^2 m_L\,\omega^2 - \frac{27{EI_0}^3\,\alpha^2 m_L\,\omega^2}{EI_\infty} + \right.$$

$$\left. \sqrt{{EI_0}^3 \left(\begin{array}{l} -4\left(EI_0\,\alpha^4 + 3m_L\,\omega^2\right)^3 + \\ \\ \dfrac{EI_0\left(2\,EI_0\,EI_\infty\,\alpha^6 + 9\left(-3EI_0 + EI_\infty\right)\alpha^2 m_L\,\omega^2\right)^2}{{EI_\infty}^2} \end{array} \right)} \right]^{1/3} \tag{4.33}$$

The other terms of matrix $\mathbf{\Omega}\left(X\right)$, concerning the eigenfunctions of rotation, bending moment, shear force, individual layer axial force and the elastic interlaminar shear force, respectively, according to Eqs(4.22-4.26), are simply obtained from the following relationships:

$$\Omega_{\mathrm{O}_g}(X) = \frac{d\Omega_{\Phi_g}\left(X\right)}{dX} \tag{4.34}$$

$$\Omega_{\mathrm{Y}_g}(X) = -EI_\infty \frac{d^2\Omega_{\Phi_g}\left(X\right)}{dX^2} + \frac{EI_\infty}{\alpha^2}\left(\frac{d^4\Omega_{\Phi_g}\left(X\right)}{dX^4} - \frac{m_L\,\omega^2}{EI_0}\Omega_{\Phi_g}\left(X\right) \right) \tag{4.35}$$

$$\Omega_{\Gamma_g}(X) = -EI_\infty \frac{d^3\Omega_{\Phi_g}\left(X\right)}{dX^3} + \frac{EI_\infty}{\alpha^2}\left(\frac{d^5\Omega_{\Phi_g}\left(X\right)}{dX^5} - \frac{m_L\,\omega^2}{EI_0}\frac{d\Omega_{\Phi_g}\left(X\right)}{dX} \right) \tag{4.36}$$

$$\Omega_{\Sigma_g}(X) = -\frac{1}{r}\left[\left(EI_0 - EI_\infty\right)\frac{d^2\Omega_{\Phi_g}\left(X\right)}{dX^2} + \frac{EI_\infty}{\alpha^2}\left(\frac{d^4\Omega_{\Phi_g}\left(X\right)}{dX^4} - \frac{m_L\,\omega^2}{EI_0}\Omega_{\Phi_g}\left(X\right) \right) \right] \tag{4.37}$$

$$\Omega_{\Psi_g}(X) = \frac{1}{r}\left[\left(EI_0 - EI_\infty\right)\frac{d^3\Omega_{\Phi_g}\left(X\right)}{dX^3} + \frac{EI_\infty}{\alpha^2}\left(\frac{d^5\Omega_{\Phi_g}\left(X\right)}{dX^5} - \frac{m_L\,\omega^2}{EI_0}\frac{d\Omega_{\Phi_g}\left(X\right)}{dX} \right) \right] \tag{4.38}$$

with $g = 2, 3, ..., 6$.

At this stage, the eigenvalue problem can be formulated using Eq.(4.27) together with the boundary conditions of the beam, obtaining six equations expressed in the same general form used for the previous chapters:

$$\mathbf{Bc} = \mathbf{0} \tag{4.39}$$

Notice that each equation corresponds to a component of vector $\mathbf{Y}(X)$ in Eq.(4.27) evaluated at the beam ends $X_b = 0, L$. For example, see the following typical boundary conditions in term of eigenfunctions:

(*i*) Simply supported end:

$$\Phi(X_b) = 0 \qquad \Upsilon(X_b) = 0 \qquad \Sigma(X_b) = 0 \tag{4.40}$$

(*ii*) Clamped end:

$$\Phi(X_b) = 0 \qquad \mathrm{O}(X_b) = 0 \qquad \Psi(X_b) = 0 \tag{4.41}$$

(*iii*) Free end:

$$\Upsilon(X_b) = 0 \qquad \Gamma(X_b) = 0 \qquad \Sigma(X_b) = 0 \tag{4.42}$$

where $X_b = 0, L$.

The characteristic equation of the eigenvalue problem is the determinant of matrix $\mathbf{B}$, i.e:

$$\det \mathbf{B} = 0 \tag{4.43}$$

whose roots ω_n are the natural frequencies of the beam (subscript n is added to indicate the infinite number of eigensolutions). Once vector $\mathbf{c}$ is derived as non-trivial solution of Eq.(4.39) for the nth natural frequency ω_n, the exact closed analytical expression for the corresponding vector of eigenfunctions $\mathbf{Y}_n(X)$ is finally built by Eq.(4.27).

4.4 Beam response to moving loads

Based on modal analysis, the beam deflection response $W(X,t)$ under moving multi-loads may be expressed as:

$$W(X,t) = \sum_{n=1}^{\infty} R_n(t)\,\Phi_n(X) \tag{4.44}$$

where $\Phi_n(X)$ denotes the nth deflection eigenfunction derived in Section 4.3, while $R_n(t)$ is the corresponding time-dependent modal coordinate.

Modal series Eq.(4.44) is substituted into the equation of motion Eq.(4.12), multiplied by the mth eigenfunction $\Phi_m(X)$, and integrated over beam length L. Then, considering the orthogonality relations [96]:

$$\begin{aligned} &-\frac{m_L}{EI_0}\int_0^L \frac{d^2\Phi_m(X)}{dX^2}\Phi_n\,dX + \frac{m_L\alpha^2}{EI_\infty}\int_0^L \Phi_n\Phi_m\,dX + \\ &+\sum_{h=1}^{2}\Phi_n(X_b)C_h\left[\Phi_m(X_b)\right] = m_m\delta_{mn} \end{aligned} \tag{4.45}$$

where $X_b = 0, L$, δ_{mn} is the Kronecker delta, C_h denotes a linear homogeneous differential operator containing derivatives of the boundaries.

(i) Simply supported or clamped end:

$$C_1 = C_2 = 0 \tag{4.46}$$

(ii) Free end:

$$C_1 = \frac{m_L}{EI_0}() \qquad C_2 = \frac{m_L}{EI_0}\frac{d}{dX}() \tag{4.47}$$

Variable m_m is the modal mass:

$$\begin{aligned} m_m = &-\frac{m_L}{EI_0}\int_0^L \frac{d^2\Phi_m(X)}{dX^2}\Phi_m(X)\,dX + \frac{m_L\alpha^2}{EI_\infty}\int_0^L \Phi_m^2(X)\,dX + \\ &\sum_{h=1}^{2}\Phi_m(X_b)C_h\left[\Phi_m(X_b,t)\right] \end{aligned} \tag{4.48}$$

The ordinary equation for modal coordinate $R_m(t)$, is written as:

$$\frac{d^2R_m(t)}{dt^2} + \omega_m^2 R_m(t) = \frac{1}{m_m} V_m(t) \quad , \quad m = 1, ..., \infty \tag{4.49}$$

with modal loading V_m:

$$V_m(t) = \frac{\alpha^2}{EI_\infty} \int_0^L \Phi_m(X) \sum_{ii=1}^{NL} F_{ii}\delta\left(X - V_0\, t + S_{ii}\right)\left[H\left(t - t_{ii}^0\right) - H\left(t - t_{ii}^E\right)\right] dX$$

$$-\frac{1}{EI_0} \int_0^L \Phi_m(X) \sum_{ii=1}^{NL} F_{ii}\delta^{(2)}\left(X - V_0\, t + S_{ii}\right)\left[H\left(t - t_{ii}^0\right) - H\left(t - t_{ii}^E\right)\right] dX \tag{4.50}$$

Within a linear theory, assuming proportional viscous damping, Eq.(4.49) can be modified as:

$$\frac{d^2R_m(t)}{dt^2} + 2\zeta_m\omega_m \frac{dR_m(t)}{dt} + \omega_m^2 R_m(t) = \frac{1}{m_m} V_m(t) \tag{4.51}$$

For quiet initial conditions, the time domain solution of Eq.(4.51) is given by the well-known Duhamel's convolution integral:

$$R_m(t) = \frac{1}{m_m\omega_{dm}} \int_0^t V_m(\tau)\, exp\left[-\zeta_m\omega_m(t-\tau)\right] sin\left[\omega_{dm}(t-\tau)\right] d\tau \tag{4.52}$$

with the mth damped natural frequency $\omega_{dm} = \omega_m\sqrt{1-\zeta_m^2}$.

4.5 Numerical Applications

In the following numerical applications, both free vibrations and dynamic response to moving multi-loads are analyzed, for two different layered beams.

4.5.1 Example A

Consider the simply-supported two-layered beam of length $L = 40\ m$ composed of a concrete deck (upper layer) and two symmetrically arranged steel girders (lower layer), as shown in Fig.4.4. The layer parameters are [5]:

$A_1 = 2.08\ m^2, E_1 = 33\ 10^9\ N/m^2, E_1 I_1 = 61.2\ 10^7\ Nm^2$ for the upper layer and $A_2 = 0.195\ m^2$, $E_2 = 210\ 10^9\ N/m^2$, $E_2 I_2 = 42.5\ 10^9\ Nm^2$ for the lower layer. The mass per unit length is $m_L = 15000\ kg/m$, and $r = 1.98\ m$ is the distance between the centroids of the individual layers. The effect of the steel anchor bolts, which couple flexibly the two layers, is modeled as continuous elastic connection with slip modulus $k_s = 10^7\ N/m^2$.

The bridge is subjected to the high-speed train used in chapter 3, but in this application in dimensional way. In particular, according to Fig. 4.4: $h = c = 2.80\,m$, $b = e = 2.27\,m$, $g = 13\ m$, and $d = 24.34\,m$. The axle loads of the rail cars and passenger cars are respectively 200 kN and 116.5 kN. In the current application it is assumed that the loads cross the beam with the first critical speed of first order, i.e. $V_0 = \omega_1 d/2\pi$ [105], yielding $V_0 = 43.22\,m/s$ for the fundamental circular beam frequency $\omega_1 = 11.16\,rad/s$.

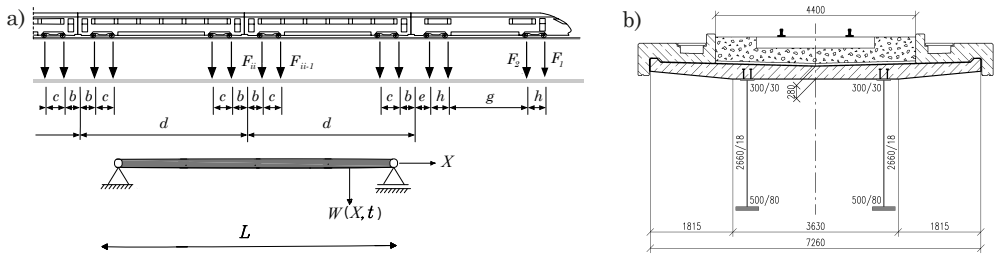

Figure 4.4: Simply-supported two-layered beam under multi-moving loads [1]

In Table 4.1 the first five natural frequencies of the beam, built by using Eq.(4.43), are listed. Additionally, in Table 4.1 the natural frequencies of the rigidly bonded beam (i.e. without interlayer slip) are specified. The frequencies of this beam configuration are much larger, emphasizing the importance of the interlayer connection.

Figure 4.5 shows the eigenfunctions of mode 1 for all response variables of the two-layered elastically bonded beam. The corresponding eigenfunctions of the rigidly bonded beam are also reported for comparison.

Next, the dynamic beam response to the high-speed train, shown in (Fig.4.4), is investigated.

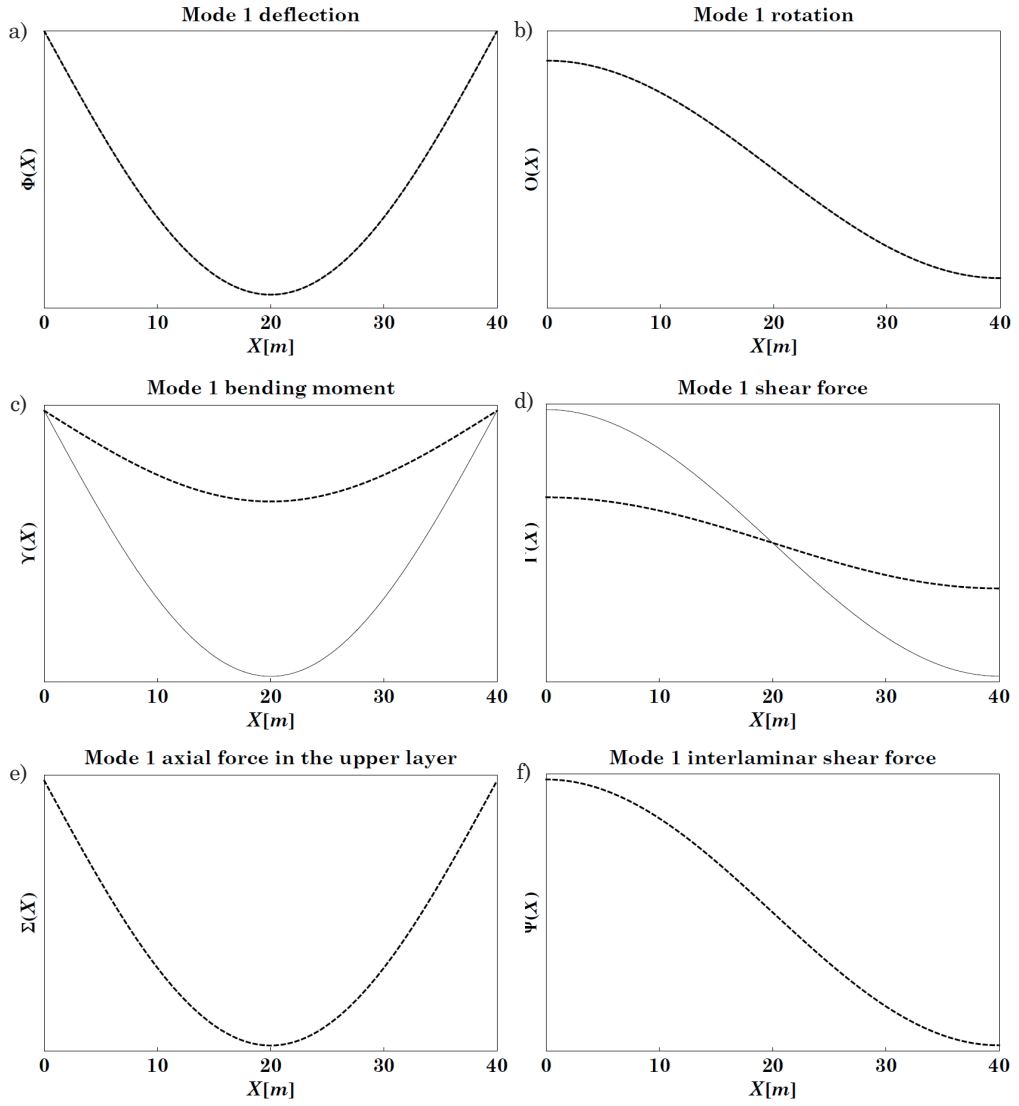

Figure 4.5: Beam in Fig.4.4: mode 1 eigenfunctions for the elastically bonded beam (black dashed line) and for the rigidly bonded beam (black solid line): (a) deflection, (b) rotation, (c) total bending moment, (d) axial force in the upper layer, (e) shear force, (f) interlaminar shear force.

Table 4.1: First five natural frequencies of the elastically bonded beam in Fig.4.4 (first column) and the corresponding rigidly bonded beam (second column)

Natural frequency [*rad/s*]	
Elastically bonded beam	Rigidly bonded beam
11.16	19.09
42.58	76.36
94.88	171-81
168.08	305.44
262.20	477.25

In particular Fig. 4.6 shows the deflection at the mid span of the two-layered elastically bonded beam and the corresponding rigidly bonded beam.

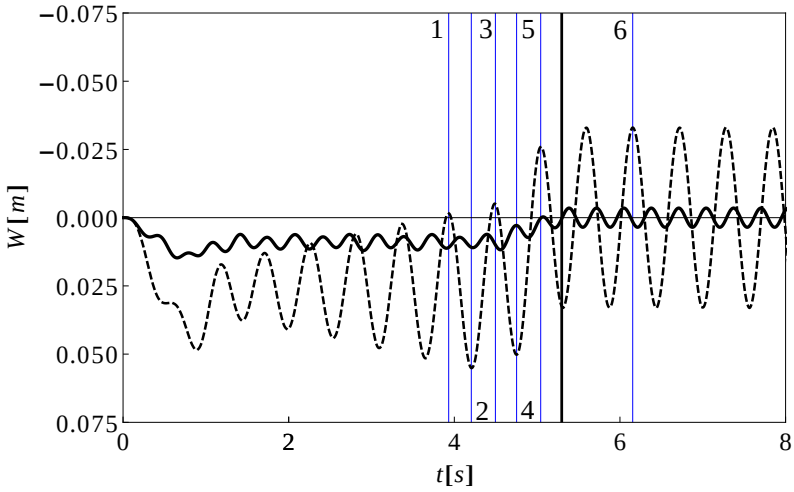

Figure 4.6: Time history of the mid-span deflection of the two-layered elastically bonded beam shown in Fig.4.4 (black dashed line) and for the rigidly bonded beam (black solid line)

The deflection over the whole domain at six time instants, specified in Fig.4.6 by numbers 1 to 6, for the two-layered elastically bonded beam, is depicted in Fig.4.7. Additionally, also the displacement considering only the first eigenfunction for time instant 5 is shown (red solid line). No significant

changes are found when considering more than four modes in the proposed solution, thus, the results shown are based on a five mode series approximation.

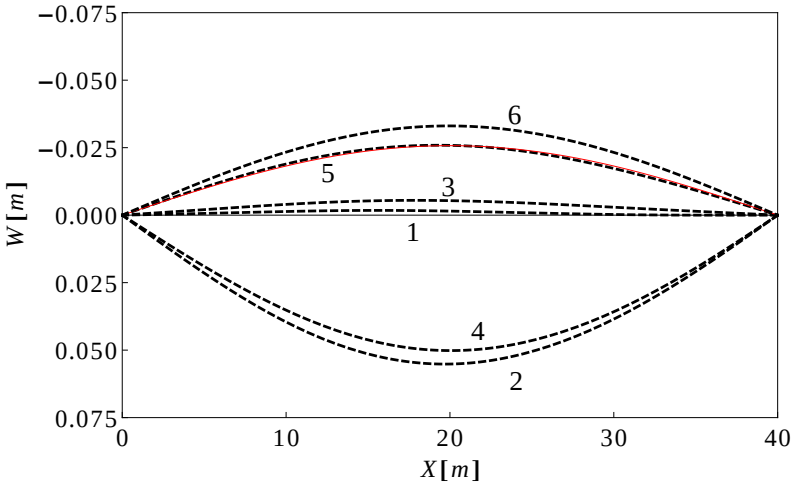

Figure 4.7: Deflection over span of the the two-layered elastically bonded beam shown in Fig.4.4. Black dashed lines: multi-mode response at six time instants specified in Fig.4.6 ($t_1 = 3.93\ s$, $t_2 = 4.20\ s$, $t_3 = 4.49\ s$, $t_4 = 4.75\ s$, $t_5 = 5.04\ s$, $t_6 = 6.15\ s$). Red solid line: first mode response at time instant t_5. Red solid line: first mode response at time instant t_5

Finally, the deflection at the mid span of the two-layered elastically bonded viscous beam is shown in Fig. 4.8. Modal damping with with coefficient $\zeta_m = 0.05$ for all modes is considered.

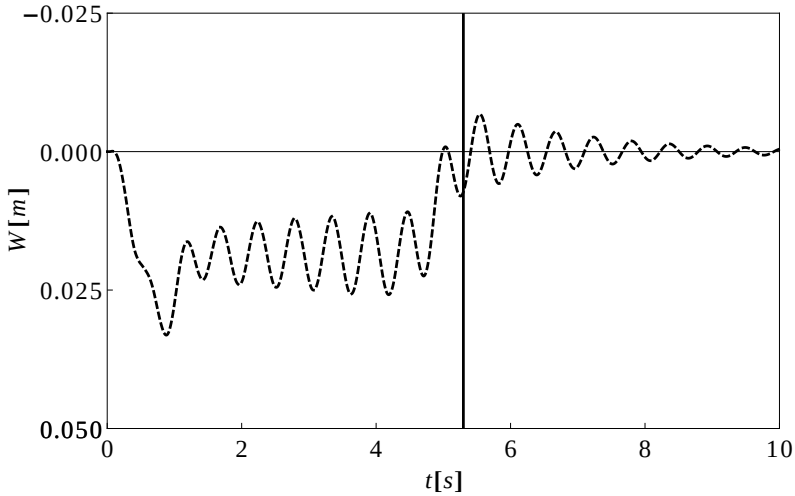

Figure 4.8: Time history of the mid-span deflection of the two-layered elastically bonded viscous beam shown in Fig.4.4

4.5.2 Example B

The two-layered elastically bonded beam of the previous example is now considered in clamped-clamped boundary condition Fig.4.9.

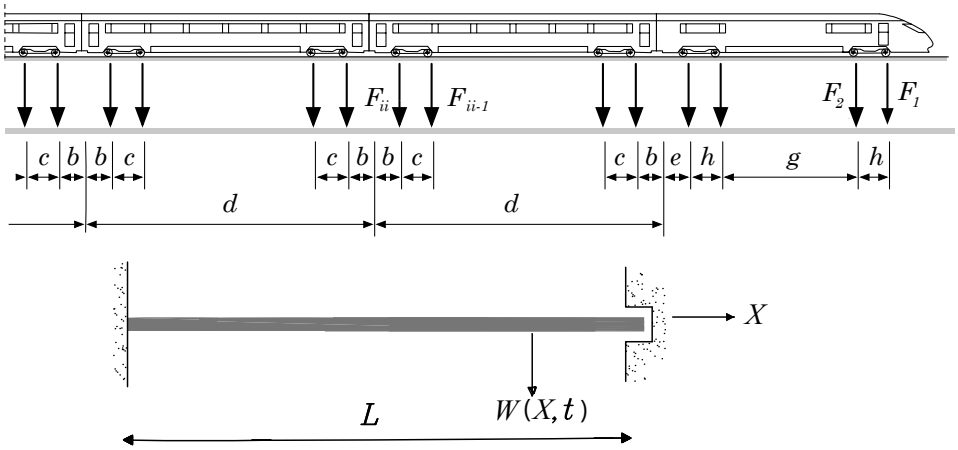

Figure 4.9: Clamped-clamped two-layered elastically bonded beam [1]

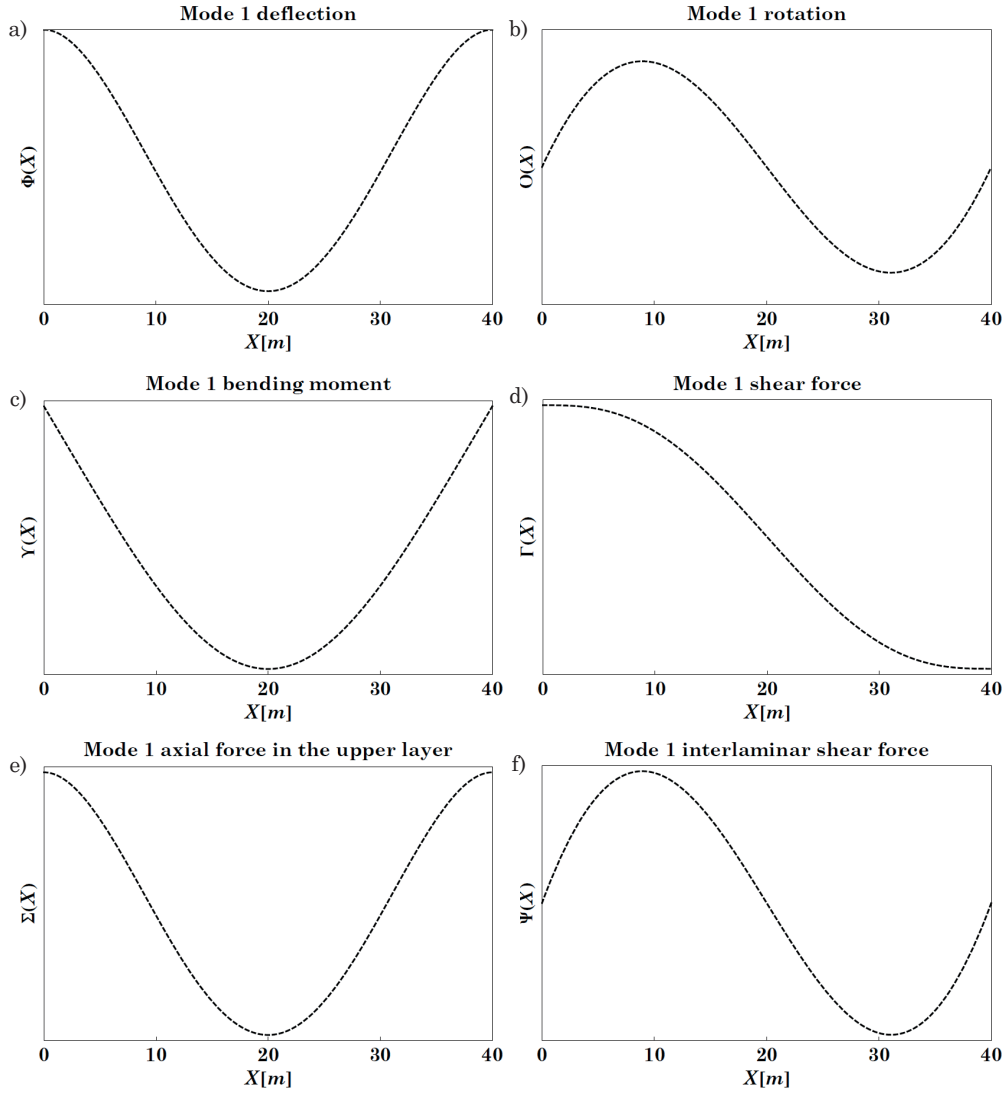

Figure 4.10: Beam in Fig.4.9: mode 1 eigenfunctions for the elastically bonded beam: (a) deflection, (b) rotation, (c) total bending moment, (d) axial force in the upper layer, (e) shear force, (f) interlaminar shear force.

Figure 4.10 shows the eigenfunctions of mode 1 for all response variables of the two-layered elastically bonded beam in Fig.4.9 while the first five natu-

ral frequencies, built by using Eq.(4.43), are listed in Table 4.2.

Table 4.2: First five natural frequencies of the elastically bonded beam in Fig.4.9

Modes	Natural frequency [*rad/s*]
1	24.12
2	65.91
3	128.73
4	212.42
5	317.02

Figure 4.11 shows the deflection at the mid span of the two-layered elastically bonded beam subjected to the high-speed train, shown in (Fig.4.9) that cross the beam with the first critical speed of first order, $V_0 = 93.43\,m/s$. Five modes have been considered also in this example, because no significant changes were found when considering more than four modes.

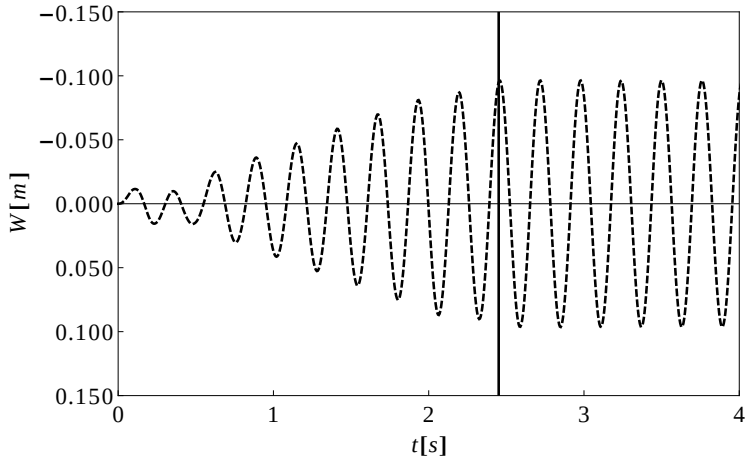

Figure 4.11: Time history of the mid-span deflection of the two-layered elastically bonded beam shown in Fig.4.9

Finally, for comparison, the deflection at the mid span of the two-layered elastically bonded viscous beam subjected to the same loads conditions, is shown in Fig. 4.12. Modal damping with with coefficient $\zeta_m = 0.05$ for all modes is considered.

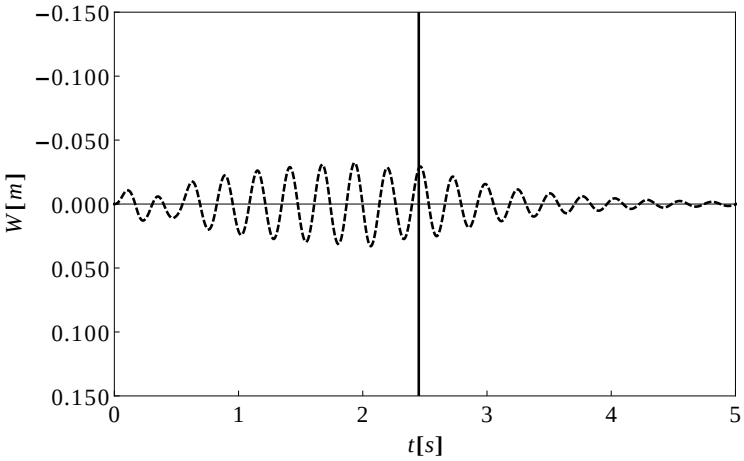

Figure 4.12: Time history of the mid-span deflection of the two-layered elastically bonded viscous beam shown in Fig.4.9

4.6 Concluding remarks

The dynamic flexural behavior of two-layered elastically bonded beams has been presented. From a characteristic equation built as determinant of a 6 x 6 matrix, the exact eigenfunctions of all response variables has been derived. Based on pertinent orthogonality conditions for deflection modes, the dynamic response has been built in time domain by modal superposition. Efficiency and accuracy of the proposed method have been shown for a two-layered elastically bonded beam in two different boundary conditions configuration.

Chapter 5

Novel approach to the moving multi-loads problem in discontinuous beam structures with interlayer slip

This chapter addresses the dynamic flexural behavior of two-layered elastically bonded beams carrying an arbitrary number of elastic translational supports and rotational joints, under moving multi-loads. As discussed for the continuous layered elastically bonded beams, the Euler-Bernoulli hypothesis is assumed to hold for each layer separately, and a linear constitutive relation between the horizontal interlayer slip and the interlaminar shear force is considered. Based on the theory of generalized functions to handle the discontinuities of response variables due to supports/joints, exact beam modes are obtained from a characteristic equation built as determinant of a 6 x 6 matrix, regardless of the number of supports/joints. On using pertinent orthogonality condition for the deflection modes, the dynamic response of the beam under moving multi-loads is derived in time domain. Remarkably, all response variables are presented in a closed analytical form. Four numerical applications illustrate the efficiency of the proposed method.

5.1 Preliminary remarks

In practical applications, beams have one or several in-span elastic supports, and in-span local flexibility may arise from cracks and imperfections, whether the beams are layered or not [9, 10, 12, 106–110]. In this case, the corresponding structural model is a *discontinuous* beam, for the presence of the elastic translational supports and elastic rotational joints, as mentioned several times in this thesis.

For discontinuous homogeneous beams, i.e beams made of a single material, an innovative modal superposition approach, based on exact analytical modes derived by the theory of generalized functions [31–42], has been discussed in chapters 2 and 3 and published in Refs.[29, 30, 68].

In the present chapter, the theory of generalized functions is used to reformulate and solve the moving multi-loads problem of the two-layered elastically bonded beams with elastic translational supports and rotational joints. This approach has been proposed in a paper published by myself and co-authors in the International journal "Composites Part B" [111] and in Refs. [112, 113]

First, the governing equations of motion are presented. Then, a modal superposition approach is applied to build the dynamic response of the discontinuous layered elastically bonded beams under moving multi-loads. The exact modes derived from an eigenvalue problem involving a 6×6 matrix, for any number of supports/joints. This result is obtained thanks to novel solutions of the equation of motion, built via the theory of generalized functions. Finally four illustrative examples are reported.

5.2 Equation of motion for discontinuous layered beam under moving multi-loads

The dynamic response of a beam composed of two elastically bonded layers, under moving multi-loads and carrying an arbitrary number N of elastic translational supports and elastic rotational joints at abscissas X_j along the longitudinal (X-) axis, as shown in Fig.5.1, is analyzed. As in the previous chapter, the beam, composed by two layers disposed about the transverse (Z-) beam axis, is subjected to a series of NL concentrated loads F_{ii} ($i = 1, ..., NL$) along the longitudinal (X-), with constant velocity V_0.

The dynamic lateral beam deflection $W(X,t)$, is assumed to be the same

for each fiber at given X, under the assumption of small deformations.

Also in this case, neglecting the effect of rotatory and longitudinal inertia and in absence of external axial forces [95], conservation of momentum in transverse direction, conservation of the angular momentum about the Y-axis, and conservation of momentum in axial direction for the beam element, yield the following equations of motion:

$$\begin{aligned}
&\frac{\bar{\partial} Q\left(X,t\right)}{\partial X} = -\sum_{ii=1}^{NL} F_{ii}\delta\left(X - V_0\ t + S_{ii}\right)\left[H\left(t - t_{ii}^{0}\right) - H\left(t - t_{ii}^{E}\right)\right] - \\
&P_j(t)\ \delta\left(X - X_j\right) + m_L \frac{\partial^2 W\left(X,t\right)}{\partial t^2} \\
&\frac{\bar{\partial} M\left(X,t\right)}{\partial X} = Q\left(X,t\right) \\
&\frac{\bar{\partial} N\left(X,t\right)}{\partial X} = -T_1(X,t) + T_2(X,t) = 0
\end{aligned} \tag{5.1}$$

in which the space-derivatives are generalized derivatives, as denoted by the over-bar, to capture the discontinuities of response variables at the elastic supports and joints.

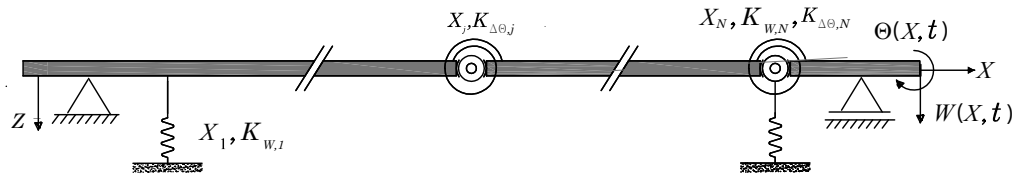

Figure 5.1: Discontinuous two-layered elastically bonded beam

Dirac's delta function $\delta()$ describes the effect of the reaction force $P_j(t)$ exerted by the j-th elastic translational support of stiffness $K_{W,j}$:

$$P_j(t) = -K_{W,j} W\left(X_j, t\right) \tag{5.2}$$

As discussed in chapter 4, it is possible to express the total shear force $Q(X,t)$, the total bending moment $M(X,t)$ and the total axial force $N(X,t)$ in

terms of the layer stress resultants Eq.(4.2) that in this case, in according with Fig.4.2 result to be:

$$
\begin{aligned}
Q_i(X,t) &= \frac{\partial M_i\left(X,t\right)}{\partial X} + T_i(X,t)\, r_i \\
M_i(X,t) &= E_i I_i \left[-\frac{\bar{\partial}^2 W\left(X,t\right)}{\partial X^2} + \Delta\Theta_j(t)\, \delta\left(X - X_j\right) \right] \quad , \quad i = 1,2 \\
N_i(X,t) &= E_i A_i \frac{\partial U_i\left(X,t\right)}{\partial X}
\end{aligned}
\tag{5.3}
$$

The relative rotation $\Delta\Theta_j(t)$ at the jth elastic rotational joint is related to the corresponding bending moment $M\left(X_j,t\right)$ according to:

$$
\Delta\Theta_j(t) = \Theta\left(X_j^+,t\right) - \Theta\left(X_j^-,t\right) = -\frac{M\left(X_j,t\right)}{K_{\Delta\Theta,j}} \tag{5.4}
$$

where $\Theta(X,t) = \bar{\partial} W\left(X,t\right)/\partial X$ is the rotation of the cross section, assumed to be equal for both layers, while $K_{\Delta\Theta,j}$ denotes the stiffness of the j-th rotational joint.

Again, assuming the elastic behaviour $T(X,t) = k_s\, \Delta U(X,t)$, between the interlaminar shear force $T(X,t)$ and the interlaminar slip $\Delta U\left(X,t\right)$ expressed as:

$$
\Delta U\left(X,t\right) = U_2\left(X,t\right) - U_1\left(X,t\right) + r\frac{\bar{\partial} W\left(X,t\right)}{\partial X} \tag{5.5}
$$

Differentiation of $T(X,t) = k_s\, \Delta U(X,t)$ with respect to X, together with Eqs.(5.5),(5.3c),(4.2c) and $\bar{\partial} N_1\left(X,t\right)/\partial X = -T(X,t)$, yields to the following equation:

$$
r\frac{\bar{\partial}^2 W\left(X,t\right)}{\partial X^2} + \frac{1}{k_s}\frac{\bar{\partial}^2 N_1\left(X,t\right)}{\partial X^2} - N_1\left(X,t\right)\left(\frac{1}{E_1 A_1} + \frac{1}{E_2 A_2}\right) = 0 \tag{5.6}
$$

Combining Eq.(5.3b) and Eq.(4.2b) allows the axial force in the upper layer $N_1(X,t)$ to be expressed as a function of the total bending moment $M(X,t)$ and the kinematic variables $W(X,t)$ and $\Delta\Theta_j(t)$:

$$
N_1\left(X,t\right) = -\frac{1}{r}\left[M\left(X,t\right) + EI_0\left(\frac{\bar{\partial}^2 W\left(X,t\right)}{\partial X^2} - \Delta\Theta_j(t)\, \delta\left(X - X_j\right) \right) \right] \tag{5.7}
$$

Subsequently, Eq.(5.7) and its second derivative with respect to X are substituted into Eq.(5.6), obtaining:

$$\frac{\bar{\partial}^4 W(X,t)}{\partial X^4} - \alpha^2 \frac{\bar{\partial}^2 W(X,t)}{\partial X^2} + k_s \frac{EA_0}{EA_p} \Delta\Theta_j(t)\, \delta\left(X - X_j\right) - \Delta\Theta_j(t)\, \delta^{(2)}\left(X - X_j\right) =$$

$$+ \frac{\alpha^2}{EI_\infty} M(X,t) - \frac{1}{EI_0} \frac{\bar{\partial}^2 M(X,t)}{\partial X^2} \tag{5.8}$$

In this equation, $\delta^{(2)}\left(X - X_j\right)$ denotes the second derivative of the Dirac's Delta function at X_j with respect to X.

Twice differentiation of Eq.(5.8) with respect to X and using Eqs.(4.1a,b) finally yields the equation of motion in terms of $W(X,t)$,

$$\frac{\bar{\partial}^6 W(X,t)}{\partial X^6} - \alpha^2 \frac{\bar{\partial}^4 W(X,t)}{\partial X^4} + \frac{m_L}{EI_0} \frac{\bar{\partial}^4 W(X,t)}{\partial X^2 \partial t^2} - \frac{m_L\, \alpha^2}{EI_\infty} \frac{\partial^2 W(X,t)}{\partial t^2} +$$

$$+ \frac{\alpha^2}{EI_\infty} P_j(t)\, \delta\left(X - X_j\right) - \frac{P_j(t)}{EI_0}\, \delta^{(2)}\left(X - X_j\right) + k_s \frac{EA_0}{EA_p} \Delta\Theta_j(t)\, \delta^{(2)}\left(X - X_j\right)$$

$$- \Delta\Theta_j(t)\, \delta^{(4)}\left(X - X_j\right) = - \frac{\alpha^2}{EI_\infty} \sum_{ii=1}^{NL} F_{ii} \delta\left(X - V_0\, t + S_{ii}\right) \left[H\left(t - t_{ii}^0\right) - H\left(t - t_{ii}^E\right)\right]$$

$$+ \frac{1}{EI_0} \sum_{ii=1}^{NL} F_{ii} \delta^{(2)}\left(X - V_0\, t + S_{ii}\right) \left[H\left(t - t_{ii}^0\right) - H\left(t - t_{ii}^E\right)\right] \tag{5.9}$$

Note that, in Eq.(5.9), the reaction force $P_j(t)$ exerted by the j-th translational support and the relative rotation $\Delta\Theta_j(t)$ at the j-th rotational joint are unknown quantities.

In the present formulation, both limits $\alpha \to \infty$ (rigidly bonded beam) and $\alpha \to 0$ (no bonded beam) can be taken into account without numerical difficulties. If no supports and joints are present then $P_j = 0$ and $\Delta\Theta_j = 0$ for any j. In such case, Eq.(5.9) reverts to the equations of motion of two-layered elastically bonded beam without discontinuities Eq.(4.12), as shown in [95] and [96].

The solution of Eq.(5.9) is found together with the initial conditions $W(X, t = 0) = 0$, $\partial W(X, t = 0)/\partial t = 0$, and the beam boundary conditions. In the following, three classical boundary conditions are reported [96], with $X_b = 0, L$ denoting the beam ends.

(*i*) Simply supported end according to Eq.(4.13)

(*ii*) Free end according to Eq.(4.14)

(*iii*) Clamped end:

$$W\left(X_b, t\right) = 0 \qquad \frac{\bar{\partial} W\left(X_b, t\right)}{\partial X} = 0 \qquad \Delta U\left(X_b, t\right) = 0 \tag{5.10}$$

Upon solving Eq.(5.9) for $W(x, t)$, the stress resultants $M(X, t)$, $Q(X, t)$, $N_1(X, t)$ and the interlaminar shear force per unit length $T(X, t)$ can be built from Eqs.(5.8), (5.1a,b), (5.7), and (5.1c), (4.2c), respectively.

In particular, the bending moment $M(X, t)$ from Eqs.(5.8) and (5.1a,b) become

$$\begin{aligned} M\left(X, t\right) = & -EI_\infty \frac{\bar{\partial}^2 W\left(X, t\right)}{\partial X^2} + \frac{EI_\infty}{\alpha^2}\left(\frac{\bar{\partial}^4 W\left(X, t\right)}{\partial X^4} + \frac{m_L}{EI_0}\frac{\partial^2 W\left(X, t\right)}{\partial t^2}\right) + \\ & \frac{k_s\, EA_0 EI_\infty}{EA_p \alpha^2}\Delta\Theta_j(t)\, \delta\left(x - x_j\right) - \frac{EI_\infty}{\alpha^2}\Delta\Theta_j(t)\, \delta^{(2)}\left(x - x_j\right) + \\ & \frac{EI_\infty}{EI_0 \alpha^2}\left(-\sum_{ii=1}^{NL} F_{ii}\delta\left(X - V_0\, t + S_{ii}\right)\left[H\left(t - t_{ii}^0\right) - H\left(t - t_{ii}^E\right)\right] - P_j(t)\, \delta\left(X - X_j\right)\right) \end{aligned} \tag{5.11}$$

the transverse shear force from Eq.(5.1b):

$$Q\left(X,t\right)=-EI_{\infty}\frac{\bar{\partial}^{3}W\left(X,t\right)}{\partial X^{3}}+\frac{EI_{\infty}}{\alpha^{2}}\left(\frac{\bar{\partial}^{5}W\left(X,t\right)}{\partial X^{5}}+\frac{m_{L}}{EI_{0}}\frac{\bar{\partial}^{3}W\left(X,t\right)}{\partial X\partial t^{2}}\right)$$
$$+\frac{k_{s}\ EA_{0}EI_{\infty}}{EA_{p}\alpha^{2}}\Delta\Theta_{j}(t)\ \delta^{(1)}\left(X-X_{j}\right)-\frac{EI_{\infty}}{\alpha^{2}}\Delta\Theta_{j}(t)\ \delta^{(3)}\left(X-X_{j}\right)+$$
$$\frac{EI_{\infty}}{EI_{0}\alpha^{2}}\left(-\sum_{ii=1}^{NL}F_{ii}\delta^{(1)}\left(X-V_{0}\ t+S_{ii}\right)\left[H\left(t-t_{ii}^{0}\right)-H\left(t-t_{ii}^{E}\right)\right]-P_{j}(t)\ \delta^{(1)}\left(X-X_{j}\right)\right) \tag{5.12}$$

the axial force in the upper layer from Eq.(5.7)):

$$N_{1}\left(X,t\right)=-\frac{1}{r}\left[\left(EI_{0}-EI_{\infty}\right)\frac{\bar{\partial}^{2}W\left(X,t\right)}{\partial X^{2}}+\frac{EI_{\infty}}{\alpha^{2}}\left(\frac{\bar{\partial}^{4}W\left(X,t\right)}{\partial X^{4}}+\frac{m_{L}}{EI_{0}}\frac{\partial^{2}W\left(X,t\right)}{\partial t^{2}}\right)\right]+$$
$$\frac{1}{r}\Delta\Theta_{j}(t)\ \delta\left(X-X_{j}\right)-\frac{k_{s}\ EA_{0}EI_{\infty}}{r\ EA_{p}\alpha^{2}}\Delta\Theta_{j}(t)\ \delta\left(X-X_{j}\right)+\frac{EI_{\infty}}{r\ \alpha^{2}}\Delta\Theta_{j}(t)\ \delta^{(2)}\left(X-X_{j}\right)-$$
$$\frac{EI_{\infty}}{r\ EI_{0}\alpha^{2}}\left(-\sum_{ii=1}^{NL}F_{ii}\delta\left(X-V_{0}\ t+S_{ii}\right)\left[H\left(t-t_{ii}^{0}\right)-H\left(t-t_{ii}^{E}\right)\right]-P_{j}(t)\ \delta\left(X-X_{j}\right)\right) \tag{5.13}$$

the axial force in the lower layer:

$$N_{2}\left(X,t\right)=-N_{1}\left(X,t\right) \tag{5.14}$$

and the interlaminar shear force from Eqs.(5.7), and (5.1c)):

$$T(X,t) = -\frac{\bar{\partial} N_1(X,t)}{\partial X} =$$

$$\frac{1}{r}\left[\left(EI_0 - EI_\infty\right)\frac{\bar{\partial}^3 W(X,t)}{\partial X^3} + \frac{EI_\infty}{\alpha^2}\left(\frac{\bar{\partial}^5 W(X,t)}{\partial X^5} + \frac{m_L}{EI_0}\frac{\bar{\partial}^3 W(X,t)}{\partial X \partial t^2}\right)\right] -$$

$$\frac{1}{r}\Delta\Theta_j(t)\,\delta^{(1)}\left(X - X_j\right) + \frac{k_s\, EA_0 EI_\infty}{r\, EA_p \alpha^2}\Delta\Theta_j(t)\,\delta^{(1)}\left(X - X_j\right) - \frac{EI_\infty}{r\,\alpha^2}\Delta\Theta_j(t)\,\delta^{(3)}\left(X - X_j\right) +$$

$$\frac{EI_\infty}{r\, EI_0 \alpha^2}\left(-\sum_{ii=1}^{NL} F_{ii}\delta\left(X - V_0\, t + S_{ii}\right)\left[H\left(t - t_{ii}^0\right) - H\left(t - t_{ii}^E\right)\right] - P_j(t)\,\delta^{(1)}\left(X - X_j\right)\right) \tag{5.15}$$

5.3 Beam modes

Here, the forced vibration problem of the beam shown in Fig.5.1 is solved through modal analysis, thus requiring eigenfunctions and natural frequencies.

5.3.1 Eigenvalue problem

As solved in the previous chapter, based on the standard separate variables approach, the following sixth order ordinary differential equation for the deflection eigenfunction $\Phi(X)$ of the two-layered elastically bonded beam with elastic supports/joints, is obtained:

$$\frac{\bar{d}^6\Phi(X)}{dX^6} - \alpha^2\frac{\bar{d}^4\Phi(X)}{dX^4} - \frac{m_L\omega^2}{EI_0}\frac{\bar{d}^2\Phi(X)}{dX^2} + \frac{m_L\,\alpha^2\omega^2}{EI_\infty}\Phi(X) + \frac{\alpha^2}{EI_\infty}b_j\,\delta\left(X - X_j\right)$$

$$-\frac{b_j}{EI_0}\,\delta^{(2)}\left(X - X_j\right) + k_s\frac{EA_0}{EA_p}\Delta O_j\,\delta^{(2)}\left(X - X_j\right) - \Delta O_j\,\delta^{(4)}\left(X - X_j\right) = 0 \tag{5.16}$$

The eigenfunctions for the bending moment $\Upsilon(x)$, the shear force $\Gamma(x)$, the axial force in the upper layer $\Sigma(x)$, and the elastic interlaminar shear force

$\Psi(x)$, are similarly obtained from Eqs.(5.11), (5.12), (5.13) and (5.15):

$$\begin{aligned}\Upsilon(X) = &-EI_\infty \frac{\bar{d}^2\Phi(X)}{dX^2} + \frac{EI_\infty}{\alpha^2}\left(\frac{\bar{d}^4\Phi(X)}{dX^4} - \frac{m_L\,\omega^2}{EI_0}\Phi(X)\right) + \\ &\frac{k_s\,EA_0\,EI_\infty}{EA_p\,\alpha^2}\Delta O_j\,\delta(X - X_j) - \frac{EI_\infty}{\alpha^2}\Delta O_j\,\delta^{(2)}(X - X_j) - \\ &\frac{EI_\infty}{EI_0\,\alpha^2}\,b_j\,\delta(X - X_j)\end{aligned} \tag{5.17}$$

$$\begin{aligned}\Gamma(X) = &-EI_\infty \frac{\bar{d}^3\Phi(X)}{dX^3} + \frac{EI_\infty}{\alpha^2}\left(\frac{\bar{d}^5\Phi(X)}{dX^5} - \frac{m_L\,\omega^2}{EI_0}\frac{\bar{d}\Phi(X)}{dX}\right) + \\ &\frac{k_s\,EA_0\,EI_\infty}{EA_p\,\alpha^2}\Delta O_j\,\delta^{(1)}(X - X_j) - \frac{EI_\infty}{\alpha^2}\Delta O_j\,\delta^{(3)}(X - X_j) - \\ &\frac{EI_\infty}{EI_0\,\alpha^2}\,b_j\,\delta^{(1)}(X - X_j)\end{aligned} \tag{5.18}$$

$$\begin{aligned}\Sigma(X) = &-\frac{1}{r}\left[(EI_0 - EI_\infty)\frac{\bar{d}^2\Phi(X)}{dX^2} + \frac{EI_\infty}{\alpha^2}\left(\frac{\bar{d}^4\Phi(X)}{dX^4} - \frac{m_L\,\omega^2}{EI_0}\Phi(X)\right)\right] + \\ &\frac{1}{r}\Delta O_j\,\delta(X - X_j) - \frac{k_s\,EA_0\,EI_\infty}{r\,EA_p\,\alpha^2}\Delta O_j\,\delta(X - X_j) + \frac{EI_\infty}{r\,\alpha^2}\Delta O_j\,\delta^{(2)}(X - X_j) + \\ &\frac{EI_\infty}{r\,EI_0\,\alpha^2}\,b_j\,\delta(X - X_j)\end{aligned} \tag{5.19}$$

$$\Psi(X) = \frac{1}{r}\left[(EI_0 - EI_\infty)\frac{\bar{d}^3\Phi(X)}{dX^2} + \frac{EI_\infty}{\alpha^2}\left(\frac{\bar{d}^5\Phi(X)}{dX^4} - \frac{m_L\,\omega^2}{EI_0}\frac{\bar{d}\Phi(X)}{dX}\right)\right] -$$

$$\frac{1}{r}\Delta O_j\,\delta^{(1)}(X - X_j) + \frac{k_s\,EA_0\,EI_\infty}{r\,EA_p\,\alpha^2}\Delta O_j\,\delta^{(1)}(X - X_j) -$$

$$\frac{EI_\infty}{r\,\alpha^2}\Delta\Theta_j\,\delta^{(3)}(X - X_j) - \frac{EI_\infty}{r\,EI_0\,\alpha^2}\,b_j\,\delta^{(1)}(X - X_j) \tag{5.20}$$

The eigenfunction of rotation $O(X)$ is found considering that:

$$O(x) = \frac{\bar{d}\Phi(X)}{dX} \tag{5.21}$$

Unknown quantities b_j and ΔO_j, appearing in Eq.(5.16) at the application points of the supports/joints, are given by Eq.(5.2) and Eq.(5.4), respectively:

$$b_j = -K_{W,j}\Phi(X_j) \tag{5.22}$$

$$\Delta O_j = -\frac{\Upsilon(X_j)}{K_{\Delta O,j}} \tag{5.23}$$

Next, based on a procedure proposed in [29] a novel approach for evaluation of the eigenfunctions of the discontinuous two-layered elastically bonded beam problem is introduced.

For this purpose, as proposed in the previous Chapter for the two-layered elastically bonded beam, the eigenfunctions of the response variables are collected in the vector $\mathbf{\Upsilon}(X) = \left[\begin{array}{cccccc}\Phi(X) & O(X) & \Upsilon(X) & \Gamma(X) & \Sigma(X) & \Psi(X)\end{array}\right]^T$, and $T_j = \left[\begin{array}{cc} b_j & \Delta O_j \end{array}\right]$ is the vector of the unknown quantities b_j and ΔO_j at the application points of the elastic supports and joints. Based on the linear superposition principle, vector $\mathbf{\Upsilon}(X)$ is built as the sum of the solution $\mathbf{\Omega}(X)\,\mathbf{c}$ to the homogeneous equation associated with Eq.(5.16), representing the eigenfunctions of the two-layered elastically bonded beam considered in Chapter 4 (i.e. the beam without supports/joints) Eq.(4.34-4.38), and the particular solution $\mathbf{J}(X, X_j)\mathbf{\Lambda}_j$ associated with the unknowns b_j and ΔO_j, which account for the discontinuities of the response variables at support and joint locations, respectively:

$$\mathbf{Y}(X) = \mathbf{\Omega}(X)\,\mathbf{c} + \sum_{j=1}^{N} \mathbf{J}\left(X, X_j\right)\,\mathrm{T}_j \tag{5.24}$$

In Eq.(5.24), all terms associated with a unit transverse force $b_j = 1$ and a unit relative rotation $\Delta\mathrm{O_j} = 1$, applied at $X = X_j$, respectively, and defined as:

$$\mathbf{J}\left(X, X_j\right) = \left[\begin{array}{cc} \mathbf{J}^{(b)} & \mathbf{J}^{(\Delta\mathrm{O})} \end{array}\right] = \left[\begin{array}{cc} J_{\Phi}^{(b)} & J_{\Phi}^{(\Delta\mathrm{O})} \\ J_{\mathrm{O}}^{(b)} & J_{\mathrm{O}}^{(\Delta\mathrm{O})} \\ J_{\mathrm{Y}}^{(b)} & J_{\mathrm{Y}}^{(\Delta\mathrm{O})} \\ J_{\Gamma}^{(b)} & J_{\Gamma}^{(\Delta\mathrm{O})} \\ J_{\Sigma}^{(b)} & J_{\Sigma}^{(\Delta\mathrm{O})} \\ J_{\Psi}^{(b)} & J_{\Psi}^{(\Delta\mathrm{O})} \end{array}\right] \tag{5.25}$$

are available through Mathematica [52] after some mathematical manipulations in the following simple analytical form, involving the generalized functions:

$$\begin{aligned} J_{\Phi}^{(P)} = {} & H(X - X_j)\left[EI_{\infty}\,{EI_0}^2/b\right](R_2 - R_3)(R_1 - R_3)(R_1 - R_2) \\ & \left\{\left[\left(\frac{R_2 - R_3}{\sqrt{R_1}}\right)\left(EI_{\infty}R_1 - EI_0\alpha^2\right)\right]\sinh\left(\sqrt{R_1}(X - X_j)\right)\right. \\ & -\left[\left(\frac{R_1 - R_3}{\sqrt{R_2}}\right)\left(EI_{\infty}R_2 - EI_0\alpha^2\right)\right]\sinh\left(\sqrt{R_2}(X - X_j)\right) \\ & \left.+\left[\left(\frac{R_1 - R_2}{\sqrt{R_3}}\right)\left(EI_{\infty}R_3 - EI_0\alpha^2\right)\right]\sinh\left(\sqrt{R_3}(X - X_j)\right)\right\} \end{aligned} \tag{5.26}$$

while the following particular integral $J_{\Phi}^{(\Delta\mathrm{O})}$ for a relative rotation $\Delta\mathrm{O_j} = 1$ at $X = X_j$ is obtained via successive differentiation of Eq.(5.26), taking into account Eq.(5.16):

$$J_{\Phi}^{(\Delta O)}(X) = H(X - X_j)\left[\left(EI_{\infty}^2\ {EI_0}^3\right) / \left(b\ EA_p\right)\right](R_2 - R_3)(R_1 - R_3)(R_1 - R_2)$$
$$\left\{\left[\sqrt{R_1}\,(R_2 - R_3)\left(-EA_0\ k_s\ + EA_p\ R_1\right)\right]\sinh\left(\sqrt{R_1}(X - X_j)\right)\right.$$
$$-\left[\sqrt{R_2}\,(R_1 - R_3)\left(-EA_0\ k_s\ + EA_p\ R_2\right)\right]\sinh\left(\sqrt{R_2}(X - X_j)\right)$$
$$\left.+\left[\sqrt{R_3}\,(R_1 - R_2)\left(-EA_0\ k_s\ + EA_p\ R_3\right)\right]\sinh\left(\sqrt{R_3}(X - X_j)\right)\right\} \tag{5.27}$$

Symbol b is a constant defined as:

$$b = m_L\,\omega^2\left[4{EI_0}^3 EI_{\infty}\,\alpha^8 + EI_0\left(-27{EI_0}^2 + 18EI_0\ EI_{\infty} + EI_{\infty}^2\right)\alpha^4 m_L\,\omega^2\right.$$
$$\left.+\ 4EI_{\infty}^2\ m_L^2\omega^4\right] \tag{5.28}$$

Once again, according to Eqs.(5.17-5.21), the remaining particular integrals in vector $\mathbf{J}^{(p)}$ are obtained by the following relationships:

$$J_{\mathrm{O}}^{(b)}(X) = \frac{\bar{d}J_{\Phi}^{(b)}(X)}{dX} \tag{5.29}$$

$$J_{\mathrm{Y}}^{(b)}(X) = -EI_{\infty}\frac{\bar{d}^2 J_{\Phi}^{(b)}(X)}{dX^2} + \frac{EI_{\infty}}{\alpha^2}\left(\frac{\bar{d}^4 J_{\Phi}^{(b)}(X)}{dX^4} - \frac{m_L\omega^2}{EI_0}J_{\Phi}^{(b)}(X)\right) -$$
$$\frac{EI_{\infty}}{EI_0\,\alpha^2}\,\delta\left(X - X_j\right) \tag{5.30}$$

$$J_{\Gamma}^{(b)}(X) = -EI_{\infty}\frac{\bar{d}^3 J_{\Phi}^{(b)}(X)}{dX^3} + \frac{EI_{\infty}}{\alpha^2}\left(\frac{\bar{d}^5 J_{\Phi}^{(b)}(X)}{dX^5} - \frac{m_L\omega^2}{EI_0}\frac{\bar{d} J_{\Phi}^{(b)}(X)}{dX}\right) - \frac{EI_{\infty}}{EI_0\,\alpha^2}\,\delta^{(1)}\left(X - X_j\right) \tag{5.31}$$

$$J_{\Sigma}^{(b)}(X) = -\frac{1}{r}\left[\left(EI_0 - EI_{\infty}\right)\frac{\bar{d}^2 J_{\Phi}^{(b)}(X)}{dX^2} + \frac{EI_{\infty}}{\alpha^2}\left(\frac{\bar{d}^4 J_{\Phi}^{(b)}(X)}{dX^4} - \frac{m_L\omega^2}{EI_0}J_{\Phi}^{(b)}(X)\right)\right] + \frac{EI_{\infty}}{r\,EI_0\,\alpha^2}\,\delta\left(X - X_j\right) \tag{5.32}$$

$$J_{\Psi}^{(b)}(X) = \frac{1}{r}\left[\left(EI_0 - EI_{\infty}\right)\frac{\bar{d}^3 J_{\Phi}^{(b)}(X)}{dX^3} + \frac{EI_{\infty}}{\alpha^2}\left(\frac{\bar{d}^5 J_{\Phi}^{(b)}(X)}{dX^5} - \frac{m_L\omega^2}{EI_0}\frac{\bar{d} J_{\Phi}^{(b)}(X)}{dX}\right)\right] - \frac{EI_{\infty}}{r\,EI_0\,\alpha^2}\,\delta^{(1)}\left(X - X_j\right) \tag{5.33}$$

and analogously, for $\mathbf{J}^{(\Delta O)}$ as:

$$J_{O}^{(\Delta O)}(X) = \frac{\bar{d}\,J_{\Phi}^{(\Delta O)}(X)}{dX} \tag{5.34}$$

$$J_{Y}^{(\Delta O)}(X) = -EI_{\infty}\frac{\bar{d}^2 J_{\Phi}^{(\Delta O)}(X)}{dX^2} + \frac{EI_{\infty}}{\alpha^2}\left(\frac{\bar{d}^4 J_{\Phi}^{(\Delta O)}(X)}{dX^4} - \frac{m_L\omega^2}{EI_0}J_{\Phi}^{(\Delta O)}(X)\right) + \frac{k_s\,EA_0\,EI_{\infty}}{EA_p\,\alpha^2}\,\delta\left(X - X_j\right) - \frac{EI_{\infty}}{\alpha^2}\,\delta^{(2)}\left(X - X_j\right) \tag{5.35}$$

$$J_{\Gamma}^{(\Delta O)}(X) = -EI_{\infty}\frac{\bar{d}^3 J_{\Phi}^{(\Delta O)}(X)}{dX^3} + \frac{EI_{\infty}}{\alpha^2}\left(\frac{\bar{d}^5 J_{\Phi}^{(\Delta O)}(X)}{dX^5} - \frac{m_L\omega^2}{EI_0}\frac{\bar{d} J_{\Phi}^{(\Delta O)}(X)}{dX}\right) + \frac{k_s\, EA_0\, EI_{\infty}}{EA_p\, \alpha^2}\,\delta^{(1)}\left(X - X_j\right) - \frac{EI_{\infty}}{\alpha^2}\,\delta^{(3)}\left(X - X_j\right) \tag{5.36}$$

$$J_{\Sigma}^{(\Delta O)}(X) = -\frac{1}{r}\left[\left(EI_0 - EI_{\infty}\right)\frac{\bar{d}^2 J_{\Phi}^{(\Delta O)}(X)}{dX^2} + \frac{EI_{\infty}}{\alpha^2}\left(\frac{\bar{d}^4 J_{\Phi}^{(\Delta O)}(X)}{dX^4} - \frac{m_L\omega^2}{EI_0}J_{\Phi}^{(\Delta O)}(X)\right)\right] + \frac{1}{r}\,\delta\left(X - X_j\right) - \frac{k_s\, EA_0\, EI_{\infty}}{r\, EA_p\, \alpha^2}\,\delta\left(X - X_j\right) + \frac{EI_{\infty}}{r\,\alpha^2}\,\delta^{(2)}\left(X - X_j\right) \tag{5.37}$$

$$J_{\Psi}^{(\Delta O)}(X) = \frac{1}{r}\left[\left(EI_0 - EI_{\infty}\right)\frac{\bar{d}^3 J_{\Phi}^{(\Delta O)}(X)}{dX^3} + \frac{EI_{\infty}}{\alpha^2}\left(\frac{\bar{d}^5 J_{\Phi}^{(\Delta O)}(X)}{dX^5} - \frac{m_L\omega^2}{EI_0}\frac{\bar{d} J_{\Phi}^{(\Delta O)}(X)}{dX}\right)\right] - \frac{1}{r}\,\delta^{(1)}\left(X - X_j\right) + \frac{k_s\, EA_0\, EI_{\infty}}{r\, EA_p\, \alpha^2}\,\delta^{(1)}\left(X - X_j\right) - \frac{EI_{\infty}}{r\,\alpha^2}\,\delta^{(3)}\left(X - X_j\right) \tag{5.38}$$

In Eqs(5.29-5.38), the space-derivatives are generalized derivatives, as denoted by the over-bar.

It is important to note that, in this context, novel exact closed analytical expressions are obtained for the particular integrals.

Considering Eq.(5.24) together with Eqs.(5.22) and (5.23) allows vector T_j to be expressed in terms of vector **c**, resulting in the following general form for $\mathbf{Y}(X)$:

$$\mathbf{Y}(X) = \tilde{\mathbf{Y}}(X)\,\mathbf{c} \tag{5.39}$$

where $\tilde{\mathbf{Y}}(X)$ is:

$$\begin{aligned}\tilde{\mathbf{Y}}(X) = \boldsymbol{\Omega}(X) + \sum_{j=1}^{N} \mathbf{J}(X, X_j)\, \boldsymbol{\Pi}_{\boldsymbol{\Omega}}(X_j) + \\ + \sum_{j=2}^{N} \mathbf{J}(X, X_j) \sum_{2\le q\le j} \sum_{(\underbrace{j,m,n,...,r,s}_{q})\in N_q^{(j)}} \boldsymbol{\Pi}_{\mathbf{J}}(X_j, X_m)\, \boldsymbol{\Pi}_{\mathbf{J}}(X_m, X_n) \\ \cdot\cdot\cdot\cdot\cdot \boldsymbol{\Pi}_{\mathbf{J}}(X_r, X_s)\, \boldsymbol{\Pi}_{\boldsymbol{\Omega}}(X_s)\end{aligned} \tag{5.40}$$

with:

$$\boldsymbol{\Pi}_{\boldsymbol{\Omega}}(X_j) = \begin{bmatrix} -K_{W,j}\boldsymbol{\Omega}(X_j)_1 \\ \\ -\left(K_{\Delta\Theta,j}\right)^{-1}\boldsymbol{\Omega}(X_j)_3 \end{bmatrix} \qquad \boldsymbol{\Pi}_{\mathbf{J}}(X_j, X_k) = \begin{bmatrix} -K_{W,j}\mathbf{J}(X_j, X_k)_1 \\ \\ -\left(K_{\Delta\Theta,j}\right)^{-1}\mathbf{J}(X_j, X_k)_3 \end{bmatrix} \tag{5.41}$$

In Eq.(5.40), $N_q^{(j)} = \{(\underbrace{j,m,n,...r,s}_{q}) : j > m > n > ... > r > s; m, n, ...r, s = 1, 2, ..., (j-1)\}$ is the set including all possible $q$ples of index $(\underbrace{j,m,n,...r,s}_{q})$ such that $j > m > n > ... > r > s$ being $2 \le q \le j$.

At this stage, the eigenvalue problem can be formulated using Eq.(5.39) together with the boundary conditions of the beam, obtaining six equations expressed in the general form:

$$\mathbf{Bc} = \mathbf{0} \tag{5.42}$$

Each equation corresponds to a component of vector $\mathbf{Y}(X)$ in Eq.(5.39) evaluated at the beam ends $X_b = 0, L$, as described in the previous chapter where there are also reported the typical boundary conditions in term of eigenfunctions Eq.(4.40-4.42)

It is worth underscoring that matrix $\mathbf{B}$ in Eq.(4.39) is always a 6×6 matrix, independently of the number of elastic supports and joints along the beam. The characteristic equation of the eigenvalue problem is the determinant of matrix $\mathbf{B}$, i.e:

$$\det \mathbf{B} = 0 \tag{5.43}$$

whose roots ω_n are the natural frequencies of the beam (subscript n is added to indicate the infinite number of eigensolutions). Once vector $\mathbf{c}$ is derived

as non-trivial solution of Eq.(5.42) for the nth natural frequency ω_n, the exact closed analytical expression for the corresponding vector of eigenfunctions $\mathbf{Y}_n(x)$ is finally built by Eq.(5.39). The eigenfunctions satisfy intrinsically all the required conditions at the application points of support/joints, thanks to the generalized functions involved in the particular integrals (5.25).

In contrast, the exact classical approach requires six integration constants for each beam segment between two consecutive application points of supports/joints, totalling $6 \times (N+1)$ constants for N application points. Furthermore, when using the classical approach, the coefficient matrix associated with the equations to be solved must be updated whenever positions of supports and joints change, and its size inevitably increases with the number of supports and joints.

The proposed procedure remains valid also when a single translational support or rotational joint occurs at given abscissa X_j. If no support occurs at $X = X_j$, $K_{W,j} = 0$ shall be set at $X = X_j$. This will automatically set equal to zero the first row in matrices $\mathbf{\Pi_\Omega}(X_j)$, $\mathbf{\Pi_J}(X_j, X_k)$. Being the reaction force $b_j = 0$ at $X = X_j$, the 1st column of matrix $\mathbf{\Pi_J}(X_j, X_k)$ shall be set equal to zero for all $X_k > X_j$. Obviously, if no joint occurs at $X = X_j$, $K_{\Delta\Theta,j} = \infty$ shall be set at $X = X_j$. As a result, the second row of matrices $\mathbf{\Pi_\Omega}(X_j)$, $\mathbf{\Pi_J}(X_j, X_k)$ will be equal to zero. Also, being $\Delta O_j = 0$ at $X = X_j$, the 2nd column of matrix $\mathbf{\Pi_J}(X_j, X_k)$ shall be set equal to zero for all $X_k > X_j$.

5.4 Beam response to moving loads

Based on modal analysis, the beam deflection response $W(X,t)$ for a discontinuous two-layered elastically bonded beam, under moving multi-loads, may be expressed through the same relationship proposed in chapter 4, here repeated for convenience of reading:

$$W(X,t) = \sum_{n=1}^{\infty} R_n(t)\,\Phi_n(X) \tag{5.44}$$

where $\Phi_n(X)$ denotes the nth deflection eigenfunction derived in section 5.1, that, unlike the previous chapter, include the discontinuities of the response variables at support and joint locations.

Instead, the corresponding time-dependent modal coordinate $R_n(t)$ for the discontinuous two-layered elastically bonded beam remains unchanged if compared to the one proposed for the layered beam without supports and

joints, since the discontinuities only cause variations in the eigenfunctions of the beam.

Furthermore, because the supports and joints are considered as perfectly elastic, also the orthogonality relations [96] remains unchanged.

At this stage, to solve this problem, consider the equations of section 4.4 of this thesis only by being careful that in this case the derivatives of the eigenfunction are denoted by the over-bar since the presence of the discontinuities of the response variables at support and joint locations

5.5 Numerical Applications

In the following subsection, four numerical applications on the moving multi-loads in discontinuous two-layered elastically bonded beam are analyzed. In particular, example A is refereed to a simply-supported discontinuous two-layered elastically bonded beam for the presence of a mid-span translational support while in example B, rotational joints are considered. Again, in example C, both the discontinuities, rotational and translational are included in a clamped-clamped two-layered elastically bonded beam. Finally in example D, a two-layered elastically bonded beam with elastic discontinuities at the end is analysed. This last example wants to emphasize that the procedure proposed in this thesis is also valid for non-homogeneous B.C. due to end discontinuities. Modelling end discontinuities as internal discontinuities located at $x_1 = 0^+$ and $x_N = L^-$, the B.C. can still be taken as homogeneous.

5.5.1 Example A

Consider the compound high-speed train bridge of length $L = 40\,m$, analysed in Chapter 4, simply supported at both ends and equipped with an elastic translational support of stiffness $K_{W,1} = 20\,10^7\,N/m$ at the center (see Fig. 5.2).

It is assumed that the loads cross the beam with the first critical speed of first order, i.e. $V_0 = \omega_1 d/2\pi$ [105], yielding $V_0 = 104.91\,m/s$ for the fundamental circular beam frequency $\omega_1 = 27.08\,rad/s$. The next three natural frequencies are: $\omega_2 = 42.6\,rad/s$, $\omega_3 = 98.5\,rad/s$, $\omega_4 = 168\,rad/s$. To show the effect of the elastic bond on the beam response, alternatively the response of the beam bridge with rigid interlayer bond is also derived. In this case, the natural frequencies become larger (i.e. $\omega_1 = 31.83\,rad/s$, $\omega_2 = 76.36\,rad/s$, $\omega_3 = 173.77\,rad/s, \omega_4 = 305.44\,rad/s$) because of increased global lateral beam stiffness.

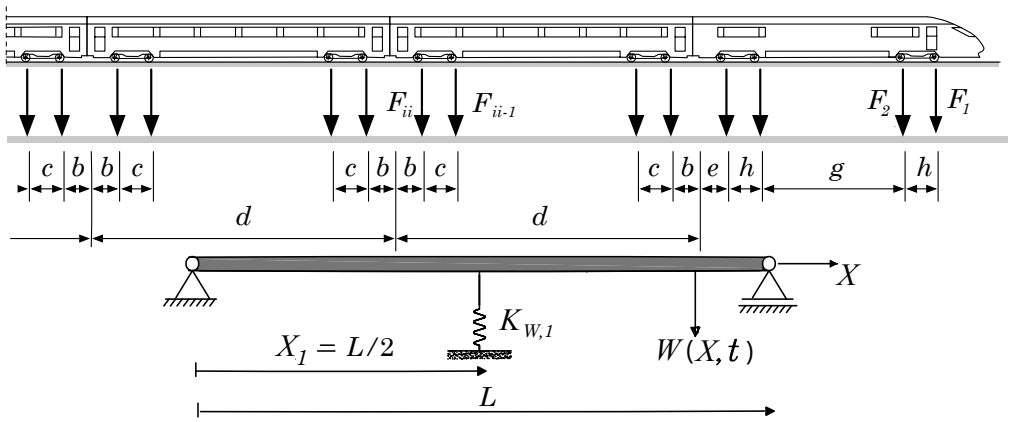

Figure 5.2: Simply-supported discontinuous two-layered beam under multi-moving loads (modified from [1]))

Figure 5.3 shows the eigenfunctions of mode 1 for all response variables of the discontinuous two-layered elastically bonded beam and alternatively of the discontinuous rigidly bonded beam, derived by the proposed method and the classical method. In the latter method, the free-vibration response is represented by twelve integration constants, six for each segment, respectively left and right of the translational support. Instead, in the proposed more efficient method only six integration constants appear. The fundamental deflection mode of the two-layered elastically bonded beam exhibits a slope (see Fig. 5.3a), indicating the impact of the flexible support. In contrast, the corresponding mode of the rigidly bonded beam looks like more the mode of the simply supported beam without elastic spring at mid-span (see Fig. 5.3b). As observed, the translational support causes a slope discontinuity in the bending moment, mirroring the corresponding jump discontinuity in the shear force. The eigenfunctions, built by the proposed method, satisfy inherently all the required conditions at the support/joint locations, and are in perfect agreement with those built by the classical method.

The dynamic lateral beam deflection induced by the series of repetitive loads is shown in Figs. 5.4 and 5.5. In particular, in Fig. 5.4 the time history of the deflection at $x = L/2$ is depicted. As observed, the beam with interlayer slip (black dashed line) is excited to resonance because the loads move with a critical speed related to the first mode of this structure. In contrast, the beam model with rigid interlayer bond underpredicts significantly the actual

response, emphasizing the importance of correct consideration of the interlayer slip stiffness. This response behavior can be led back to detuning of the critical speed from the actual fundamental frequency, as it has been shown above. Figure 5.5 shows the beam deflection over span at six time instants, specified in Fig. 5.4 by numbers 1 to 6. Additionally, also the displacement considering only the first eigenfunction for time instant 3 is shown (red line). No significant changes are found when considering more than four modes in the proposed solution, thus, the results shown are based on a five mode series approximation.

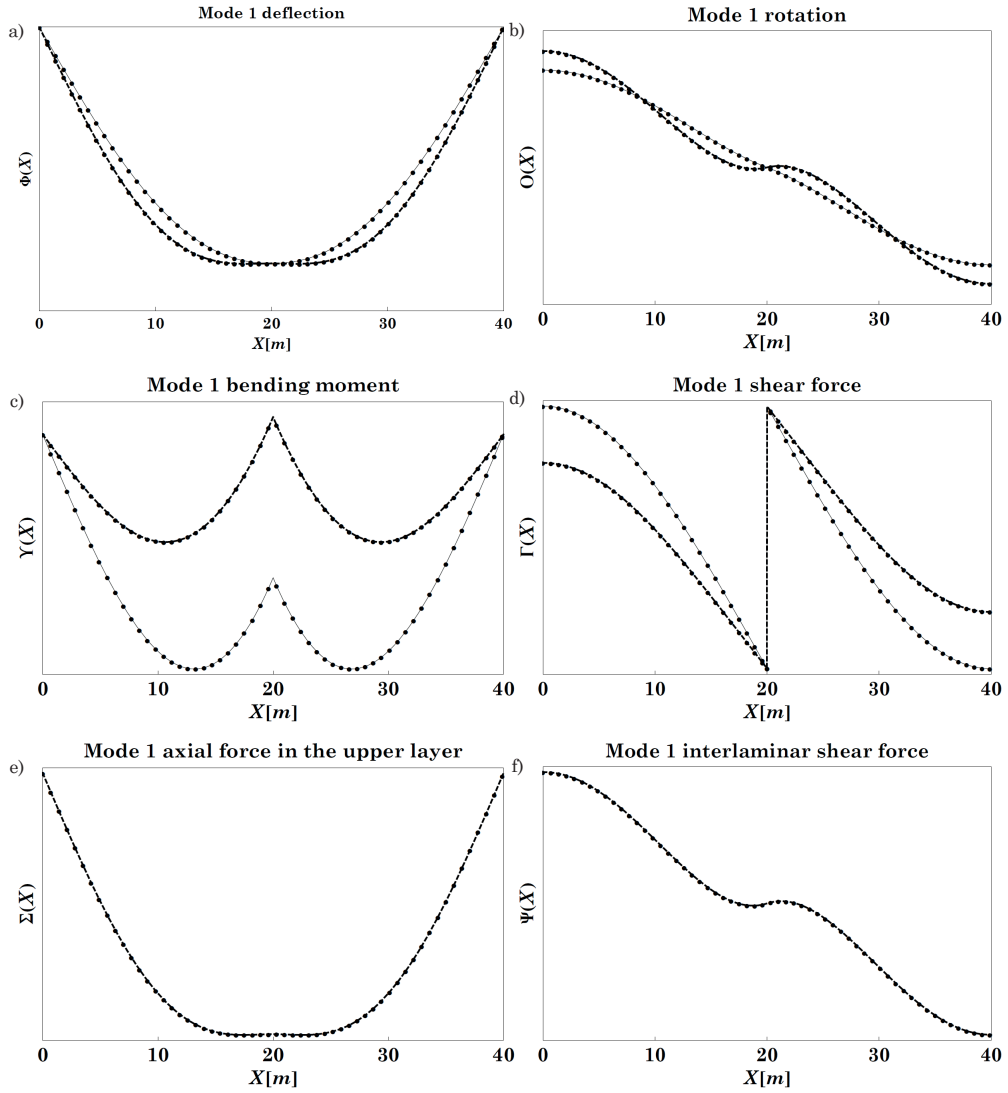

Figure 5.3: Beam in Fig.5.2: mode 1 eigenfunctions for the elastically bonded beam (black dashed line) and for the rigidly bonded beam (black solid line): (a) deflection, (b) rotation, (c) total bending moment, (d) axial force in the upper layer, (e) shear force, (f) interlaminar shear force. Solution based on the proposed method and on the classical procedure (black markers)

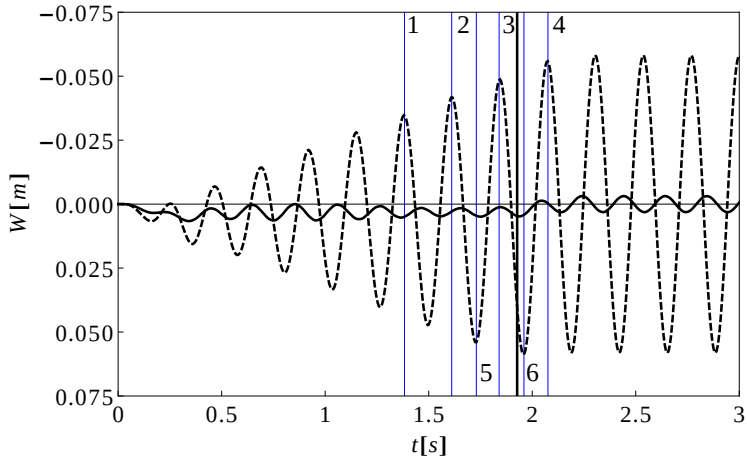

Figure 5.4: Time history of the mid-span deflection of the discontinuous two-layered elastically bonded beam shown in Fig.5.2 (black dashed line) and for the rigidly bonded beam (black solid line)

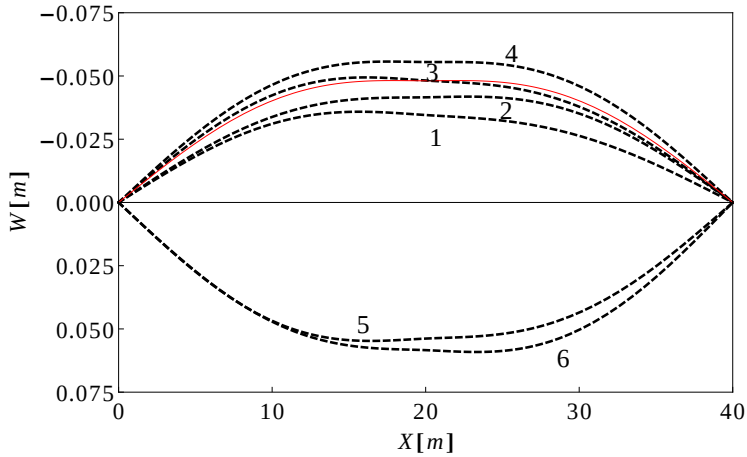

Figure 5.5: Deflection over span of the the discontinuous two-layered elastically bonded beam shown in Fig.5.2. Black dashed lines: multi-mode response at six time instants specified in Fig.4.6 ($t_1 = 1.383\ s$, $t_2 = 1.611\ s$, $t_3 = 1.84\ s$, $t_4 = 2.076\ s$ $t_5 = 1.73\ s$, $t_6 = 1.96\ s$). Red solid line: first mode response at time instant t_3. Red solid line: first mode response at time instant t_3

Finally, the deflection at the mid span of the two-layered elastically bonded

viscous beam is shown in Fig. 5.6. Modal damping with with coefficient $\zeta_m = 0.05$ for all modes is considered.

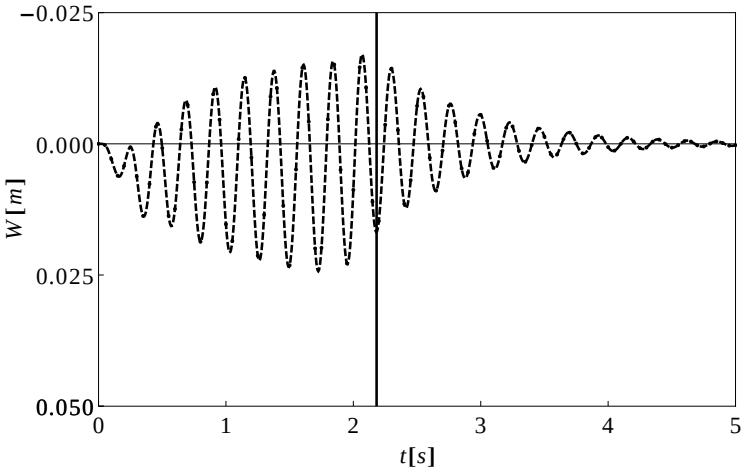

Figure 5.6: Time history of the mid-span deflection of the two-layered elastically bonded viscous beam shown in Fig.5.2

5.5.2 Example B

Consider now the same high-speed train bridge analysed in the previous examples, with local damage modeled by three in-span elastic rotational joints Fig. 5.7, whose stiffness are fixed as $K_{\Delta\Theta} = 10^{10} Nm$ connecting the beam sections at $X_1 = L/4$, $X_2 = L/2$, $X_3 = 3L/4$, respectively. In the current application it is assumed that the loads cross the beam with the first critical speed of first order, i.e. $V_0 = \omega_1 d/2\pi = 36.13\, m/s$ for the fundamental circular beam frequency $\omega_1 = 9.32\, rad/s$. The next four natural frequencies are: $\omega_2 = 35.57\, rad/s$, $\omega_3 = 78.74\, rad/s$, $\omega_4 = 168.08\, rad/s$, $\omega_5 = 230.96\, rad/s$.

Fig. 5.8 shows the eigenfunctions of mode 1 for all response variables of the cracked beam as built by proposed and classical method. In the latter method, the free-vibration response is represented by eighteen integration constants, six for each segment. Instead, in the proposed more efficient method only six integration constants are involved. A rotational joint induces a jump discontinuity in the rotation while the displacement eigenfunction of the damaged beam exhibits a slope discontinuity at the joint, mirroring the jump discontinuity in the rotation. Furthermore, the joint produces a

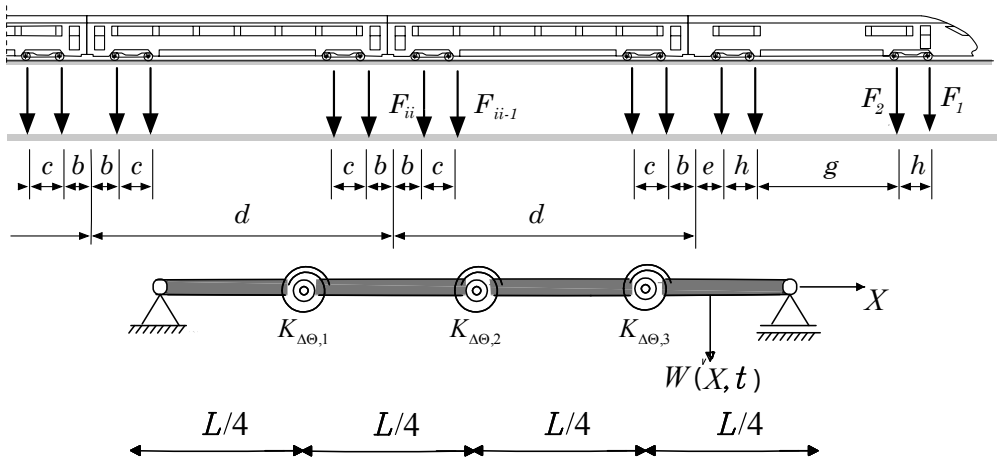

Figure 5.7: Cracked beam bridge subjected to a series of concentrated forces

slope discontinuity in the axial force $N_1(X,t)$ in the upper layer of the elastically bonded beam, and, likewise, in the axial force $N_2(X,t) = -N_1(X,t)$ in the lower layer of the elastically bonded beam, mirroring the jump discontinuity in the interlaminar shear force, since $T(X,t) = -\bar{\partial}N_1(X,t)/\partial X = \bar{\partial}N_2(X,t)/\partial X$ (see Fig.4.2). The eigenfunctions, built by the proposed method, satisfy inherently all the required conditions at the joint locations, and are in perfect agreement with those built by the classical method.

The time history displacement at $x = L/2$ of the damaged beam and the beam without imperfections, induced by the series of repetitive loads is shown in Fig. 5.9. The damaged beam is excited to resonance because the loads move with a critical speed related to the first mode of this damaged structure. In contrast, the beam model without imperfection underpredicts significantly the actual response, emphasizing the importance of correct consideration of the damage in the beam with interlayer slip. No significant changes are found when considering more than four modes in the proposed solution, thus, the results shown are based on a five mode series approximation.
Finally, the deflection at the mid span of the two-layered elastically bonded viscous beam is shown in Fig. 5.10. Modal damping with coefficient $\zeta_m = 0.05$ for all modes is considered.

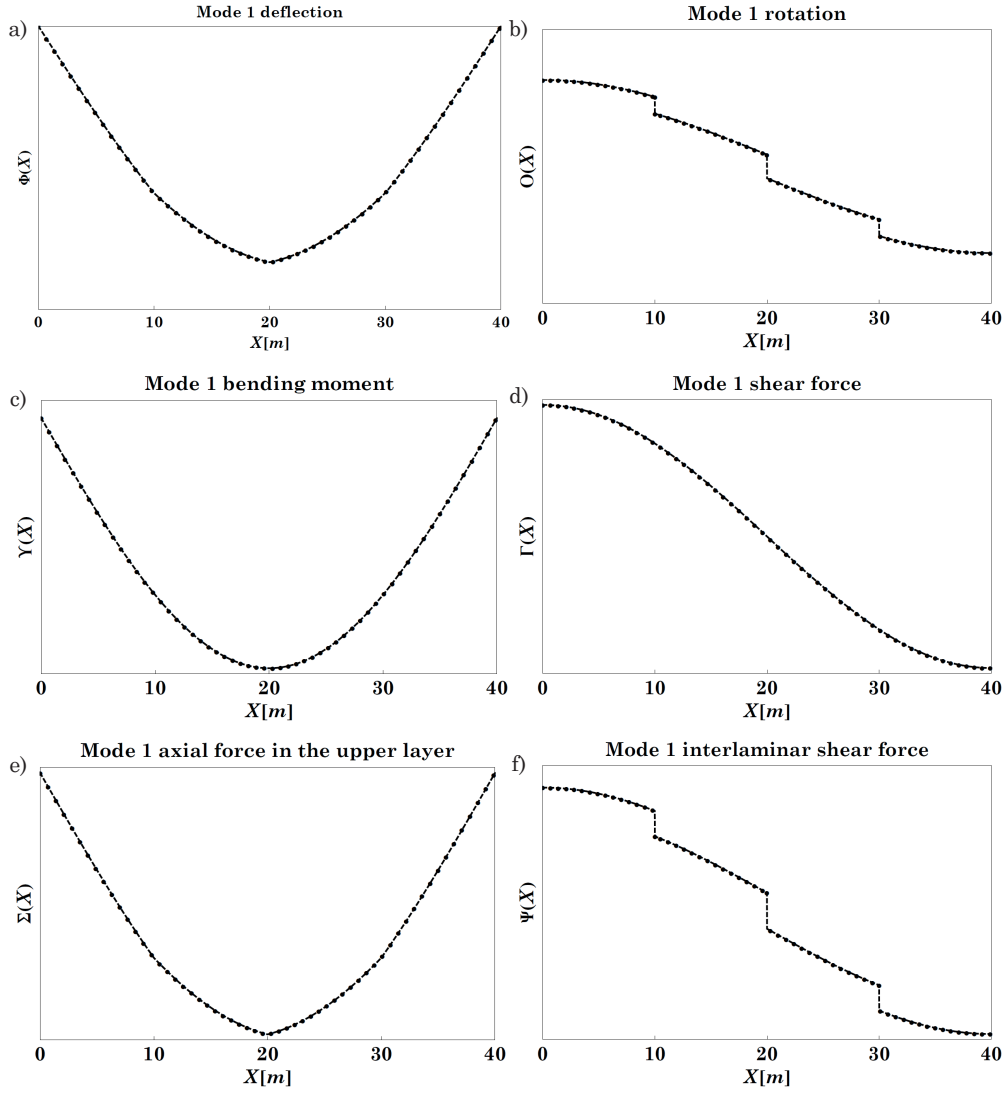

Figure 5.8: Beam in Fig.5.7: mode 1 eigenfunctions for the elastically bonded cracked beam (black dashed line): (a) deflection, (b) rotation, (c) total bending moment, (d) axial force in the upper layer, (e) shear force, (f) interlaminar shear force. Solution based on the proposed method and on the classical procedure (black markers)

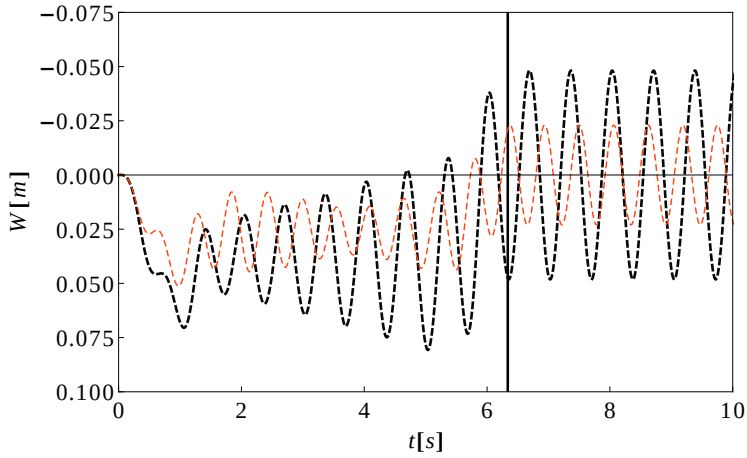

Figure 5.9: Time history beam response at mid-span to moving multi-loads at critical speed $V_0 = 36.13 m/s$. Beam without local damage (black dashed thick line) and with local damage (red dashed line)

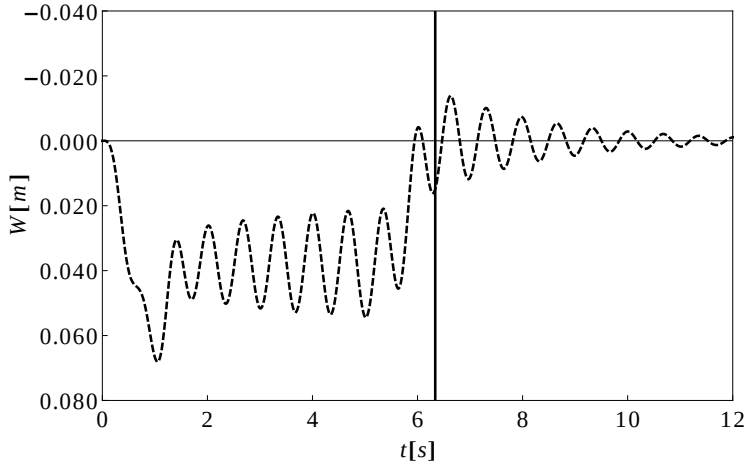

Figure 5.10: Time history of the mid-span deflection of the two-layered elastically bonded viscous beam shown in Fig.5.7

5.5.3 Example C

Consider now the high-speed train bridge analysed in Section 4.5.2, with one translation elastic support located at $X_1 = L/4$ and one in-span elastic rotational joints at $X_2 = L/2$ Fig. 5.11.

Parameters are selected as follows: $K_{W,1} = 5\,10^8 N/m$, for the translational supports and $k_{\Delta\Theta,1} = 10^{10} Nm$ for the rotational joint.

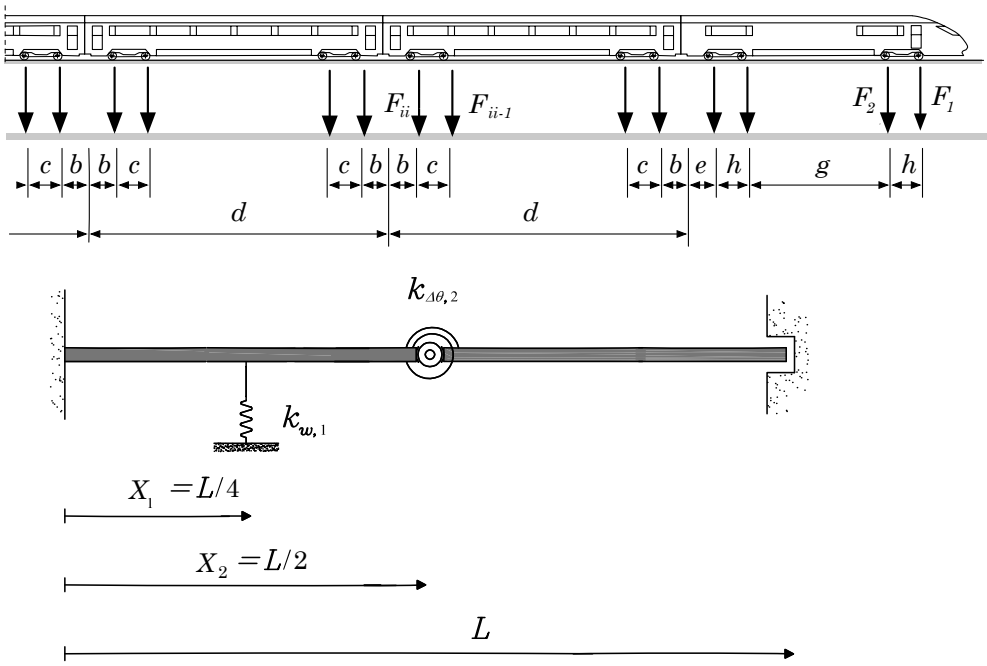

Figure 5.11: Clamped-Clamped discontinuous two-layered elastically bonded beam subjected to a series of concentrated forces

The loads cross the beam with the first critical speed of first order, i.e. $V_0 = \omega_1 d/2\pi = 113.3\,m/s$ for the fundamental circular beam frequency $\omega_1 = 29.22\,rad/s$. The next four natural frequencies are shown in the following Table 5.1.

Fig. 5.12 shows the eigenfunctions of mode 1 for all response variables of the discontinuous beam as built by proposed and classical method. As observed, the rotational joint induces a jump discontinuity in the rotation and in the interlaminar shear force, while the translational support induces a jump discontinuity in the shear force. The deflection of the elastically bonded beam exhibits a slope discontinuity at the joint, mirroring the jump discontinuity in the rotation.

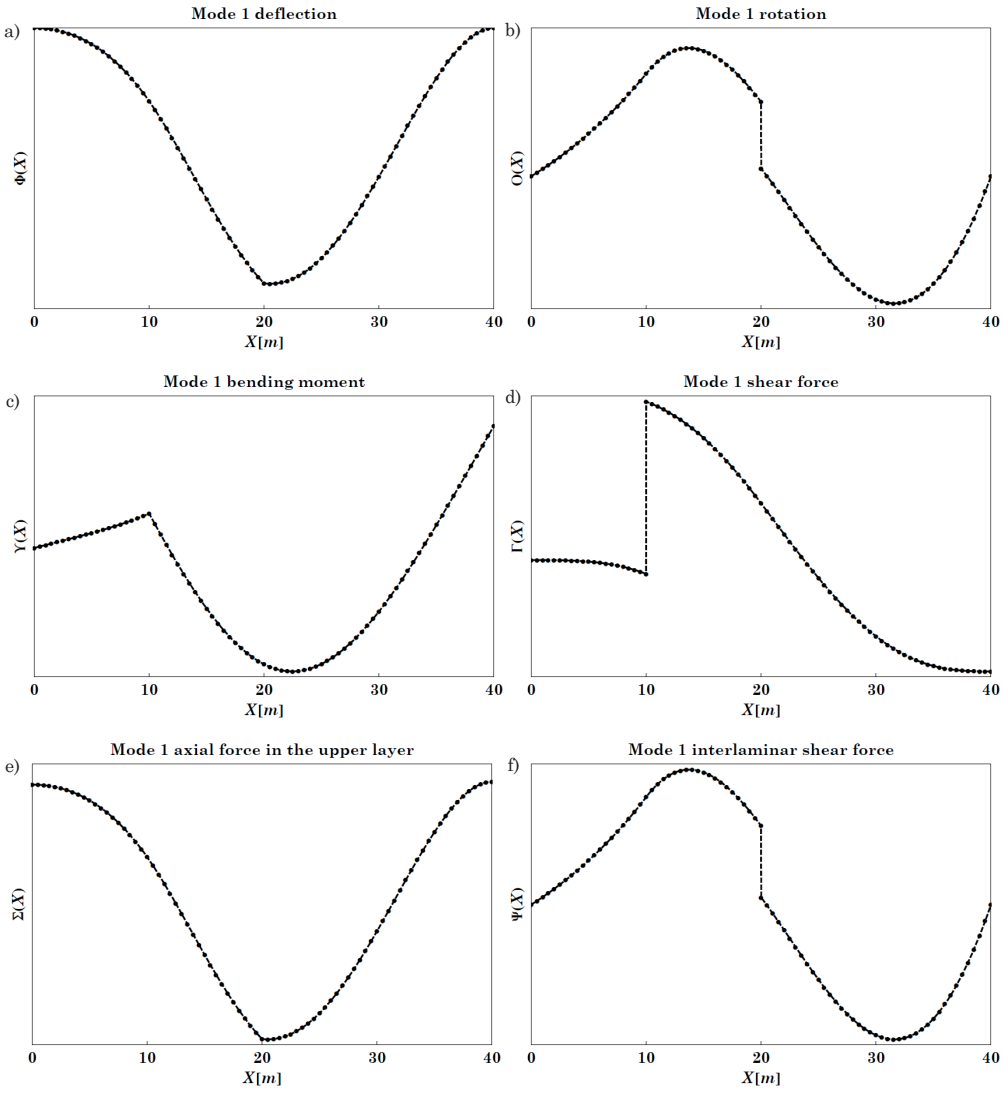

Figure 5.12: Beam in Fig.5.11: mode 1 eigenfunctions for the elastically bonded cracked beam (black dashed line): (a) deflection, (b) rotation, (c) total bending moment, (d) axial force in the upper layer, (e) shear force, (f) interlaminar shear force. Solution based on the proposed method and on the classical procedure (black markers)

Table 5.1: First five natural frequencies of the discontinuous elastically bonded beam shown in Fig.5.11

Modes	Frequency [*rad/s*]
1	29.22
2	126.33
3	213.12
4	295.51
5	444.11

Furthermore, the joint produces a slope discontinuity in the axial force $N_1(X,t)$ in the upper layer of the elastically bonded beam, and, likewise, in the axial force $N_2(X,t) = -N_1(X,t)$ in the lower layer of the elastically bonded beam, mirroring the jump discontinuity in the interlaminar shear force, since $T(X,t) = -\bar{\partial}N_1(X,t)/\partial X = \bar{\partial}N_2(X,t)/\partial X$ (see Fig.4.2). The translational support causes a slope discontinuity in the bending moment, mirroring the corresponding jump discontinuity in the shear force. The eigenfunctions, built by the proposed method, satisfy inherently all the required conditions at the support/joint locations, and are in perfect agreement with those built by the classical method.

The time history displacement at $X = L/2$ and $X = 3L/2$ of the discontinuous beam, induced by the series of repetitive loads, as built by the proposed and the classical method, is shown in Fig. 5.13a and Fig. 5.13b, respectively. No significant changes are found when considering more than four modes in the proposed solution, thus, the results shown are based on a five mode series approximation. Finally, the deflection at $X = L/2$ and $X = 3L/2$ of the two-layered elastically bonded viscous beam, as built by proposed and classical method, is shown in Fig. 5.14. Modal damping with coefficient $\zeta_m = 0.05$ for all modes is considered.

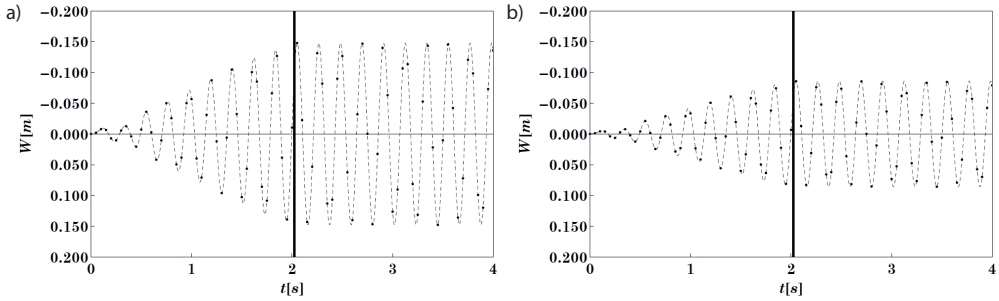

Figure 5.13: Time history beam response to moving multi-loads at critical speed $V_0 = 113.22 m/s$ at: a) $X = L/2$ b) $X = 3L/2$. Solution based on the proposed method and on the classical procedure (black markers)

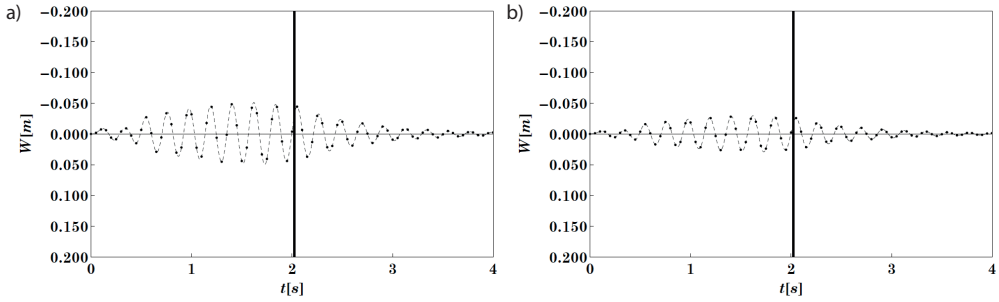

Figure 5.14: Time history of the two-layered elastically bonded viscous beam shown in Fig.5.11 at: a) $X = L/2$ b) $X = 3L/2$. Solution based on the proposed method and on the classical procedure (black markers)

5.5.4 Example D

Consider once again the two-layered elastically bonded beam with the same cross section and material properties as in the previous examples, but at this time with elastic translational/rotational supports at the ends, as shown in Fig.5.15.

The stiffness properties are $K_{W,1} = k_{W,2} = 5\ 10^8\ N/m$ for the translational supports, while for the rotational supports consider $k_{\Delta\Theta,1} = k_{\Delta\Theta,2} = 10^{10} Nm$. Modal damping with coefficient $\zeta_n = 0.05$ for all modes is considered. In literature, homogeneous beams with end rotational joints are found in [114]. Here, the beam shown in Fig.5.15 is considered to emphasize that the proposed procedure is valid also for layered elastically bonded beams equipped with elastic

translational/rotational supports applied at the beam ends. Specifically, in the proposed method, homogeneous boundary conditions are considered (end rotation $\Theta(0,t) = \Theta(L,t) = 0$, end shear force $Q(0,t) = Q(L,t) = 0$), while the translational/rotational supports at the ends are modelled respectively as internal translational supports and internal rotational joints, at $X = 0^+ = \varepsilon$ and $X = L^- = L - \varepsilon$, with $\varepsilon = 10^{-10} m$.

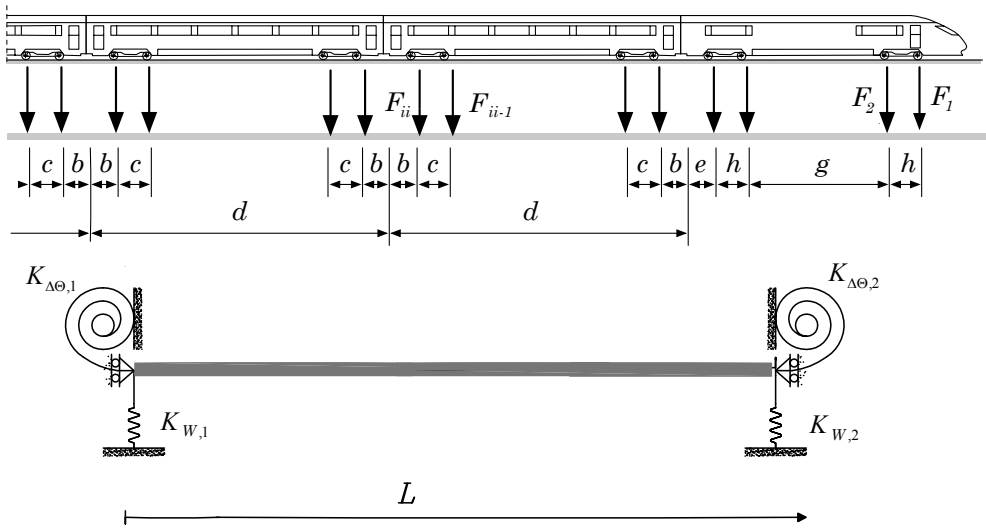

Figure 5.15: Two-layered elastically bonded beam with elastic translational and rotational supports at the ends, subjected to a series of concentrated forces

In the current application the first critical speed of first order is $V_0 = 65.97\, m/s$ for the fundamental circular beam frequency $\omega_1 = 17.03\, rad/s$. Note that the train crosses the bridge with this critical speed. The next four natural frequencies are: $\omega_2 = 120.25\, rad/s$, $\omega_3 = 214.14\, rad/s$, $\omega_4 = 293.06\, rad/s$, $\omega_5 = 424.4\, rad/s$.

Figure 5.16 shows the eigenfunctions of mode 1 for all response variables of the discontinuous beam as built by proposed method, while the dynamic response under moving multi-loads is analysed in Fig.5.17. Specifically, in Fig.5.17(a) the mid-span deflection of the discontinuous two-layered elastically bonded beam is displayed, while the mid-span deflection of the discontinuous two-layered elastically bonded viscous beam is depicted in Fig.5.17(b). Five modes have been considered also in this example.

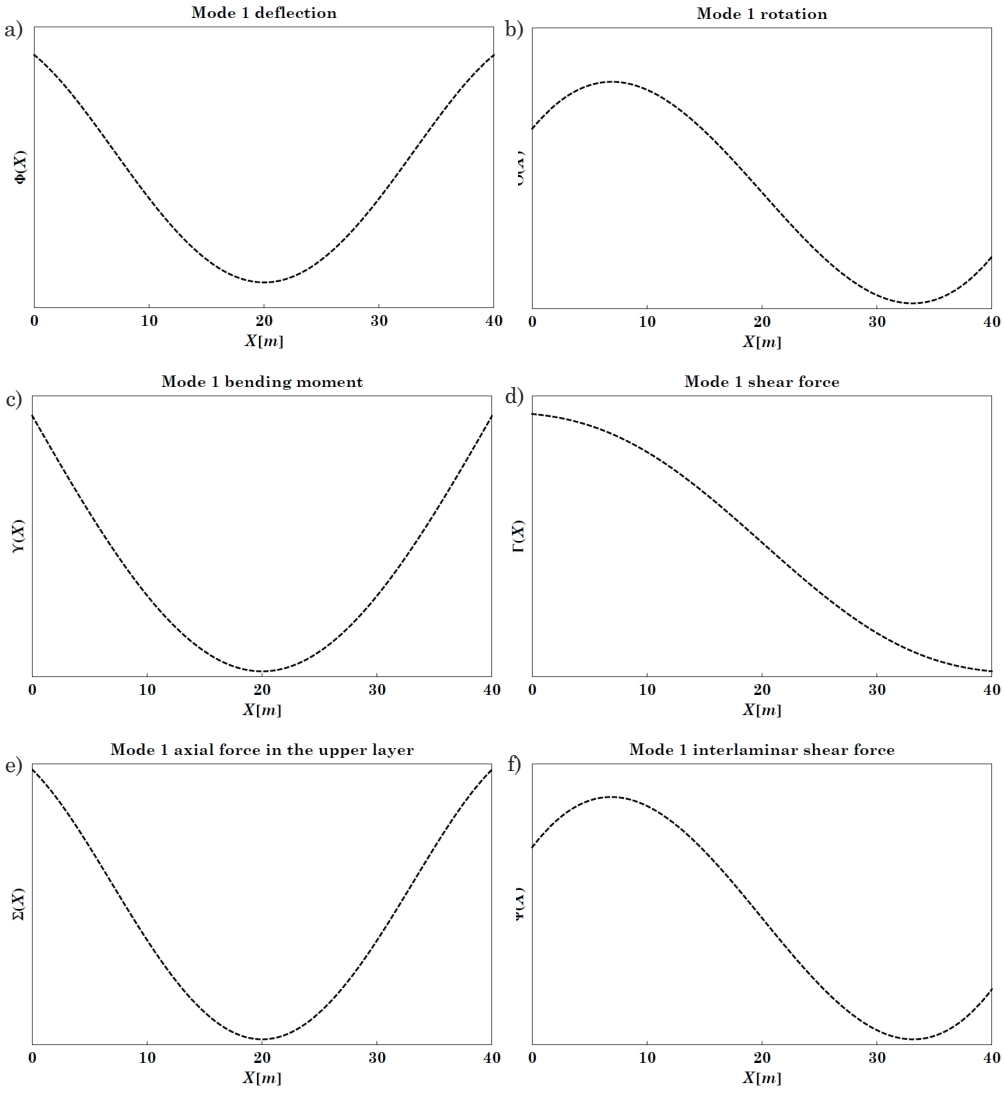

Figure 5.16: Beam in Fig.5.15: mode 1 eigenfunctions for the elastically bonded cracked beam (black dashed line): (a) deflection, (b) rotation, (c) total bending moment, (d) axial force in the upper layer, (e) shear force, (f) interlaminar shear force

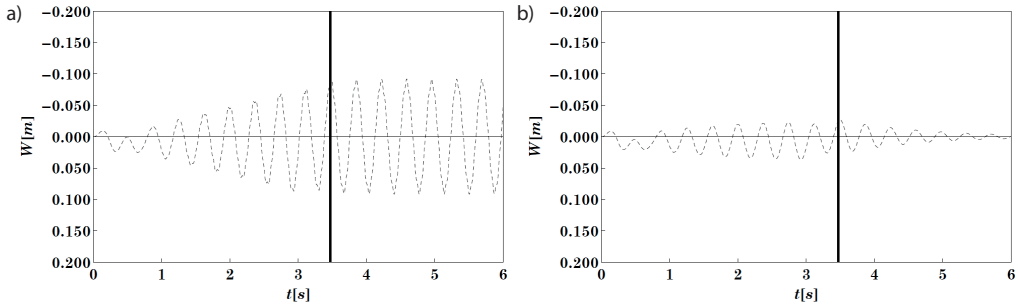

Figure 5.17: Time history mid-span beam response to moving multi-loads at critical speed $V_0 = 65.97 m/s$: a) deflection of the discontinuous two-layered elastically bonded beam b) deflection of the discontinuous two-layered elastically bonded viscous beam

5.6 Concluding remarks

An efficient approach for analyzing the dynamic flexural behavior under moving multi-loads of two-layered elastically bonded beams, featuring an arbitrary number of elastic translational supports and rotational joints, has been presented. The theory of generalized function has been used to derive the exact eigenfunctions of all response variables, from a characteristic equation built as determinant of a 6 x 6 matrix, independently of the number of discontinuities associated with the supports and joints. Based on pertinent orthogonality conditions for deflection modes, the dynamic response has been built in time domain by modal superposition. Efficiency and accuracy of the proposed method have been shown for a two-layered elastically bonded beam with various elastic supports/joints and in various boundary conditions.

Summary and conclusions

This thesis contains a novel and efficient approach to study the moving multi-loads problem in discontinuous beam with external viscoelastic supports, internal rotational joints and alternatively tuned mass damper.

The proposed solution accounts for non-proportional damping with significant benefits over existing modal superposition methods, where only proportional damping or, alternatively, no damping is considered.

The method also exceeds the limitations found using the Finite Element methods that generally require numerical integration, accuracy depends on the grid mesh, and nodes must be inserted at any location of external translational/rotational supports, internal rotational joints, and tuned mass damper. This is a significant disadvantage, especially in the early stages of design, when different solutions have to be built and compared at various locations of supports, joints or dampers.

In the present thesis, this novel modal superposition approach is applied to homogeneous beams and two-layered elastically bonded beams.

Based on the theory of generalized functions to handle the discontinuities of response variables due to supports/joints/TMDs, exact beam modes are obtained regardless of the number of discontinuities. Instead, in the classical method the free-vibration response is represented through integration constants over each segment between two consecutive damper/support locations, and the matching conditions are enforced at the subdivision points along with the boundary conditions.

On using pertinent orthogonality condition for the deflection modes, the dynamic response of the beam under moving loads is derived in time domain. All response variables are presented in a closed analytical form by using the relationship equations of the beam. Several numerical applications illustrate the efficiency of the proposed method.

Bibliography

[1] C. Adam, P. Salcher, Dynamic effect of high-speed trains on simple bridge structures, Struct. Eng. Mech 51 (2014) 581–599.

[2] R. Heuer, C. Adam, Piezoelectric vibrations of composite beams with interlayer slip, Acta Mechanica 140 (2000) 247–263.

[3] H. Ouyang, Moving-load dynamic problems: A tutorial (with a brief overview), Mech. Syst. Signal Proc 25 (2011) 2039–2060.

[4] L. Fryba, Vibration of solids and structures under moving loads, Noordhoff International Publishing, Groningen, 1972.

[5] C. Adam, R. Heuer, F. Ziegler, Reliable dynamic analysis of an uncertain compound bridge under traffic loads, Acta Mechanica 223 (2012) 1567–1581.

[6] P. Salcher, H. Pradlwarter, C. Adam, Reliability assessment of railway bridges subjected to high-speed trains considering the effects of seasonal temperature changes, Engineering Structures 126 (2016) 712–724.

[7] J. Wang, P. Qiao, Vibration of beams with arbitrary discontinuities and boundary conditions, J. Sound Vib 308 (2007) 12–27.

[8] F. Ziegler, Mechanics of Solids and Fluids, Springer Science & Business Media, 2012.

[9] C. Johansson, C. Pacoste, R. Karoumi, Closed-form solution for the mode superposition analysis of the vibration in multi-span beam bridges caused by concentrated moving loads, Computers & Structures 119 (2013) 85–94.

[10] X. Q. Zhu, S. S. Law, Moving load identification on multi-span continuous bridges with elastic bearings, Mechanical Systems and Signal Processing 20 (2006) 1759–1782.

[11] T. H. T. Chan, D. B. Ashebo, Theoretical study of moving force identification on continuous bridges, Journal of Sound and Vibration 295 (2006) 870–883.

[12] Y. A. Dugush, M. Eisenberger, Vibrations of non-uniform continuous beams under moving loads, Journal of Sound and Vibration 254 (2002) 911–926.

[13] K. Henchi, M. Fafard, G. Dhatt, M. Talbot, Dynamic behaviour of multi-span bemas under moving loads, Journal of Sound and Vibration 199 (1997) 33–50.

[14] A. Greco, A. Santini, Dynamic response of a flexural non-classically damped continuous beam under moving loadings, Comput. Struct 80 (2002) 1945–1953.

[15] A. E. Martínez-Castro, P. Museros, A. Castillo-Linares, Semi-analytic solution in the time domain for non-uniform multi-span Euler–Bernoulli beams traversed by moving loads, Journal of Sound and Vibration 294 (2006) 278–297.

[16] D. Y. Zheng, Y. K. Cheung, F. T. K. Au, Y. S. Cheng, Vibration of multi-span non-uniform beams under moving loads by using modified beam vibration functions, Journal of Sound and Vibration 212 (1998) 455–467.

[17] V. De Salvo, G. Muscolino, A. Palmeri, A substructure approach tailored to the dynamic analysis of multi-span continuous beams under moving loads, Journal of Sound and Vibration 329 (2010) 3101–3120.

[18] X. Q. Zhu, S. S. Law, Precise time-step integration for the dynamic response of a continuous beam under moving loads, Journal of Sound and Vibration 240 (2001) 962–970.

[19] H. Xu, W. L. Li, Dynamic behavior of multi-span bridges under moving loads with focusing on the effect of the coupling conditions between spans, Journal of Sound and Vibration 312 (2008) 736–753.

[20] P. Museros, M. Martinez-Rodrigo, Vibration control of simply supported beams under moving loads using fluid viscous dampers, J. Sound Vib 300 (2007) 292–315.

[21] F. Samani, F. Pellicano, Vibration reduction on beams subjected to moving loads using linear and nonlinear dynamic absorbers, J. Sound Vib 325 (2009) 742–754.

[22] H. P. Lee, Dynamic response of a beam with intermediate point constraints subject to a moving load, Journal of Sound and Vibration 171 (1994) 361–368.

[23] H. P. Lee, T. Y. Ng, Dynamic response of a cracked beam subject to a moving load, Acta Mechanica 106 (1994) 221–230.

[24] J. J. Wu, A. R. Whittaker, M. P. Cartmell, The use of finite element techniques for calculating the dynamic response of structures to moving loads, Computers & Structures 78 (2000) 789–799.

[25] J. R. Rieker, Y. H. Lin, M. W. Trethewey, Discretization considerations in moving load finite element beam models, Finite Elements in Analysis and Design 21 (1996) 129–144.

[26] V. Sarvestan, H. R. Mirdamadi, M. Ghayour, M. A, Spectral finite element for vibration analysis of cracked viscoelastic Euler–Bernoulli beam subjected to moving load, Acta Mechanica 226 (2015) 4259–4280.

[27] N. Azizi, M. M. Saadatpour, M. Mahzoon, Using spectral element method for analyzing continuous beams and bridges subjected to a moving load, Applied Mathematical Modelling 36 (2012) 3580–3592.

[28] L. Sun, A closed-form solution of beam on viscoelastic subgrade subjected to moving loads, Comput. Struct 80 (2002) 1–8.

[29] S. Di Lorenzo, M. Di Paola, G. Failla, A. Pirrotta, On the moving load problem in Euler–Bernoulli uniform beams with viscoelastic supports and joints, Acta Mechanica 228 (2016) 805–821.

[30] G. Failla, On the dynamics of viscoelastic discontinuous beams, Mechanics Research Communications 60 (2014) 52–63.

[31] A. Yavari, S. Shahram, E. T. Moyer, On applications of generalized functions to beam bending problems, International Journal of Solids and Structures 37 (2000) 5675–5705.

[32] A. Yavari, S. Sarkani, On applications of generalized functions to the analysis of Euler–Bernoulli beam–columns with jump discontinuities, International Journal of Mechanical Sciences 43 (2001) 1543–1562.

[33] A. Yavari, S. Sarkani, J. N. Reddy, Generalized solutions of beams with jump discontinuities on elastic foundations, Archive of Applied Mechanics 71 (2001) 625–639.

[34] G. Falsone, The use of generalised functions in the discontinuous beam bending differential equations, International Journal of Engineering Education 18 (2002) 337–343.

[35] B. Biondi, S. Caddemi, Euler–Bernoulli beams with multiple singularities in the flexural stiffness, European Journal of Mechanics - A/Solids 26 (2007) 789–809.

[36] G. Failla, A. Santini, A solution method for Euler–Bernoulli vibrating discontinuous beams, Mechanics Research Communications 35 (2008) 517–529.

[37] G. Failla, An exact generalised function approach to frequency response analysis of beams and plane frames with the inclusion of viscoelastic damping, Journal of Sound and Vibration 360 (2016) 171–202.

[38] A. Burlon, G. Failla, F. Arena, Exact frequency response analysis of axially loaded beams with viscoelastic dampers, International Journal of Mechanical Sciences 115-116 (2016) 370–384.

[39] S. Caddemi, A. Morassi, Multi-cracked Euler–Bernoulli beams: Mathematical modeling and exact solutions, International Journal of Solids and Structures 50 (2013) 944–956.

[40] S. Caddemi, I. Caliò, Exact reconstruction of multiple concentrated damages on beams, Acta Mechanica 225 (2014) 3137–3156.

[41] S. Caddemi, I. Caliò, F. Cannizzaro, Influence of an elastic end support on the dynamic stability of Beck's column with multiple weak sections, International Journal of Non-Linear Mechanics 69 (2015) 14 – 28.

[42] R. P. Kanwal, Generalized Functions Theory and Applications, Academic Press, New York, 1983.

[43] A. Shukla, T. Datta, Optimal use of viscoelastic dampers in building frames for seismic force, J. Struct. Eng. 125 (1999) 401–409.

[44] M. Sing, L. Moreschi, Optimal placement of dampers for passive response control, Earth. Eng. Struct. Dyn 31 (2002) 955–976.

[45] J. Ou, X. Long, Q. Li, Seismic response analysis of structures with velocity-dependent dampers, J. Constr. Steel Res 63 (2007) 628–638.

[46] Y. Xu, W. Zhang, Modal analysis and seismic response of steel frames with connection dampers, Eng. Struct 23 (2001) 385–396.

[47] S. Kawashima, T. Fujimoto, Vibration analysis of frames with semi-rigid connections, Comput. Struct 19 (1984) 85–92.

[48] M. Sekulovic, R. Salatic, M. Nefovska, Dynamic analysis of steel frames with flexible connections, Comput. Struct. 80 (2002) 935–955.

[49] G. Failla, Closed-form solutions for Euler–Bernoulli arbitrary discontinuous beams, Archive of Applied Mechanics 81 (2011) 605–628.

[50] A. Veletsos, C. Ventura, Modal analysis of non-classically damped linear systems, Earthq. Eng. Struct. Dyn 14 (1986) 217–243.

[51] G. Oliveto, A. Santini, E. Tripodi, Complex modal analysis of a flexural vibrating beam with viscous end conditions, J. Sound Vib. 200(3) (1997) 327–345.

[52] Mathematica Version 7.0. Wolfram Research Inc, Champaign (2008).

[53] ADINA Version 8.2. ADINA R & D Inc, Watertown (2004).

[54] N. Impollonia, G. Ricciardi, F. Saitta, Dynamic behaviour of stay cables with rotational dampers, ASCE J. Eng. Mech. 136 (2010) 697–709.

[55] A. Tributsch, C. Adam, Evaluation and analytical approximation of tuned mass damper performance in an earthquake environment, Smart Structures and Systems 10 (2012) 155–179.

[56] B. Schmelzer, M. Oberguggenberger, C. Adam, Efficiency of tuned mass dampers with uncertain parameters on the performance of structures under stochastic excitation, Proceedings of the Institution of Mechanical Engineers, Part O: Journal of Risk and Reliability 4 (2010) 297–308.

[57] C. Adam, R. Heuer, A. Pirrotta, Experimental dynamic analysis of elastic-plastic shear frames with secondary structures, Experimental Mechanics 43 (2003) 124–130.

[58] B. Schmelzer, M. Oberguggenberger, C. Adam, Set-valued processes induced by parameterised stochastic differential equations with an application to tuned mass dampers, PAMM Proc. Appl. Math. Mech 11 (2011) 705–706.

[59] C. Adam, M. Oberguggenberger, B. Schmelzer, Seismic performance of Tuned Mass Dampers with uncertain parameters, Computational Engineering (Hofstetter, G., ed.), Springer, 2014, pp. 57–83.

[60] C. Adam, T. Furtmüller, Seismic performance of Tuned Mass Dampers., Mechanics and Model Based Control of Smart Materials and Structures (Irschik, H., Krommer, M., Watanabe, K., eds), Wien, New York: Springer, 2010, pp. 11–18.

[61] B. Schmelzer, C. Adam, M. Oberguggenberger, Seismic performance of tuned mass dampers with uncertain parameters, in: J. Eberhardsteiner, et al (Eds.), Proc. European Congress on Computational Methods in Applied Sciences and Engineering (ECCOMAS 2012), 2012, p. 20 pages.

[62] A. Tributsch, C. Adam, Simplified assessment of structure - tuned mass damper assemblies under earthquakes, in: A. Del Grosso, P. Basso (Eds.), Proc. 5th European Conference on Structural Control (EACS 2012), no. 125, 2012, p. 10 pages.

[63] A. Tributsch, C. Adam, T. Furtmüller, Mitigation of earthquake induced vibrations by tuned mass dampers, in: G. De Roeck, G. Degrande, G. Lombaert, G. Müller (Eds.), Structural Dynamics - EURODYN2011, Proc. of 8th European Conference on Structural Dynamics, 2011, pp. 1742–1749.

[64] C. Adam, R. Heuer, A. Pirrotta, Earthquake excited elastic-plastic shear buildings with tuned mass dampers: Numerical and experimental sim-

ulation, in: P. Bisch, P. Labbé, A. Pecker (Eds.), Proc. of 11th European Conference on Earthquake Engineering (XI ECEE), 1998, p. 9 pages.

[65] Y. Chen, D. Chen, Timoshenko beam with tuned mass dampers to moving loads, J Bridge Eng 9 (2004) 167–177.

[66] C. Lin, J. Wang, B. Chen, Train-induced vibration control of high-speed railway bridges equipped with multiple tuned mass dampers, J Bridge Eng 10 (2005) 398–414.

[67] L. Miguel, R. Lopez, A. Torii, L. Miguel, B. A.T, Robust design optimization of TMDs in vehicle-bridge coupled vibration problems, Engineering Structures 126 (2016) 703–711.

[68] C. Adam, S. Di Lorenzo, G. Failla, A. Pirrotta, On the moving load problem in beam structures equipped with tuned mass dampers, Meccanica 52 (2017) 1843–1850.

[69] P. Den Hartog, J, Mechanical vibrations, McGraw-Hill, New York., 1962.

[70] J. M. Whitney, N. J. Pagano, Shear deformation in heterogeneous anisotropic plates, Journal of Applied Mechanics 37 (1970) 1031–1036.

[71] A. Apuzzo, R. Barretta, R. Luciano, Some analytical solutions of functionally graded Kirchhoff plates, Composites Part B: Engineering 68 (2015) 266 – 269.

[72] G. W. Swift, R. A. Heller, Layered beam analysis, Journal of the Engineering Mechanics Division 100 (1974) 267–282.

[73] A. Apuzzo, R. Barretta, R. Luciano, F. M. de Sciarra, R. Penna, Free vibrations of Bernoulli-Euler nano-beams by the stress-driven nonlocal integral model, Composites Part B: Engineering 123 (2017) 105 – 111.

[74] R. Heuer, Static and dynamic analysis of transversely isotropic, moderately thick sandwich beams by analogy, Acta Mechanica 91 (1992) 1–9.

[75] A. Apuzzo, R. Barretta, M. Canadija, L. Feo, R. Luciano, F. M. de Sciarra, A closed-form model for torsion of nanobeams with an enhanced nonlocal formulation, Composites Part B: Engineering 108 (2017) 315 – 324.

[76] J. N. Reddy, An evaluation of equivalent-single-layer and layerwise theories of composite laminates, Composite Structures 25 (1993) 21–35.

[77] R. Barretta, L. Feo, R. Luciano, F. M. de Sciarra, R. Penna, Functionally graded Timoshenko nanobeams: A novel nonlocal gradient formulation, Composites Part B: Engineering 100 (2016) 208 – 219.

[78] H. Irschik, On vibrations of layered beams and plates, ZAMM 73 (1993) T34–T45.

[79] R. Barretta, R. Luciano, Analogies between Kirchhoff plates and functionally graded Saint-Venant beams under torsion, Continuum Mechanics and Thermodynamics 27 (3) (2015) 499–505.

[80] A. Pagani, Y. Yan, E. Carrera, Exact solutions for static analysis of laminated, box and sandwich beams by refined layer-wise theory, Composites Part B: Engineering 131 (Supplement C) (2017) 62 – 75.

[81] V. Kahya, Buckling analysis of laminated composite and sandwich beams by the finite element method, Composites Part B: Engineering 91 (Supplement C) (2016) 126 – 134.

[82] M. Filippi, E. Carrera, Bending and vibrations analyses of laminated beams by using a zig-zag-layer-wise theory, Composites Part B: Engineering 98 (Supplement C) (2016) 269 – 280.

[83] A. Caporale, L. Feo, R. Luciano, Eigenstrain and fourier series for evaluation of elastic local fields and effective properties of periodic composites, Composites Part B: Engineering 81 (Supplement C) (2015) 251 – 258.

[84] J. R. Goodman, E. P. Popov, Layered beam systems with interlayer slip, Journal of the Structural Division 94 (1968) 2535–2548.

[85] U. A. Girhammar, V. K. A. Gopu, Composite beam-columns with interlayer slip-exact analysis, Journal of Structural Engineering 119 (1993) 1265–1282.

[86] E. S. Mistakis, K. Thomopoulos, A. Avdelas, P. D. Panagiotopoulos, On the nonmonotone slip effect in the shear connectors of composite beams, Int. J. Eng. Anal. Des. 1 (1994) 395–409.

[87] S. Schnabl, I. Planinc, M. Saje, B. Čas, G. Turk, An analytical model of layered continuous beams with partial interaction, Structural Engineering and Mechanics 22 (2006) 263–278.

[88] S. Simon, S. Miran, T. Goran, P. Igor, Analytical solution of two-layer beam taking into account interlayer slip and shear deformation, Journal of Structural Engineering 113 (2007) 886–894.

[89] M. João Batista, J. Sousa, R. Amilton, Analytical and numerical analysis of multilayered beams with interlayer slip, Engineering Structures 32 (2010) 1671 – 1680.

[90] K.-B. Choi, W.-C. Choi, L. Feo, S.-J. Jang, H.-D. Yun, In-plane shear behavior of insulated precast concrete sandwich panels reinforced with corrugated gfrp shear connectors, Composites Part B: Engineering 79 (Supplement C) (2015) 419 – 429.

[91] I. Choi, J. Kim, Y.-C. You, Effect of cyclic loading on composite behavior of insulated concrete sandwich wall panels with gfrp shear connectors, Composites Part B: Engineering 96 (Supplement C) (2016) 7 – 19.

[92] D. Zabulionis, O. Kizinievič, L. Feo, An analysis of the stress-strain state of a timber-concrete T cross section, Composites Part B: Engineering 45 (2013) 148–158.

[93] L. Feo, M. Latour, R. Penna, G. Rizzano, Pilot study on the experimental behavior of gfrp-steel slip-critical connections, Composites Part B: Engineering 115 (Supplement C) (2017) 209 – 222.

[94] S. Chonan, Vibration and stability of sandwich beams with elastic bonding, Journal of Sound and Vibration 85 (1982) 525–537.

[95] U. A. Girhammar, D. Pan, Dynamic analysis of composite members with interlayer slip, International Journal of Solids and Structures 30 (1993) 797–823.

[96] C. Adam, R. Heuer, A. Jeschko, Flexural vibrations of elastic composite beams with interlayer slip, Acta Mechanica 125 (1997) 17–30.

[97] S. W. Hansen, R. D. Spies, Structural damping in laminated beams due to interfacial slip, Journal of Sound and Vibration 204 (1997) 183–202.

[98] C. Adam, R. Heuer, A. Raue, F. Ziegler, Thermally induced vibrations of composite beams with interlayer slip, Journal of Thermal Stresses 23 (2000) 747–772.

[99] R. Xu, Y. Wu, Static, dynamic, and buckling analysis of partial interaction composite members using Timoshenko's beam theory, International Journal of Mechanical Sciences 49 (2007) 1139 – 1155.

[100] S. Lenci, F. Clementi, Effects of shear stiffness, rotatory and axial inertia, and interface stiffness on free vibrations of a two-layer beam, Journal of Sound and Vibration 331 (2012) 5247–5267.

[101] S. Lenci, G. Rega, An asymptotic model for the free vibrations of a two-layer beam, European Journal of Mechanics - A/Solids 42 (Supplement C) (2013) 441 – 453.

[102] R. Heuer, C. Adam, F. Ziegler, Sandwich panels with interlayer slip subjected to thermal loads., Journal of Thermal Stresses 26 (2003) 1185–1192.

[103] C. Adam, R. Heuer, F. Ziegler, Composite beams with interlayer slip, in: Recent Advances in Applied Mechanics, Honorary Volume for Professor A.N. Kounadis, J.T. Katsikadelisand D.E. Beskos and E.E. Gdoutos, 2000, pp. 3–10.

[104] R. Heuer, C. Adam, F. Ziegler, Thermally stressed sandwich panels with interlayer slip, in: L. Librescu, P. Marzocca (Eds.), Proc. of 5th International Congress on Thermal Stresses and Related Topics, June 8-11, 2003, Blacksburg, VA, 2003, pp. 1–3.

[105] Y. B. Yang, J. D. Yau, Y. S. Wu, Vehicle-bridge interaction dynamics: with applications to high-speed railways, World Scientific Publishing, Singapore, 2004.

[106] H.-P. Lin, S. Chang, Free vibration analysis of multi-span beams with intermediate flexible constraints, Journal of Sound and Vibration 281 (2005) 155 – 169.

[107] C. W. Bert, A. L. Newberry, Improved finite element analysis of beam vibration, Journal of Sound and Vibration 105 (1986) 179–183.

[108] P. A. A. Laura, R. E. Rossi, J. L. Pombo, D. Pasqua, Dynamic stiffening of straight beams of rectangular cross-section: A comparison of finite element predictions and experimental results, Journal of Sound and Vibration 150 (1991) 174–178.

[109] T. S. Balasubramanian, G. Subramanian, On the performance of a four-degree-of-freedom per node element for stepped beam analysis and higher frequency estimation, Journal of Sound and Vibration 99 (1985) 563–567.

[110] T. S. Balasubramanian, G. Subramanian, T. S. Ramani, Significance and use of very high order derivatives as nodal degrees of freedom in stepped beam vibration analysis, Journal of Sound and Vibration 137 (1990) 353–356.

[111] S. Di Lorenzo, C. Adam, A. Burlon, G. Failla, A. Pirrotta, Flexural vibrations of discontinuous layered elastically bonded beams, Composites Part B 135 (2018) 175–188.

[112] S. D. Lorenzo, C. Adam, G. Failla, A. Pirrotta, Moving multi-loads problem in layered cracked beams with interlayer slip, in: L. Ascione, V. Berardi, L. Feo, F. Fraternali, A. M. Tralli (Eds.), AIMETA 2017, XXIII Conference, The Italian Association of Theoretical and Applied Mechanics, 2017.

[113] S. D. Lorenzo, C. Adam, G. Failla, A. Pirrotta, On the moving multi-loads problem in discontinuous beam structures with interlayer slip., in: F. Vestroni, V. Gattulli, F. Romeo (Eds.), Procedia Engineering, no. 199, 2017, pp. 2531–2536.

[114] I. A. Karnovsky, O. I. Lebed, Formulas for Structural Dynamics: Tables, Graphs and Solutions, McGraw-Hill, Inc., 2001.

Acknowledgements

The course of doctoral studies is not only a path of academic training but also a moment of personal growth, where you can measure yourself, through conference presentations, university lessons, respect of deadlines, responsibility in finishing a path, commitment to writing a thesis. You are under the judgment of others, students, colleagues and professors, in a very competitive atmosphere, growing and acquiring awareness of own skills, limits and propensities.

It is precisely on the basis of these considerations that I would like to thank my Phd tutor, Professor Antonina Pirrotta, who, with careful and constant guidance, teaching ability and scientific dedication, has always believed in me, instigating in me curiosity and desire for learning, which has made this period fruitful, interesting and unforgettable.

A big thanks goes to my illustrious external supervisor, Prof. Christoph Adam of the University of Innsbruck, for his incomparable hospitality during my stay in Austria, for his valuable suggestions and teachings that have improved this thesis in a significant way and for the respect and esteem shown to me as a loyal friend before being a professor.

I wish to thank Prof. Giuseppe Failla for his constant support in my doctoral studies, clarifying the doubts and tackling together the thesis topics.

Thanks to Prof. Mario Di Paola, Prof. Liborio Cavaleri, Prof. Piero Colajanni, Prof. Salvatore Caddemi, Prof. Antonino Valenza, Prof. Francesco Paolo La Mantia, for academic and friendly moments spent together.

Thanks to my colleagues, Francesco Paolo, Alberto, Gioacchino, Nino, Emma, Natalia, Marco, Francesco, Gabriele, Giuseppe, Chiara, Iain, for the scientific discussions, collaborations, and friendly moments.

Thanks to my colleagues of the University of Innsbruck, Thomas, Ivan, Benjamin, Maximilian, Nadia, Johannes, Stella, Carina, Helmuth, Franz, for the welcome shown me and the nice moments to warm up the cold days of

work.

An important and invaluable thanks goes to my parents for their constant encouragement and moral and economic support. Thanks to my sister Federica who has endured me since she was born:) Thank you.

Last, but not least, a special thanks goes to Martina, always ready to encourage me in the most difficult moments, always believing in me with esteem and love.

To her and my family this manuscript is dedicated.

Salvatore Di Lorenzo
Palermo, December 2017